Measurement of Semi-Leptonic Decay Width $\Gamma(D^0 \to K^-\mu^+\nu_\mu)$

DISSERTATION

Presented in Partial Fulfillment of the Requirements
for the Degree of Doctor of Philosophy
in the Graduate School of Toho University

By

Shoji WATANABE

Toho University
1992

Dissertation Committee:

Jun Kondo
Kiyoshi Kamimura
Hiroshi Shibuya
Osamu Kusumoto
Mitsuko Kazuno

Approved By:

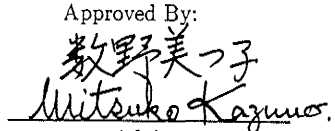

Adviser
Department of Physics

ABSTRACT

Title: Measurement of Semi-leptonic Decay Width $\Gamma(D^0 \to K^-\mu^+\nu_\mu)$

Physics Course Shoji Watanabe

Particle physics is considered to be one of the most fundamental subject in physical science. Elementary particles and forces between them govern the behavior of Nature. To understand the nature of the interactions among the elementary particles (quarks and leptons) is the central question in particle physics. Quarks and leptons are thought to be described within a unified framework by the standard electro-weak theory of SU(2)×U(1) using the Cabibbo-Kobayashi-Maskawa matrix. Many particle physicists wish to establish the consistency of this standard theory by determining the C-K-M matrix elements experimentally.

However, one can only observe the interactions through the decays of hadrons which are composite particles. We are only able to see the interplay of the strong and weak interactions. Thus, the theoretical treatment and the comparison with experiments is difficult due to the uncertaint state of our knowledge concerning strong interaction between quarks.

In this respect, the semi-leptonic decay of heavy flavor meson is more suitable than the non-leptonic decay for the determination of the structure of the interaction among the elementary particles. In particular, for the determination of the C-K-M matrix element, the semi-leptonic decay process is theoretically simple and is easily calculated at the quark level.

However, in reality the detection and the identification of the heavy flavor particle is extremely difficult because of its very low production cross section and the variety of decay modes. Furthermore, the semi-leptonic decay mode involves the unobservable neutrino.

The original result of this dissertation is the evaluation of the decay width $\Gamma(D^0 \to K^-\mu^+\nu_\mu)$ based on the value obtained from the relative branching fraction of the decay mode $D^0 \to K^-\mu^+\nu_\mu$ to $D^0 \to \mu X$ by the investigation of the selected semi-muonic decays, extracted from 1×10^8 interactions. The interactions were produced in the experiment E653 which was composed of the emulsion-counter hybrid apparatus. At present, this apparatus is the most powerful system available with both spatial and time resolution.

The author was at Fermilab from August to October 1987 to carry out the emulsion target construction, the beam exposure and the target mover operation etc. with an international team of collaborators on this experiment.

The author also produced and assembled very accurate motor-driven microscope stages

with their interface DOMS. There were both installed into the on-line system to improve the measuring performance.

The 124 D^0 semi-muonic decays were selected as the most reliable genuine $D^0 \rightarrow K^-\mu^+\nu_\mu$ events after the rigorous selection from 1084 charm decays. The values were calculated for the transverse momentum of individual decay muons P_{T_μ} and the minimum invariant mass M_{min} of $K\mu\nu$ system. From these values, the distributions of P_{T_μ} and of M_{min} were obtained and compared with the theoretical Monte Carlo simulation. Using maximum-likelihood method, the relative branching fraction f for $D^0 \rightarrow K^-\mu^+\nu_\mu$ was evaluated as:

$$f = 0.32 \pm 0.05(statistic) \pm 0.05(systematic)$$

As the value of "f" critically depends on the accurate measurement of the decay vertex. This analysis is therefore a unique feature of our experiment.

By combining this f value with the branching fraction and lifetime from other experiments, the partial width of the $D^0 \rightarrow K^-\mu^+\nu_\mu$ was found to be

$$\Gamma\left(D^0 \rightarrow K^-\mu^+\nu_\mu\right) = (5.6 \pm 0.9 \pm 1.2) \times 10^{10} sec^{-1}.$$

To our knowledge this is the first measurement of the partial decay width.

Assuming that there are only three generations for quarks and leptons, the form factor can be estimated with the above decay width to be

$$|f_+(0)| = 0.62 \pm 0.05 \pm 0.07.$$

On the other hand, if one assumes the form factor value of $|f_+(0)| = 0.7 \pm 0.1$, one finds the C-K-M matrix element experimentally V_{cs} to be

$$|V_{cs}| = 0.86 \pm 0.14 \pm 0.16.$$

To summarize, the central result of this dissertation is the first measurement of the partial decay width of the semi-muonic decay $D^0 \rightarrow K^-\mu^+\nu_\mu$. Even if semi-electronic decay data from other experiments are considered, assuming the electron-muon universality, there are only a few reports of measurements of the partial width. Thus more experimental data are greatly needed.

ACKNOWLEDGEMENTS

I sincerely appreciate my adviser Professor Mitsuko Kazuno, in particular, for her continuous encouragement and various discussion for this analysis and many support during the study of the high energy physics. I would like to thank Dr. Hiroshi Shibuya who was also an irreplaceable adviser and always provide precious advice for me when I got stuck on some problems of this analysis and other physics problems. Without their help, my thesis could not have been completed.

Many thanks to all of the members of fundamental particle laboratory at Toho university for their support and kindness. I especially express my thanks to graduate students, Etsuko Niu and Mayuko Adachi who have been engaged in the emulsion scanning with me, and offered me countless enjoyable discussions, Yasushi Umezawa, Masaru Tairadate, and Takahiro Jinya who have given me many helps in our graduated course.

I would like to thank Drs. Shigeki Aoki, Kouichi Kodama, and Ario Ito who gave me various helps and advice for my research work. My thanks are due to Dr. Søren G. Frederiksen with whom useful and stimulating discussion were exchanged.

I received a lots of kindness from many collaborators, from emulsion group and from counter group, who are greatly acknowledged for their guidance during the beam exposure to the emulsion target at the Fermi National Accelerator Laboratory, U. S. A. I wish to especially thank Profs. Neville W. Reay, Noel R. Stanton, Philip M. Yager, Shuichi Kuramata and Dr. Hiroyasu Tajima for their help in various stages of my graduate research.

It is impossible to mention all the kindness of many, many people. I would like to acknowledge the implicit and the explicit contributions of all the members of the

E653 collaboration.

Last, but certainly not least, thanks to my family and relatives for allowing me to study the physics with their support.

Shoji Watanabe

December 20, 1991

Contents

ACKNOWLEDGEMENTS ii

LIST OF FIGURES vii

LIST OF TABLES ix

1 INTRODUCTION 1
- 1.1 The Status of Weak Decay in High Energy Physics 1
- 1.2 Progress of Charm Physics with Emulsion Target 2

2 THEORY OF WEAK DECAY 5
- 2.1 Introduction 5
- 2.2 Quarks and Leptons 6
- 2.3 Weak Interaction 7
- 2.4 Cabibbo-Kobayashi-Maskawa Matrix 8
- 2.5 Spectator Quark Model 10
- 2.6 Kinematics of $P \to X\ell\nu$ 11
- 2.7 Form Factor 12
- 2.8 Model Calculations for Partial Width 13
  - 2.8.1 Quark model 13
  - 2.8.2 Lattice QCD calculations 14
  - 2.8.3 QCD sum rules 14

3 DESCRIPTION OF THE E653 EXPERIMENT 16
- 3.1 Experimental Apparatus 16
  - 3.1.1 Purpose of Fermilab E653 experiment 16
  - 3.1.2 800 GeV/c proton beam 21
  - 3.1.3 Emulsion target 21
  - 3.1.4 Target mover control 26
  - 3.1.5 Beam exposure 26
- 3.2 Counter System 28
  - 3.2.1 Vertex detectors 28
  - 3.2.2 Liquid argon calorimeter (LAC) 34
  - 3.2.3 Hadron calorimeter (HADCAL) 34

3.4 Emulsion Analysis System 42
3.4.1 Mini plate method 42
3.4.2 Toho on-line measuring system 44
3.4.3 Production of improved motor driven microscope stage 48
3.4.4 Digitized on-line microscope system (DOMS) 52

4 METHODS OF EMULSION ANALYSIS 56
4.1 Outline of Nuclear Emulsion Analysis 56
4.1.1 Description of charm events 57
4.2 Flow Chart of Emulsion Scanning Procedures 60
4.3 Event Location 64
4.3.1 Graphic matching method 65
4.4 Decay Search 67
4.4.1 Follow down method 67
4.4.2 Scan back method 67
4.4.3 Heavy track check at decay vertex 68
4.4.4 Graphic scan method 69
4.4.5 Measurement of the bottom emulsion plate 72
4.4.6 Emulsion tape 73

5 SUMMARY OF DATA 77
5.1 Event Summary 77
5.1.1 Summary of emulsion scanning 77
5.1.2 Events sample for $\Gamma(D^0 \rightarrow K^-\mu^+\nu_\mu)$ analysis 80
5.2 List of Background in Decay Candidates 81
5.3 Estimation of Neutral Backgrounds 83
5.3.1 Electron pair 83
5.3.2 Strange particle decay 84
5.3.3 Inelastic interaction 84
5.3.4 Backgrounds from hadronic feedthrough 85

6 ANALYSIS OF CHARM DECAYS 86
6.1 Introduction 86
6.2 Analysis of Muon Transverse Momentum Distribution 87
6.2.1 Generation of charm particle 89
6.2.2 Semi-muonic decay of D meson 92
6.2.3 P_{T_μ} correction for experimental conditions 97
6.3 Analysis of Mass Distribution 99
6.3.1 Invariant mass 99
6.3.2 Momentum balance 100
6.3.3 Minimum mass distribution 102

7 EXPERIMENTAL RESULTS AND DISCUSSION 106
7.1 The Fraction f 106
7.1.1 Fitting for P_{T_μ} distribution 106
7.1.2 Maximum likelihood fit for M_{min} distribution 110
7.1.3 Multi-neutral decay mode 113
7.1.4 Effect of Systematic errors 114
7.2 Decay Width of $D^0 \rightarrow K^-\mu^+\nu_\mu$ 117
7.3 V_{cs} ; C-K-M Matrix Element 118
7.4 Form Factor 119
7.5 Semi-electronic Decay Mode 119

8 CONCLUSIONS 121
8.1 Beam Exposure and Target Mover Control 122
8.2 Constructions of Semi-automated Microscope Stage and its Interface . 122
8.2.1 Semi-automated stage 122
8.2.2 DOMS interface 122
8.3 Evaluation of Relative Branching Fraction of $D^0 \rightarrow K^-\mu^+\nu_\mu$ 123
8.3.1 P_{T_μ} distribution analysis 123
8.3.2 M_{min} distribution analysis 123
8.4 C-K-M Matrix Element and Form Factor 124
8.5 Future Prospects 124

SUMMARY OF EVENT SAMPLE 126

REFERENCES 131

List of Figures

3.1 Fermilab E653 experimental apparatus. 20
3.2 Vertical emulsion target module. 24
3.3 Horizontal emulsion target module. 25
3.4 Target mover. 27
3.5 The vertex SSD from the circuit line side(photograph). 30
3.6 Cross section of silicon strip detector (SSD). 30
3.7 Cell structure and wire configuration of the SDC. 32
3.8 Space resolution of nearly collinear tracks in the SDC. 33
3.9 Typical event in the LAC. 35
3.10 Geometry of the HADCAL pad pattern. 35
3.11 Structure of muon chamber. 37
3.12 Definition of Impact Parameter (I.P.). 43
3.13 Mini plate method. 45
3.14 Mini plate (photograph). 46
3.15 Toho on-line system. 47
3.16 Semi-automated analyzing system (photograph). 48
3.17 Plan view of improved motor drive stage. 50
3.18 Improved motor drive stage(photograph). 51
3.19 Crossed roller way. 51
3.20 Stage and DOMS system (photograph). 52
3.21 DOMS controller(photograph). 53
3.22 Block diagram for data acquisition of DOMS. 53

4.1 Configurations of charm events. 58
4.2 Method of event measurement. 61
4.2 Method of event measurement (continued). 62
4.3 Graphic matching method (photograph). 66
4.4 Decay search event by graphic scan system. 71
4.5 Box diagram of track selector. 74
4.6 Emulsion tape. 75
4.7 E653 2nd run target system with emulsion tape. 75

6.1 Theoretical energy spectra for semi-leptonic decays. 88
6.2 Differential solid angle in polar coordinates. 94
6.3 $P_{T\mu}$ distribution in various decay modes. 98

6.4 $P_{T\mu}$ distribution in various categories cut. 98
6.5 Total momentum vectors in the laboratory frame. 101
6.6 –1C fit in semi-muonic two-prong decay. 103
6.7 M_{min} distribution with perfect vertex resolution. 105
6.8 M_{min} distribution with 1 mrad vertex resolution. 105

7.1 Comparison of the experimental $P_{T\mu}$ distribution with Monte Carlo $P_{T\mu}$ distributions. 107
7.2 Experimental $P_{T\mu}$ distribution with fitted Monte Carlo $P_{T\mu}$ distributions. 109
7.3 Comparison of the experimental M_{min} distribution with fitted Monte Carlo M_{min} distributions. 111

List of Tables

2.1 Theoretical predictions for $D^0 \to K^- \mu^+ \nu_\mu$ 14

3.1 Fermilab E653 experiment collaborators. 17
3.2 The yields of charm for various beams. 18
3.3 Chemical composition of Fuji ET-7B nuclear emulsion 23
3.4 Emulsion target module material properties 23
3.5 Summary data of beam exposure 28
3.6 Wire parameter for the SDC. 33
3.7 Summary of spectrometer resolutions. 39
3.8 Categories of physical cuts on the triggered sample. 41

4.1 On-line programs for emulsion analysis. 63

5.1 Summary of location of events. 78
5.2 Summary of scanning in Toho Univ. 79
5.3 Result of blob check at decay vertex. 82

7.1 Detection efficiencies for various decay modes. 112
7.2 The fraction f for multi-neutral decay modes. 112
7.3 Measurements data of emulsion plate thickness. 115

CHAPTER 1

INTRODUCTION

1.1 The Status of Weak Decay in High Energy Physics

Weak decays of hadrons play an important role for our understanding of the interplay of weak and strong interactions. The semi-leptonic decays of heavy mesons are particularly interesting because the underlying interaction is simple and they provide clear information on the internal structure of hadron systems consisting of quarks of unequal mass. However, experimental data are not sufficient even for the semi-leptonic decays of D meson. In particular, there is almost no report on semi-muonic D decays[1]. About 60 % of all D meson decay modes have been observed and their branching fractions have been measured[1]. However the remaining 40 % are not yet understood.

The field of high energy physics is one of the most interesting and active areas of modern physics. Because it is related to the most fundamental matter and the forces with which the universe is made up.

Heavy quark physics is one of the latest frontier of high energy physics. In particular, charm physics is an interesting part of particle physics today because the study of charm particle give information on the search for top particle which

has not been yet discovered. Main emphasis in the investigation is now quantitative analysis of the weak interaction phenomena with high statistics of charm data.

We have tried to study weak decays of charmed mesons produced in 800 GeV/c proton-emulsion interactions using the "Emulsion-counter hybrid system", the experiment was run at Fermilab National Accelerator Laboratory (Fermilab). Since this experiment, Fermilab E653[2], is designed to tag muons from weak decay of bottom(beauty)/charm particles, we obtained a large number of semi-muonic charmed particle decays.

1.2 Progress of Charm Physics with Emulsion Target

In 1971, Niu *et al.*[3] observed X particles by nuclear emulsion chambers exposed to cosmic rays. Japanese-theoretician group [4] pointed out this particle as a charmed particle.

In 1980's, there was the epoch-making experiment Fermilab-E531 that was first determination of the lifetimes[5, 6, 7] of various types of charmed particles with high statistics in those days. E531, a fixed target experiment, consisted of emulsion target and counter hybrid system in order to get precise measurements of event vertex positions, the slope and the momentum for individual tracks.

In 1985, CERN WA75 experiment[8, 9, 10], a first direct observation was made for a pair of bottom particles and their decays in the emulsion-counter hybrid system which was the first experiment the author took part in as a researcher.

Learning from WA75 experiment, the same collaboration group designed a new experiment E653 to get higher statistics and more precise information for the heavy flavor quarks. Fermilab E653 thus introduced the techniques of the hybrid emulsion

spectrometer which has been performed in WA75.

In the field of charm physics, there are many interesting topics, such as the properties of weak decay, the production cross section, the production mechanism, the pair correlations and so forth.

In particular, the studies of exclusive semi-leptonic decays are very interesting. Because semi-leptonic decays are easier to interpret than the non-leptonic decays. Non-leptonic decays of charm particle have a rather implicated final state interactions or interferences. Thus many theoretical assumptions and many experimental inputs are needed when one tries to determine the properties of non-leptonic decays.

On the other hand, semi-leptonic decay is theoretically simple because the weak current is clearly understood by the electro-weak standard theory[11]. Hence the understanding of semi-leptonic decay provide some information to strong interaction physics.

However, the semi-leptonic decay modes always include missing neutrino(s), thus in practice, it is difficult to investigate them. It is a reason why very few experimental report exist on this subject until present.

In this dissertation, I present an investigation on the semi-muonic decays of neutral charm particle by means of "P_{T_μ} analysis" and "Minimum parent mass analysis". The evaluation is carried out for the relative branching fractions and the decay width Γ of semi-muonic charm decays $D^0 \to K^-\mu^+\nu_\mu$ which were produced in the first running period of E653 experiment. With the value of decay width, Cabibbo–Kobayashi–Maskawa matrix element $|V_{cs}|$ and form factor are estimated.

The decay mode $D^0 \to K^-\mu^+\nu_\mu$ [a] is the simplest in various semi-muonic charm decay modes, and it has only one Feynman diagram. It means that this decay

[a] Throughout the dissertation, the charge-conjugate states are implicitly included.

mode has no final interactions or interferences and there is no vector term in the theoretical calculations because $D^0 \to K^-\mu^+\nu_\mu$ is a decay mode in which a pseudoscalar particle decay into another pseudoscalar particle and leptons. Study for $D^0 \to K^-\mu^+\nu_\mu$ may hence be a good trial for giving information to the strong interaction and understanding the charm physics. The contents of this thesis are the topics which the particle physicist are striving to develop at present.

CHAPTER 2

THEORY OF WEAK DECAY

2.1 Introduction

Semi-leptonic decays of the mesons containing heavy quarks have been studied during the recent years. In these processes, the leptonic part of the amplitude can be easily separated, so their investigation is rather simple. Both the experimental and theoretical studies of these decays are of great importance since they allow to obtain the restriction on the corresponding Cabibbo-Kobayashi-Maskawa (C-K-M) matrix elements. Extracting the C-K-M matrix elements from the experiment of semi-leptonic decay rates necessarily involves theory since the rates depend on hadronic dynamics. The calculations for $D^0 \to K^-\mu^+\nu_\mu$, in particular, can be made reliably, and should be emphasized in the extraction of V_{cs}, it is clearly important to have an independent experimental check on the value deduced from other matrix elements by assuming theoretical constraints. On the contrary, the theory of non-leptonic decay is too complicated to be studied because there are too many diagrams to be checked when the theoretical and the experimental result do not agree. Therefore semi-leptonic decays are suitable for evaluating fundamental parameters of the weak interaction. In this chapter, a review is given for the theory and some models of semi-leptonic decay via weak interaction.

2.2 Quarks and Leptons

Nowadays, generally accepted concept is that most fundamental particles of the matter are quarks and leptons. Kobayashi and Maskawa predicted[12] that at least three generations of quarks and leptons are needed in order to incorporate the CP violation in the framework of the standard theory. On the other hand, from the experimental result, strong evidence that number of light neutrino type is only three[13, 14, 15, 16, 17] was obtained from the study of Z^0 's cross section in e^+e^- annihilation into hadronic final states. Of course this result is only valid for light neutrinos and it does not necessarily mean that this world consists of only three generations. Fermions of which existence have been established are:

$$\begin{pmatrix} \nu_e \\ e^- \end{pmatrix} \begin{pmatrix} \nu_\mu \\ \mu^- \end{pmatrix} \begin{pmatrix} \nu_\tau \\ \tau^- \end{pmatrix} \tag{2.1}$$

$$\begin{pmatrix} u \\ d \end{pmatrix} \begin{pmatrix} c \\ s \end{pmatrix} \begin{pmatrix} t? \\ b \end{pmatrix} = \begin{pmatrix} u_i \\ d_i \end{pmatrix} \quad (i = 1,2,3)\ , \tag{2.2}$$

where $u_i (i = 1,2,3)$ have charge of 2/3 in unit of e, and $d_i (i = 1,2,3)$ have charge of -1/3. Particles consisting of quarks, for example, are as follows:

$$\begin{aligned} p(proton) = uud, \quad n(neutron) = udd \\ \pi^+ = u\bar{d}, \quad \pi^0 = (u\bar{u} - d\bar{d})/\sqrt{2}, \quad \pi^- = \bar{u}d \\ K^+ = u\bar{s}, \quad K^0 = d\bar{s} \\ D^+ = c\bar{d}, \quad D^0 = c\bar{u}, \quad D_s^+ = c\bar{s} \end{aligned} \tag{2.3}$$

In the present viewpoint in which the fundamental particles are quarks and leptons, β decay of neutron is understood as $d \to u + e^- + \bar{\nu}_e$ while at the hadron level the reaction is described as $n \to p + e^- + \bar{\nu}_e$.

2.3 Weak Interaction

Weak interactions are phenomena which are induced by exchanging weak bosons between fundamental particles, i.e. quarks and leptons.

Hamiltonian of weak interactions mediated by the charged weak boson $W^\pm$ is given by

$$H_{weak} = \frac{g}{2\sqrt{2}}[(j_\mu + J_\mu)W^{+\mu} + (j_\mu^\dagger + J_\mu^\dagger)W^{-\mu}]\ , \tag{2.4}$$

where the lepton current j_μ is

$$j_\mu = \sum_i (\bar{\nu_{ei}}\gamma_\mu(1 - \gamma_5)e_i)\ , \tag{2.5}$$

and the quark current J_μ is

$$J_\mu = \sum_i (\bar{u_i^w}\gamma_\mu(1 - \gamma_5)d_i^w). \tag{2.6}$$

If the weak boson mass m_W is sufficiently heavier than the mass of decay particle, the effective Hamiltonian can be written as

$$H_{weak}^{eff} = \frac{G_F}{\sqrt{2}}(j_\mu + J_\mu)(j_\mu^\dagger + J_\mu^\dagger)\ , \tag{2.7}$$

where the coupling constant $G_F/\sqrt{2}$ is given by

$$\frac{G_F}{\sqrt{2}} = \left(\frac{g}{2\sqrt{2}}\right)^2 \frac{1}{m_W^2} = \frac{1}{\sqrt{2}} \times 1.16637(2) \times 10^{-5} \quad GeV^{-2}\ . \tag{2.8}$$

Weak interaction acts on three doublets of left handed quarks

$$\begin{pmatrix} u \\ d' \end{pmatrix} \begin{pmatrix} c \\ s' \end{pmatrix} \begin{pmatrix} t \\ b' \end{pmatrix} = \begin{pmatrix} u_i^w \\ d_i^w \end{pmatrix} \quad (i = 1,2,3)\ . \tag{2.9}$$

Quarks(u_i^w, d_i^w) (i=1,2,3) are eigenstates of weak interaction, and not eigenstate of mass. On the other hand, quarks in hadrons (u_i, d_i) are eigenstates of mass and are generally given by mixing state of (u_i^w, d_i^w):

$$u_i = \sum_k U^u_{ik} u^w_k \tag{2.10}$$

$$d_i = \sum_\ell U^d_{i\ell} d^w_\ell \ , \tag{2.11}$$

where U^u, U^d are unitary matrices.

2.4 Cabibbo-Kobayashi-Maskawa Matrix

The quark currents(2.6) is rewritten in mass eigenstate as follows:

$$J^\mu = (\bar{u}\bar{c}\bar{t})\frac{\gamma^\mu(1-\gamma^5)}{2} V \begin{pmatrix} d \\ s \\ b \end{pmatrix} \ , \tag{2.12}$$

where V is Cabibbo-Kobayashi-Maskawa matrix, which includes three real parameters and one complex phase factor. The complex phase factor causes CP violation. Here C-K-M matrix is defined by

$$V = U^{u\dagger} U^d. \tag{2.13}$$

The C-K-M matrix is, in the case of n families, described by a total of $(n-1)^2$ independent variables. The values of individual C-K-M matrix elements can in principle all be determined from weak decays of the relevant quarks and these measurements are the most important subject in the quark and lepton physics. Kobayashi and Maskawa originally chose[12] a parametrization involving the four angles, ϑ_1 , ϑ_2 , ϑ_3 , and δ:

$$V = \begin{bmatrix} c_1 & -s_1 c_3 & -s_1 s_3 \\ s_1 c_2 & c_1 c_2 c_3 - s_2 s_3 \exp^{i\delta} & c_1 c_2 s_3 + s_2 c_3 \exp^{i\delta} \\ s_1 s_2 & c_1 s_2 c_3 + c_2 s_3 \exp^{i\delta} & c_1 s_2 s_3 + c_2 c_3 \exp^{i\delta} \end{bmatrix} \ , \tag{2.14}$$

where $c_i = \cos\vartheta_i$ and $s_i = \sin\vartheta_i$ for i= 1,2,3. In the limit $\vartheta_2 = \vartheta_3 = 0$, this matrix reduces to the usual Cabibbo mixing with ϑ_1 identified with the Cabibbo angle[18].

There are several parametrizations of the C-K-M matrix. A popular parametrization which is adopted as a "standard" in the Review of Particle Properties is,

$$V = \begin{bmatrix} c_{12}c_{13} & s_{12}c_{13} & s_{13}\exp^{-i\delta_{13}} \\ -s_{12}c_{23} - c_{12}s_{23}s_{13}\exp^{i\delta_{13}} & c_{12}c_{23} - s_{12}s_{23}s_{13}\exp^{i\delta_{13}} & s_{23}c_{13} \\ s_{12}s_{23} - c_{12}c_{23}s_{13}\exp^{i\delta_{13}} & -c_{12}s_{23} - s_{12}c_{23}s_{23}\exp^{i\delta_{13}} & c_{23}c_{13} \end{bmatrix} \ , \tag{2.15}$$

which was proposed by Chau and Keung[19]. Here $c_{ij} = \cos\vartheta_{ij}$ and $s_{ij} = \sin\vartheta_{ij}$, with i and j being "generations".

Another parametrization of the C-K-M matrix, which is often used, is due to Wolfenstein[20]

$$\begin{bmatrix} 1-\frac{1}{2}\lambda^2 & \lambda & \lambda^3 A(\rho - i\eta) \\ -\lambda & 1-\frac{1}{2}\lambda^2 & \lambda^2 A \\ \lambda^3 A(1-\rho-i\eta) & -\lambda^2 A & 1 \end{bmatrix} . \tag{2.16}$$

The 4 independent parameters are λ , A, η and ρ . Roughly speaking, "λ" is known to be 0.22 from nuclear β decay and strange particle decay. "A" is known to be close to unity from B lifetime measurements. Information on "ρ" and "η" comes from CP violation in K decay, upper limits on V_{ub}/V_{cb} and $B^0 - \bar{B}^0$ mixing.

Fundamental parameters of the C-K-M matrix must be determined by experiments. Experimental situation of the C-K-M matrix values are as follows:

$$\begin{bmatrix} V_{ud} & V_{us} & V_{ub} \\ V_{cd} & V_{cs} & V_{cb} \\ V_{td} & V_{ts} & V_{tb} \end{bmatrix} \tag{2.17}$$

$$= \begin{pmatrix} 0.9747 \ to \ 0.9759 & 0.218 \ to \ 0.224 & 0.001 \ to \ 0.007 \\ 0.218 \ to \ 0.224 & 0.9734 \ to \ 0.9752 & 0.030 \ to \ 0.058 \\ 0.003 \ to \ 0.019 & 0.029 \ to \ 0.058 & 0.9983 \ to \ 0.9996 \end{pmatrix} \ , \tag{2.18}$$

assuming that there are only three quark generations. When there are more than three generations, the allowed ranges of the matrix elements connecting the first three generations are[1]

$$\begin{pmatrix} 0.9728 \ to \ 0.9757 & 0.218 \ to \ 0.224 & 0.001 \ to \ 0.007\cdots \\ 0.182 \ to \ 0.227 & 0.865 \ to \ 0.975 & 0.030 \ to \ 0.058\cdots \\ 0. \ to \ 0.13 & 0. \ to \ 0.45 & 0. \ to \ 0.9995\cdots \\ \vdots & \vdots & \vdots \end{pmatrix} . \tag{2.19}$$

2.5 Spectator Quark Model

The theoretical value of $\Gamma(P_Q \to X_q \ell\nu)$ is approximately estimated with the spectator quark model. The spectator quark model treats the semi-leptonic decay of heavy meson P_Q as the decay of heavy quark Q which is a point like free particle; i.e.

$$\Gamma(P_Q \to X_q \ell\nu) = \Gamma(Q \to q\ell\nu), \tag{2.20}$$

where X_q expresses meson X which contains light quark q. It gives the inclusive semi-leptonic D^0 decay rate

$$\Gamma(D^0 \to X^- \mu^+ \nu_\mu) = \Gamma_0 \cdot (\frac{m_c}{m_\mu})^5 [|V_{cs}|^2 \cdot I_0(\frac{m_s}{m_c}) + |V_{cd}|^2 \cdot I_0(\frac{m_d}{m_c})] , \tag{2.21}$$

where Γ_0 is muon decay width

$$\Gamma_0(\mu \to e\bar{\nu}_e\nu_\mu) = \frac{G_F^2}{192\pi^3} m_\mu^5 , \tag{2.22}$$

with phase space suppression factor

$$I_0(x) = 1 - 8x^2 + 8x^6 - x^8 - 24x^4 \ln x . \tag{2.23}$$

Now if a simplest assumption[21] that physical-hadron masses are assigned to the quark masses; i.e.

$$m_c = m_D, \quad m_s = m_K, \quad m_d = m_\pi, \tag{2.24}$$

is taken, the resulting inclusive semi-leptonic decay width is calculated as:

$$\Gamma(D^0 \to X^- \mu^+ \nu_\mu) = 4.8 \times 10^{11} \quad sec^{-1}. \tag{2.25}$$

However, spectator quark model is too simple and it can explain only the total rate of heavy meson decay. Fractions of various exclusive decay modes would not be calculated easily. Thus we need to treat and to calculate the form factor which reflect the effect of hadron structure.

2.6 Kinematics of $P \to X\ell\nu$

The normalization of the state $|p>$ is defined by,

$$< p'|\, p >= (2\pi)^3 \delta^3(\vec{p'} - \vec{p}), \tag{2.26}$$

and also Dirac spinor u of mass m is defined by,

$$\bar{u}u = 2m . \tag{2.27}$$

In this normalization, Lorentz invariant matrix element $\mathcal{M}$ of semi-leptonic decay $P_i(p_i) \to X_f(p_f)\, \ell(p_\ell)\, \nu(p_\nu)$ is described by:

$$\mathcal{M} = \sqrt{2E_i}\sqrt{2E_f}\sqrt{2E_\ell}\sqrt{2E_\nu} < X_f(p_f)\, \ell(p_\ell)\, \nu(p_\nu)\, |H_{weak}|P_i(p_i) > . \tag{2.28}$$

Using this matrix element $\mathcal{M}$, the partial decay width is given by

$$d\Gamma = \frac{(2\pi)^4}{2m_i} |\mathcal{M}\,|^2 d\Psi, \tag{2.29}$$

$$d\Psi = \delta^4(p_i - p_f - p_\ell - p_\nu) \frac{1}{(2\pi)^9} \frac{d^3p_f}{2E_f} \frac{d^3p_\ell}{2E_\ell} \frac{d^3p_\nu}{2E_\nu}. \tag{2.30}$$

The Lorentz invariant matrix element $\mathcal{M}$ is represented by

$$\mathcal{M} = h_\mu \ell^\mu , \tag{2.31}$$

where

$$\begin{aligned} \ell_\mu &= \sqrt{2E_\ell}\sqrt{2E_\nu} < \ell^+(p_\ell)\nu(p_\nu)|j_\mu|\, 0 > \\ &= \bar{u}_\nu(p_\nu)\gamma_\mu(1-\gamma_5)v_\ell(p_\ell), \end{aligned} \tag{2.32}$$

$$h_\mu = \sqrt{2E_i}\sqrt{2E_f} < X_f(p_f)|j_\mu^\dagger|P_i(p_i) > . \tag{2.33}$$

2.7 Form Factor

In $0^- \to 0^-\ell\nu$ decay where 0^- means $(spin)^{(parity)}$ of the particle, h_μ depends only on the two four-momenta $p_{i\mu}$ and $p_{f\mu}$. There are two conventional parametrizations: One is

$$h_\mu = f_+(q^2)(p_i + p_f)_\mu + f_-(q^2)(p_i - p_f)_\mu, \tag{2.34}$$

and the other is

$$h_\mu = f_1(q^2)\left\{(p_i + p_f)_\mu - \frac{m_i^2 - m_f^2}{q^2}q_\mu\right\} + f_0(q^2)\frac{m_i^2 - m_f^2}{q^2}q_\mu \,. \tag{2.35}$$

Where q^2 has the kinematically allowed range

$$0 < q^2 \leq q^2_{max} = (m_i - m_f)^2, \quad q \equiv p_i - p_f, \tag{2.36}$$

and

$$f_1(q^2) = f_+(q^2) \ , \tag{2.37}$$

$$f_0(q^2) = f_+(q^2) \ + \frac{q^2}{m_i^2 - m_f^2}f_-(q^2) \,. \tag{2.38}$$

$f_1(q^2)$ and $f_0(q^2)$ are called vector form factor and scalar form factor, respectively. In most of the theoretical calculation, the nearest pole dominance is assumed as follows:

$$f_+(q^2) = f_+(0)\frac{1}{1 - q^2/m_v^2} \ , \tag{2.39}$$

$$f_0(q^2) = f_0(0)\frac{1}{1 - q^2/m_s^2} \ , \tag{2.40}$$

i.e. $f_+(q^2)$ and $f_0(q^2)$ are expected to be dominated by vector meson and scalar meson, respectively. These two form factors $f_+(q^2)$, $f_0(q^2)$ are independent each other. For $0^- \to 0^-\ell\nu$ decay in which $m_\ell^2 = m_\nu^2 = 0$ is a good approximation,

$$\frac{d^2\Gamma}{dxdy} = |V_{fi}|^2\frac{G_F^2}{16\pi^3}m_i^5|f_+(m_i^2 y)|^2[2x(1 - \varepsilon^2 + y) - 4x^2 - y] \tag{2.41}$$

is obtained. Where x, y, and ε are:

$$x \equiv \frac{E_\ell}{m_i}, \quad y \equiv \frac{q^2}{m_i^2}, \quad \varepsilon \equiv \frac{m_f}{m_i} \,. \tag{2.42}$$

To date, there is no experimental results which disagrees with the calculation of meson-pole dominance model concerning $f_1(q^2)$. However, in order to get information on $f_0(q^2)$, the decay mode in which $m_\ell^2 \neq 0$ namely $0^- \to 0^-\tau\nu$ decay must be studied.

2.8 Model Calculations for Partial Width

2.8.1 Quark model

As the assumption of meson-pole dominance seems to be reasonable and confirmed by some experiments[22, 23], the partial decay width of the $D \to K\ell\nu$ can be written as:

$$\Gamma(D \to K\ell\nu) = |V_{cs}|^2|f_+(0)|^2 \cdot (1.54 \times 10^{11}) \quad sec^{-1} \ , \tag{2.43}$$

here $f_+(0)$ is the form factor relevant to $D_{\ell 3}$ decay.

However, the value of $f_+(0)$ is not simply calculated because it obviously includes a non-perturbative effect. Therefore one has to rely on phenomenological approaches. This form factor is calculated on the quark model using some form of the quark potentials. Namely, the overlap of the wave functions of the initial and final mesons are calculated by assuming the orbital part of the wave function to be the solution of a relativistic scalar harmonic oscillator potential[24], the Schrödinger wave function of the usual Coulomb plus linear potential[25] or of harmonic-oscillator potential[25] etc. These phenomenological model predictions[24, 25, 26, 27] are tabulated in Table 2.1.

Table 2.1: Theoretical predictions for $D^0 \to K^-\mu^+\nu_\mu$.

Model	$\Gamma(D^0 \to K\ell\nu)$ [$\times 10^{10}$ sec^{-1}][35]	form factor $f_+(0)$
Quark Model		
GS/AW[26]	7.1	0.69
BSW[24]	8.3	0.76
GISW[25]	8.4	0.76
KS[27]	10.	0.83
Lattice QCD		
LMS[29]	4.9 ± 0.7	0.58 ± 0.04
CMHS[30]	9.5 ± 4.0	0.74 ± 0.17
BKS[31]	14.0 ± 6.0	0.90 ± 0.22
QCD sum rule		
BBD[32]	6.4 ± 3.0	$0.6^{+0.15}_{-0.10}$
DP[33]	9.7 ± 1.3	0.75 ± 0.05
AOS[34]	11.0 ± 5.0	0.8 ± 0.2

2.8.2 Lattice QCD calculations

To deal with the non-perturbative effect, the lattice QCD theory defines a gauge theory on the lattice of space-time points by using the path integral. Following Wilson's formulation[28], one can write the lattice actions as $S = S_f + S_g(U)$, where S_f is the fermionic part and $S_g(U)$ is the gauge part. On the lattice one can, in principle, determine the form factor as a function of q^2. Therefore, assumptions such as pole dominance are not needed. The predictions of this lattice QCD calculations[29, 30, 31] are also summarized in Table 2.1.

2.8.3 QCD sum rules

QCD sum rules provide an independent approach for calculating hadronic matrix elements and form factors for the system of both light and heavy quarks. The formalism of QCD sum rules is fully relativistic and field theoretic by construction,

and where the basic QCD features, such as asymptotic freedom and non-perturbative spontaneous symmetry breaking, are incorporated in a natural way. The value of $f_+(0)$ is estimated in this framework using two- or three-point function sum rules. The predictions of QCD sum rules[32, 33, 34] are shown in Table 2.1. However this estimate depends on other thing and in addition it is well known that three-point function QCD sum rules suffer from a systematic uncertainty due to their complicated structure and lack of positively of the spectral function.

The predicted values for $\Gamma(D \to K\ell\nu)$[35] by the above models are spread widely as one can see in the Table 2.1. Therefore, to check these models the experimental study is strongly desired.

CHAPTER 3

DESCRIPTION OF THE E653 EXPERIMENT

3.1 Experimental Apparatus

3.1.1 Purpose of Fermilab E653 experiment

Fermilab E653, emulsion-counter hybrid experiment, is performed by the international collaboration of Japan, U. S. A. and Korea, the names of the participating collaborators are shown in Table 3.1. The main purpose of this experiment is a study of the properties of heavy flavor quarks; in particular charm and bottom quarks.

In general, heavy quarks or heavy flavor particles have short decay lifetime of about 10^{-13} sec. Therefore the experimental set up is required a rigorous and a high precision design to detect the decay vertex of heavy flavor particles.

For this purpose, it is necessary to satisfy the following conditions in the construction of the apparatus.

1) High yields of charm and bottom particles.

2) High spatial resolution detectors.

3) Good selection for less background.

Table 3.1: Fermilab E653 experiment collaborators.

K. Kodama,[1] N. Ushida,[1] A. Mokhtarani,[2],[a] V.S. Paolone,[2] J.T. Volk,[2],[a] J.O. Wilcox,[2]
P.M. Yager,[2] R.M. Edelstein,[3] A.P. Freyberger,[3] D.B. Gibaut,[3] R.J. Lipton,[3],[a] W.R. Nichols,[3]
D.M. Potter,[3] J.S. Russ,[3] Y. Zhang,[3] H.I. Jang,[4] J.Y. Kim,[4] I.T. Lim,[4] M.Y. Pac,[4]
B.R. Baller,[5] R.J. Stefanski,[5],[b] K. Nakazawa,[6] S. Tasaka,[6] Y.S. Choi,[7] K.H. Chung,[7]
D.C. Kim,[7] I.G. Park,[7] J.S. Song,[7] C.S. Yoon,[7] M. Chikawa,[8] T. Abe,[9] T. Fujii,[9] G. Fujioka,[9]
K. Fujiwara,[9] H. Fukushima,[9] T. Hara,[9] Y. Takahashi,[9] K. Taruma,[9] Y. Tsuzuki,[9]
C. Yokoyama,[9] S.D. Chang,[10] B.G. Cheon,[10] J.H. Cho,[10] J.S. Kang,[10] C.O. Kim,[10] K.Y. Kim,[10]
T.Y. Kim,[10] J.C. Lee,[10] S.B. Lee,[10] G.Y. Lim,[10] S.W. Nam,[10] T.S. Shin,[10] K.S. Sim,[10]
J.K. Woo,[10] Y. Isokane,[11] Y. Tsuneoka,[11] S. Aoki,[12] A. Gauthier,[12],[c] K. Hoshino,[12] H. Kitamura,[12]
M. Kobayashi,[12] M. Miyanishi,[12] K. Nakamura,[12] M. Nakamura,[12] Y. Nakamura,[12]
S. Nakanishi,[12] K. Niu,[12] K. Niwa,[12] H. Tajima,[12] J.M. Dunlea,[13],[d] S.G. Frederiksen,[13],[b]
S. Kuramata,[13],[c] B.G. Lundberg,[13],[a] G.A. Oleynik,[13],[a] N.W. Reay,[13] K. Reibel,[13]
R.A. Sidwell,[13] N.R. Stanton,[13] K. Moriyama,[14] H. Shibata,[14] T.S. Jaffery,[15],[a] G.R. Kalbfleisch,[15]
P.L. Skubic,[15] J.M. Snow,[15] S.E. Willis,[15],[f] W.Y. Yuan,[15] O. Kusumoto,[16],[g] T. Okusawa,[16]
M. Teranaka,[16] T. Tominaga,[16] T. Watanabe,[16] J. Yamato,[16] H. Okabe,[17] J. Yokota,[17]
M. Adachi,[18] M. Kazuno,[18] F. Minakawa,[18] E. Niu,[18] H.Shibuya,[18] S. Watanabe,[18]
O. Fukuda,[19] Y. Sato,[19] I. Tezuka,[19] S.Y. Bahk[20] and S.K. Kim[20]

(Fermilab E653 Collaboration)

[1] *Aichi University of Education, Kariya 448, JAPAN*
[2] *University of California at Davis, Davis, CA 95616, USA*
[3] *Carnegie-Mellon University, Pittsburgh, PA 15213, USA*
[4] *Chonnam National University, Kwangju 500-757, KOREA*
[5] *Fermi National Accelerator Laboratory, Batavia, IL 60510, USA*
[6] *Gifu University, Gifu 501-11, JAPAN*
[7] *Gyeongsang National University, Jinju 660-300, KOREA*
[8] *Kinki University, Higashi-Osaka 577, JAPAN*
[9] *Kobe University, Kobe 657, JAPAN*
[10] *Korea University, Seoul 136-701, KOREA*
[11] *Nagoya Institute of Technology, Nagoya 466, JAPAN*
[12] *Nagoya University, Nagoya 464, JAPAN*
[13] *The Ohio State University, Columbus, OH 43210, USA*
[14] *Okayama University, Okayama 700, JAPAN*
[15] *University of Oklahoma, Norman, OK 73019, USA*
[16] *Osaka City University, Osaka 558, JAPAN*
[17] *Science Education Institute of Osaka Prefecture, Osaka 558, JAPAN*
[18] *Toho University, Funabashi 274, JAPAN*
[19] *Utsunomiya University, Utsunomiya 350, JAPAN*
[20] *Wonkwang University, Iri 570-749, KOREA*

Table 3.2: The yields of charm for various beams.

Beam Type	Interaction Type	Available Beam	σ_{int}	Yields Ratio	Performance
Hadron	strong	800GeV proton	40 mb	1/1000	0.04 mb
Photon	electromagnetic	$< 300 >$GeV γ	0.1 mb	1/100	0.001 mb
Neutrino	weak	$< 100 >$GeV ν	10^{-9} mb	1/10	10^{-10} mb

4) Good and efficient scanning system.

To realize the above conditions we considered the following,

1) 800 GeV/c proton beam for high yield of interaction.

2) Emulsion target connected with fine counter system.

3) Effective on-line trigger and off-line selections of raw data.

4) Facility of semi- and fully-automated scanning system.

In this beam energy region, the cross section of bottom particle has been predicted about 10nb/nucleon[36]. It means that the relative yield ratio of bottom particles to a hadron interaction is roughly estimated as 10^{-6}.

The production cross section of charm particles depends on incident beam energy and the types of incident particle. One can use hadron, electron or photon beam in accelerator according to the purpose of the experiment. The estimation of charm yields for various beam types is shown in Table 3.2.

The cross section of charm production is about 1% of the total cross section in photoproduction and is only about 0.1% in hadroproduction.

Since the luminosity of hadron beam is higher than those of neutrino or other exotic beams, hadron beam is more efficient in producing interactions, thus more high yield of charm mesons is expected within a limited time and a limited production materials.

However events produced by 800 GeV/c proton beam, in general, has a high multiplicity of charged tracks which are highly collimated in the forward direction. Therefore the high spatial resolution of individual tracks are of vital importance. Also time resolution of individual events is necessary for the fixed emulsion target.

The only property of charm which is distinctive enough to allow such a small signal to be seen clearly is the separated charm decay vertex. Furthermore most of bottom particles decay into charm particles which successively decay within 10^{-13} sec. And in good portion, both particles decay into semileptonically with muons. Thus the clear separation of each decay vertex is essential.

To solve those difficulties, a number of new inventions were made on the apparatus for this experiment such as a vertical exposure of emulsion target, a use of very fine strip silicon detectors, time resolution emulsion tape and the vector drift chamber.

All of new emulsion techniques were developed by our Japanese emulsion group and these are the vertical emulsion technique, target mover, emulsion tape method, mini plate method, semi- and fully-automated emulsion scanning system, changeable sheet et cetera.

The experimental set up of E653 is shown in Figure 3.1. It triggers muons of high transverse momentum with respect to beam direction since the transverse momentum of decay muon from bottom or charm particle is higher than that of pion

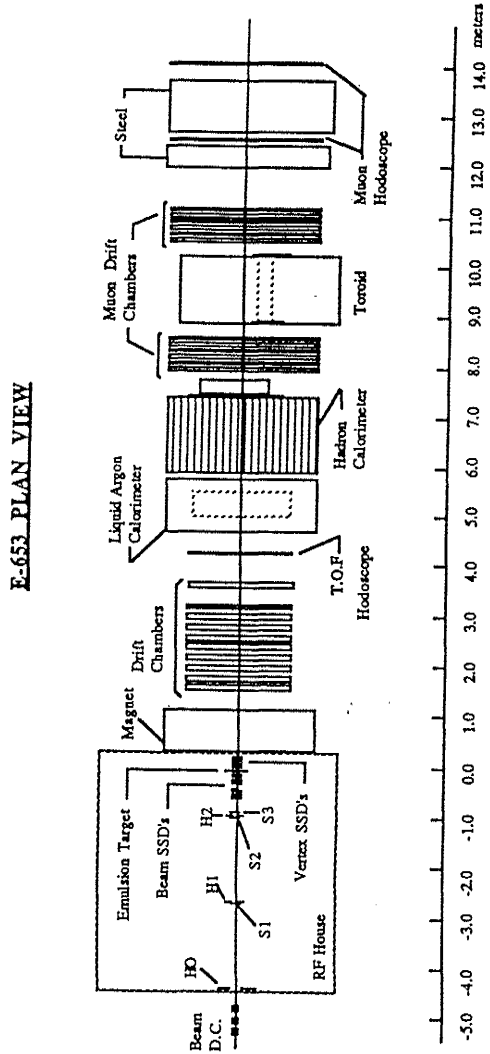

Figure 3.1: Fermilab E653 experimental apparatus.

and kaon. The total number of 800 GeV/c proton-emulsion interactions produced in this experiment is about 1×10^8 interactions.

The information of all charged tracks produced in the interactions were recorded in magnetic tapes (MTs), then they were dumped into optical disks for easy handling.

The functions and specifications of each system are described in the following[2, 37, 38, 39].

3.1.2 800 GeV/c proton beam

Although the yield of charm particles per interaction by neutrino is higher than that by hadrons, the production of neutrino beam is very restricted. Because neutrino interact only via weak interaction. Thus E653 experiment, 800 GeV/c proton beam was chosen at the first run in 1985 with the above consideration as contrast to our previous neutrino experiment E531[5, 6, 7]. The Experimental apparatus was situated Lab D in the Neutrino Area-East beamline of Fermilab.

The beam is ejected out from the main accelerator ring about 2 km apart from the experimental site, then it is guided to the site with cooled vacuum pipes collimated by a series of magnets. The size of beam, the horizontal spread is 2mm full width at half maximum (FWHM) while the vertical spread is 2.5mm FWHM. The beam was run at 2×10^5 protons per pulse and one pulse time is 57 sec with 10 sec spill.

3.1.3 Emulsion target

The lifetime of charm and bottom particles are roughly between 0.1 and 1.0 picoseconds. Thus the best target and detector for this purpose is nuclear emulsion that enables the direct observation of such short lived particles.

Nuclear emulsion target acts as the producer and the detector of charm particles

since it has the most fine space resolution among the particle detectors. This resolution is about 1 μm in three dimensions because the size of silver grain of nuclear emulsion after the processing is about 0.7 μm .

Table 3.3 shows the chemical compositions of Fuji ET-7B nuclear emulsion. Table 3.4 depicts the material properties of the emulsion target. The target consisted of modules. There are two types of emulsion module, one is a vertical type and the other is a horizontal type. The vertical type module is exposed to the beam perpendicular to the emulsion plane as shown in Figure 3.2 while the horizontal one is to parallel to the emulsion plane and are shown in Figure 3.3.

We exposed 49 modules containing a total of 33 ℓ emulsion for the first run and 53 modules amounted 38 ℓ emulsion in the second run.

We Toho-Kiso laboratory is using the vertical type module which has an advantage on the individual track discrimination of congested secondary particles of events. The each module consisted of 25 emulsion plates and honeycomb spacer as shown in Figure 3.2. The size of each emulsion plate is 250mm × 250mm × 0.73mm. The thickness of 330 μm emulsion was coated in both sides of 70μm polystyrene base.

Figure 3.2 illustrates the structure of the emulsion target module. Then each module was wrapped with laminated sheet, of four layers consists of polyethylene, paper, polyisobutylene and aluminum, while evacuating air. This way the emulsion plates are protected from humidity and from light exposure.

To minimize cosmic ray background, the emulsion modules were produced and assembled on the site of Fermilab just before the beam exposure.

Table 3.3: Chemical composition of Fuji ET-7B nuclear emulsion

Element (i)	*Weight %* (W_i)	*Atomic weight* (A_i)	*Atomic number* (Z_i)	*Number %* (N_i[a])
I	.3	126.90	53	.1
Ag	45.4	107.87	47	11.7
Br	33.4	79.90	35	11.1
S	.2	32.06	16	.2
O	6.8	16.00	8	11.3
N	3.1	14.01	7	5.9
C	9.3	12.01	6	20.6
H	1.5	1.01	1	39.6
Totals	100.0	$< A >$=26.64[b]	$< Z >$=12.42[c]	100.0

weight power x	2/3	.77	.8	1.0
$\Sigma_i\ N_i\ \times\ A_i^x$	7.18	10.62	11.94	26.64
$< A >_{eff} = \Sigma_i\ (N_i\ \times\ A_i^x)^{1/x}$	19.24	21.52	22.19	26.64

[a] *from* $N_i = < A > \times W_i/A_i$

[b] $< A >= 100\ \%/(\Sigma_i(W_i/A_i))$

[c] $< Z >= < A > \times \Sigma_i(W_i/A_i) \times Z_i$

Table 3.4: Emulsion target module material properties

Material	*Interaction length for protons (mm)*	*Radiation length (mm)*	*Density* g/cm^3
Fuji ET − 7B nuclear emulsion	359	29.5	3.73
Polystyrene	795	424	1.032
Lucite	697	338	1.20
Horizontal polystyrene spacer	10340	5523	.0793
Vertical honey − combed spacer	7962	3862	.105
Glassine paper	929	451	.9

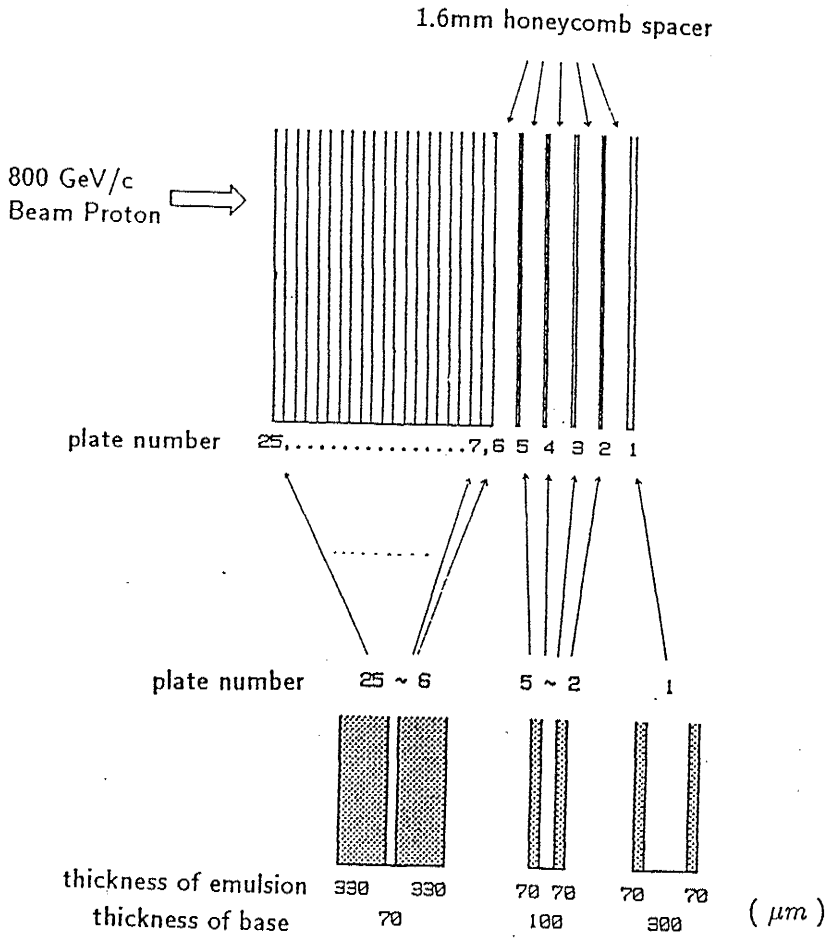

Figure 3.2: Vertical emulsion target module.

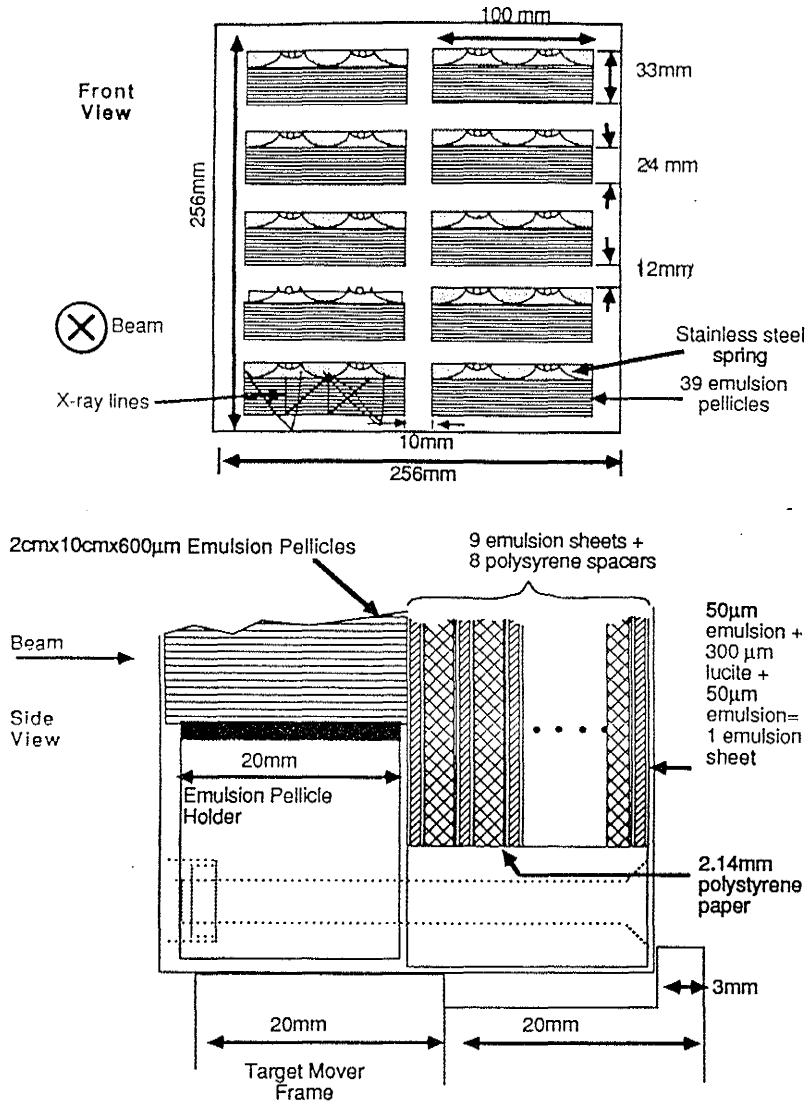

Figure 3.3: Horizontal emulsion target module.

3.1.4 Target mover control

It is very important to achieve a technique of uniform beam exposure over the emulsion modules of 250mm × 250mm within the restricted beam spill time. To realize this requirement, we have developed a target mover which controls beam expose density over the emulsion module uniformly. The target mover, as shown in Figure 3.4, holds each module in the center of beam line position and drive all directions in two dimensions so that the module is exposed to the beam from an edge to the other edge. When the beam come to one of the edge, the mover is so controlled to move upward of the module so that a new line of the emulsion module is irradiated to the beam. To secure an uniform and a specified intensity of the beam irradiation, the mover was driven in such a way that the speed of the mover coincides to the real-time beam rate obtained from an upstream scintillation counter as seen in Figure 3.1.

The target mover was driven by DC motor, and controlled by a programmed computer. The position resolution is about $10\mu m$ and read position resolution is $2.5\mu m$ unit.

3.1.5 Beam exposure

The available highest beam energy in the world was 800 GeV/c proton beam at Fermilab in 1985. Beam intensity was 10^5 particles/ cm^2. The period of beam exposure for E653 was about 3 months. The author have been to U. S. A. for 3 months to taking part of the beam exposure, the target mover control, the emulsion tape control and the emulsion target processing. The emulsion tape, will be described in Chapter 4. Table 3.5 shows the summary of event production at the beam exposure.

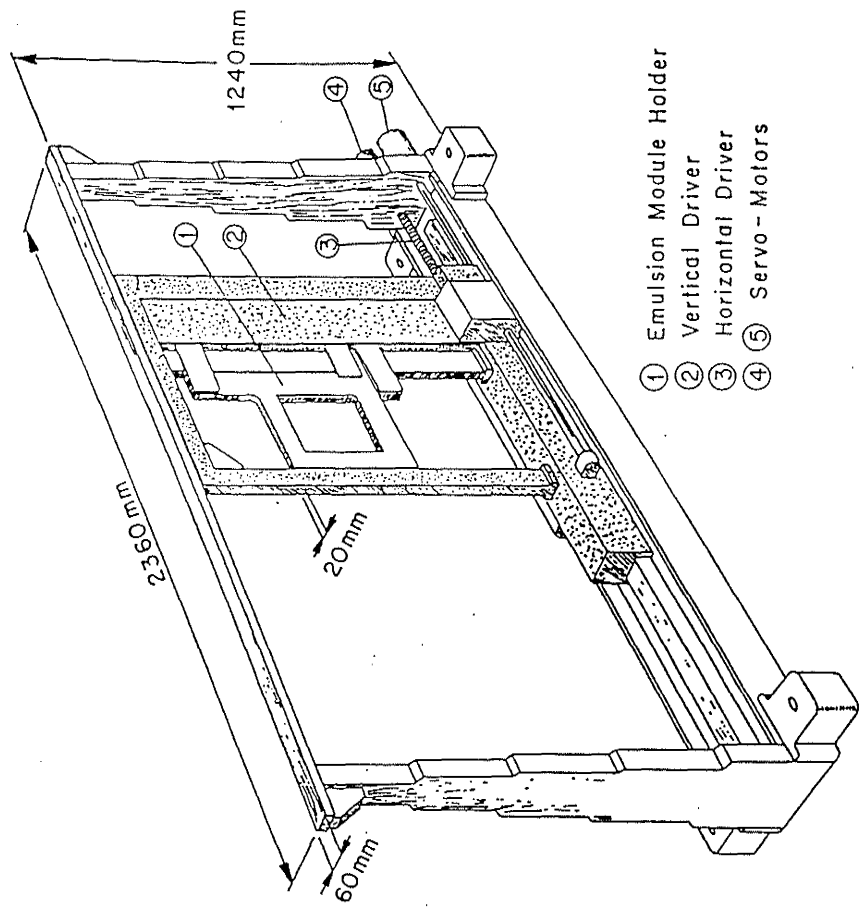

Figure 3.4: Target mover.

Table 3.5: Summary data of beam exposure

	1st Run		2nd Run	
Type	V-MOD	H-MOD	V-MOD	H-MOD
Term	1985 May~Aug.		1987 Aug.~Oct.	
Beam	800 GeV/c Proton		600 GeV/c π^-	
Nuclear Emulsion [module]	24	25	31	22
	33 ℓ		38 ℓ	
Beam Density [particles/cm^2]	1.5×10^5	0.8×10^5	3.0×10^5	1.0×10^5
Trigger Events	4×10^6	1.4×10^6	8.5×10^6	1.1×10^6
Sub Total	5.4×10^6		9.6×10^6	
Total	1.5×10^7 triggers			
Total Interaction in Emultion	trigger rate 1/20 1×10^8		trigger rate 1/30 3×10^8	

V-MOD : Vertical Module.
H-MOD : Horizontal Module.

In the second run, 600 GeV/c negative pion was chose since the quark constituent of proton is uud while that of negative pion is $\bar{u}d$, the latter is more favorable to produce charm particles according to the theoretical prediction10nb.

3.2 Counter System

The counter system of E653 consisted of emulsion target, vertex detectors, TOF, calorimeter, magnet and was described in detail elsewhere[2]. A brief description for the system is given in the following.

3.2.1 Vertex detectors

3.2.1.1 Silicon strip detector

To predict the vertex position of primary interaction and its beam position, we used silicon microstrip detector (SSD) consisted of a silicon wafer with strips of 20

μm pitch. The beam position is measured by 9 layers of SSD in which the resolution of space is achieved about 17 μm [37] at the central region. The structure of the SSD is shown in Figure 3.5, and the cross section of it is shown in Figure 3.6.

Each set of Vertex SSD (VSSD) was composed of 3 layers which are placed one layer in the vertical plane with respect to beam direction; and named it as X plane (0 degree), and the other layers placed in the positions rotating 60 degree and 120 degree relative to the first layer and named U and V planes respectively. We installed 6 sets of them, altogether 18 SSD layers.

In the second run, an improvement was made for the upstream SSD resolution. A fine prediction of vertex reconstruction can not be achieved by increasing number of SSD layers used, but must be done with the pitch of the strips. For E653 experiment, Hamamatsu Photonics Co. manufactured a fine pitch SSD for the second run. The pitch of the silicon strip is 12.5 μm . The VSSDs' system consisted of (12.5 μm pitch, 3cm $\times$ 3cm)$\times$ 3 layers, (50 μm pitch, 5cm $\times$ 5cm) $\times$ 12 layers, (50 μm pitch,10cm$\times$ 10cm)$\times$ 3 layers, then the vertex prediction resolution was improved.

The reconstruction of secondary tracks were done by computer programs from the pulse signals of SSDs in three dimensions. Thus the primary interaction vertex was able to be reconstructed and predicted its position in the emulsion target within 350 μm [37] of the beam direction and 8 μm of the transverse to the beam direction.

This helps to provide a confined scanning volume for decay search on charm and bottom particles, and thus shorten a time for event location and measurements.

3.2.1.2 Spectrometer drift chamber (SDC)

The produced secondary particles in the interactions are spread out into the space along the downstream of the apparatus. Thus the detectors must cover a large area

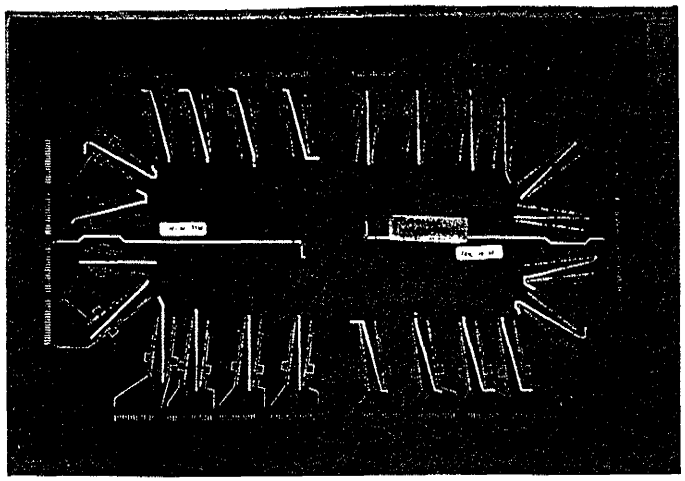

Figure 3.5: The vertex SSD from the circuit line side(photograph).

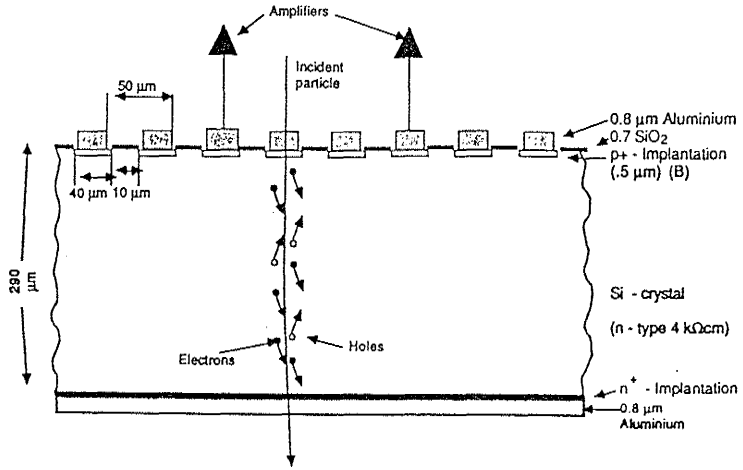

Figure 3.6: Cross section of silicon strip detector(SSD).

in the downstream. For this purpose, a set of spectrometer drift chambers (SDCs) were installed behind VSSDs and Magnet as shown in Figure 3.1. The Chambers had five sense wires along the beam direction. Figure 3.7 shows cell structure and wire configuration of SDC. These are consisted of the cathode wires(C), the field shaping wires(S', S", and F), and the sense wires. Table 3.6 shows the wire parameter for SDC.

The active area of the SDC is 1.7m × 1.7 m and arranged 3 planes in a set and one in X ; the vertical position with respect to the beam direction and the others in U and V ; the positions of 30 degrees rotating to both sides of X.

We detected all charged particles and measured their momenta at the SDC within an angle of 240 mrad. Multi-sampling chambers allowed left-right ambiguities to be resolved using track slope information. Figure 3.8 illustrates resolution of nearly collinear tracks in the SDC.

The spectrometer magnet (SCM104) was used to determine the momentum of the charged particles. It was placed close to the emulsion target and nearly 40 cm in depth and it operated at a typical current of 2400 amperes with a mean integrated magnetic field of ;

$$< \int Bdl >= 11.2 \cdot K\ Gauss\ meter \tag{3.1}$$

corresponding to a effective transverse momentum kick; P_T = 336 MeV/c was applied to the charged particles. Momentum resolution is

$$\frac{\delta P}{P} = \sqrt{(0.01)^2 + (0.00023P)^2} \qquad (P\ in\ GeV/c). \tag{3.2}$$

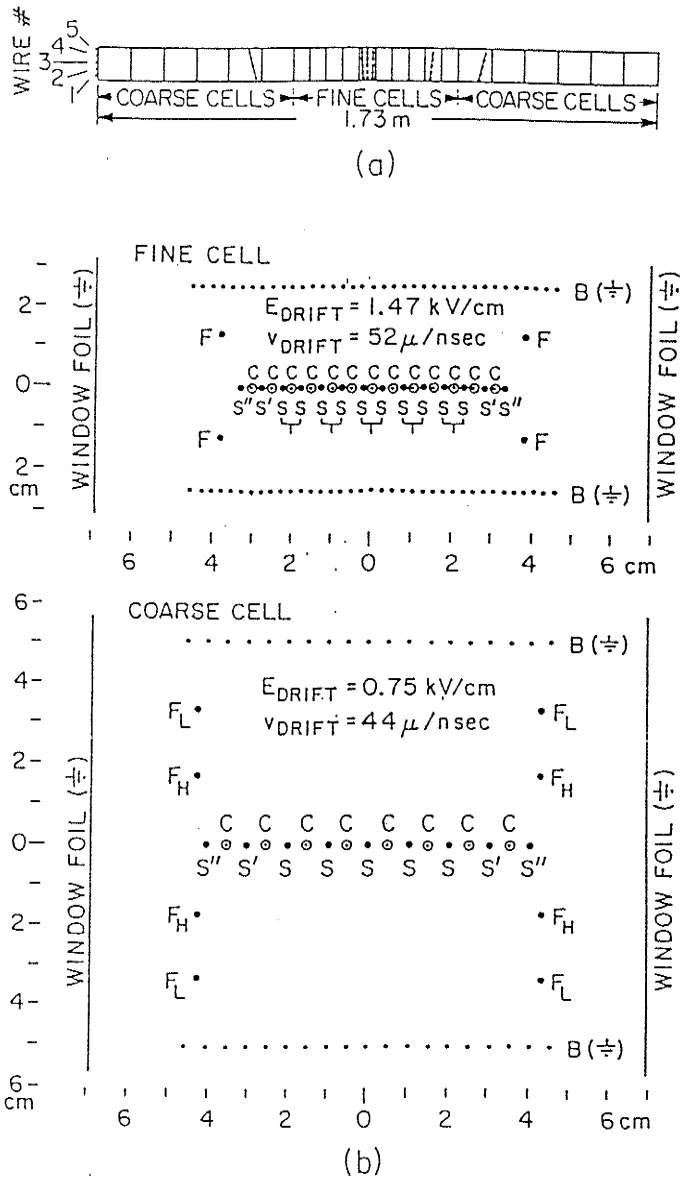

Figure 3.7: Cell structure and wire configuration of the SDC.

Table 3.6: Wire parameter for the SDC.

Wire type	Material (Au plated)	Diameter (microns)	Tension (grams)	Potential (volts)
Fine S	W	30	105	5375
Fine S′	Al	250	350	4670
Fine S″	Al	250	350	5375
Fine C	Al	250	350	3495
Fine F	Al	160	130	3145
Fine B	Al	160	130	0
Coarse S	W	30	80	5780
Coarse S′	Al	250	350	5070
Coarse S″	Al	250	350	5780
Coarse C	Al	250	350	3610
Coarse F_L	Al	160	130	1790
Coarse F_H	Al	160	130	4050
Coarse B	Al	160	130	0

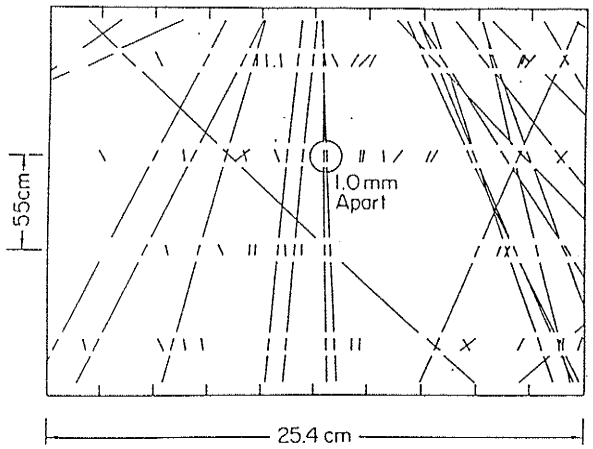

Figure 3.8: Space resolution of nearly collinear tracks in the SDC.

3.2.2 Liquid argon calorimeter (LAC)

Neutral particles are not detected directly in the target emulsion or SDCs. Thus the Liquid Argon Calorimeter (LAC) is designed to detect the neutral particles such as neutral pions by producing electromagnetic cascades. Figure 3.9 shows a typical event in the LAC.

The spatial position and the energy of electron and photon were measured in the LAC which consisted of lead-liquid-argon segmented in pads. The readout of the central pad is 2.03 cm × 2.03 cm while that of outer pads is about 16cm × 16cm. By introducing these pad-segments, it allows to determine the energy and the position of neutral particles. The resolution of energy measurement is :

$$\frac{12\%}{\sqrt{E}} + 2.5\% \tag{3.3}$$

and the position resolution is $\sim$ 1mm.

3.2.3 Hadron calorimeter (HADCAL)

This system is located downstream of LAC to measure the total energy and position of produced hadronic particles. The hadron calorimeter consisted of 16 planes of proportional counter with pad readouts covered an area of 2.34 m × 2.34 m. Figure 3.10 shows the pad pattern of the HADCAL. The steel plates were 244 cm high by 305 cm wide by 5 cm thickness. The energy resolution is

$$\sim \frac{100\%}{\sqrt{E}} \tag{3.4}$$

and the position resolution is $\sim$ 0.25 cm.

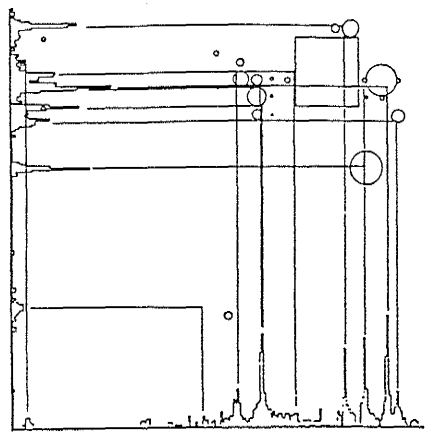

Figure 3.9: Typical event in the LAC.

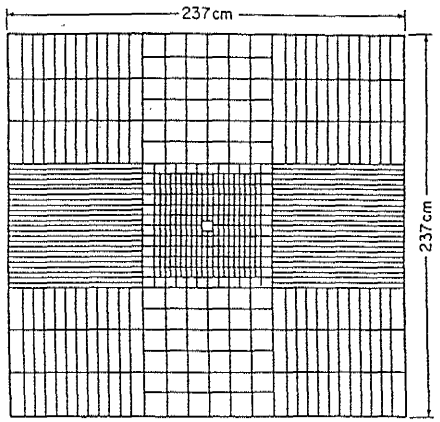

Figure 3.10: Geometry of the HADCAL pad pattern.

3.2.4 Muon system

The muon system is most important one not only to measure the particle positions but to determine whether the triggered event is useful for the analysis or not. As seen in Figure 3.1 the system was installed at the downstream of HADCAL to measure the momentum and the slope of muon tracks. Figure 3.11 shows the structure of the muon chamber. It consisted of 30cm steel block, drift chamber (DC) × 6 layers, troidal magnet (1.33m in thickness and the field of 1.7 to 2.2 T) and transverse momentum (P_T) kick is ∼ .76 GeV/c and DC×6 layers. The momentum resolution of this system is

$$\frac{\delta P}{P} = \sqrt{(.19)^2 + (.007P)^2} \qquad (P \; in \; GeV/c) \tag{3.5}$$

for triggered muon.

Twelve 3m × 3m DC were oriented in such directions: that one was aligned vertically with respect to the beam direction (Z), and the other two u and v are oriented in 12 degrees rotation in both side of Z direction.

Muon trigger required at least one hit from each sintillatior wall. This muon is required to have coincidence with upstream scintillatior. Muon is bent at troidal magnet to measure the momentum. Therefore the segments of muon tracks before the magnet and after the magnet must be matched as calculated.

The momentum was determined by the angular deflection $\delta\theta$ of muon track at the magnet;

$$p = 0.03 \times B(r) \times \frac{\delta Z}{\delta \theta}, \tag{3.6}$$

where $B(r)$ is the fit field as a function of the troidal radius r in kilogauss, δZ is the troidal thickness (1.3 m).

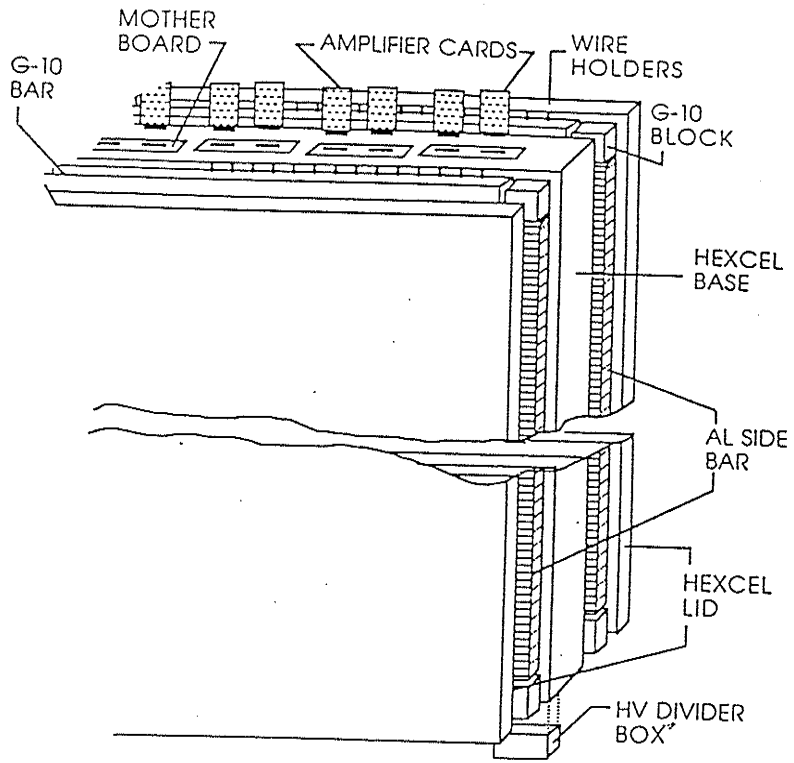

Figure 3.11: Structure of muon chamber.

Table 3.7 shows the resolution of these counters.

3.3 Data Acquisition (DAQ) in E653

This section describes how to concentrate and extract the events which accompany charm and bottom particle decays as to facilitate for efficient emulsion scanning.

3.3.1 On-line trigger

The beam is ejected once a minute and produces about 300 interactions[2]. The data of each event were written on the magnetic tape (MT) and uses 27 Kbytes per event on average. These data were such as emission angle, spatial position, charge, momentum of all charged secondary particles. On-line data acquisition (DAQ) system consisted of CAMAC (Computer Automated Measurement And Control, 1MHz, 16bit words), FASTBUS (high speed(fast) bus, 8MHz, 32bit words) and LSI11/73, VAX11/750 computer.

The main background of muons is the decayed muons from pions produced in the primary interaction. The number of produced pions in an event is about 20 at 800 GeV/c proton-emulsion interaction. In the set up of E653, pions produced at first interaction should almost be absorbed in the HADCAL and steel part, but some π mesons decay in flight. Trigger rate for the total interactions of E653 was about 1/20 at the first run and about 1/30 at the second run.

In this stage all events which accompany a muon were recorded on MTs and were numbered about 5×10^6 events.

To avoid background from wrong track matching, the on-line trigger selected a muon which had no change in its momentum between upstream end of the spectrometer magnet and downstream top of the troidal magnet. Tagged muon must

Table 3.7: Summary of spectrometer resolutions.

System	Quantity	Units	Resolution
Emulsion	Position Angular	μm mrad	1-10 1-10
Beam SSD Beam DC Combined	Position/plane Position/plane Position (z=0) Angular	μm μm μm μrad	17-35 150 10 20
Vertex SSD	Position/plane Position (z=0)[a] Angular[a]	μm μm μrad	8-24 10 70
Spectrometer DC	Position/plane Angular[a]	μm μrad	50-60 35
Primary vertex[b] Secondary vertex[c]	Position (z) Position (x,y) Position (z) Position(x,y)	μm μm μm μm	300-400 6-10 550-750 11-18
Electromagnetic Calorimeter	Position (x,y) Energy (δE/E)	mm %	1.2 $12/\sqrt{\mathrm{E}} + 2.5$
Charged particle spectrometer	Momentum $\delta p/p$	p in Gev/c	$\sqrt{(.01)^2 + (.00023p)^2}$
Muon spectrometer	Momentum $\delta p/p$	p in Gev/c	$\sqrt{(.19)^2 + (.007p)^2}$

[a] Does not include momentum dependent multiple scattering contribution.
[b] The resolution varies approximately as the square root of the charged particle multiplicity.
[c] Based on $\sqrt{10/3}$ × resolution of the primary. The average multiplicity of the primary is about 10, while the secondary is assumed to be a three prong decay.

have the momentum grater than 5 GeV/c. This selection reduces the number of recording events to a manageable rate, while enhanced the heavy flavor quark signal relative to the background events.

3.3.2 Off-line selection

The events recorded at on-line trigger into the MT were further reduced to a manageable number of selected events. To select useful events, various considerations are taken into account. Firstly, event vertices were reconstructed by using only good VSSD-fit-track and must be converged in the emulsion target. When the primary vertex is reconstructed outside of the emulsion bulk, the event is rejected. In this way we can examine each interaction vertex visually in emulsion.

To avoid muon background from pion decay and to enrich for charm and bottom particles, tagged muon was required to have the momentum greater than 8 GeV/c and the transverse momentum greater than 0.2 GeV/c. These requirements are generally satisfied if the muon originated from the decay of a heavy flavor particle. Table 3.8 shows the summary of off-line cuts. We also applied the criterion of the impact parameter, of the decay vertices relative to the primary vertex, should be greater than 50 μm . More detailed description will be given later.

To enhance the charm and bottom particles over background events, we selected events which satisfy the following 3 conditions based on MT data.

a) Event with possible secondary muonic vertex.

b) Event with transverse momentum of muon with respect to beam $P_{T\mu}$ is greater than a certain value (it varies according to the purpose of investigation).

c) Event with impact parameter of muon I. P.$_\mu$ greater than a certain value.

Table 3.8: Categories of physical cuts on the triggered sample.

	Category			
Cut variable	3	2	1	4
P_μ (GeV/c)	8.000	8.000	8.000	8.000
$P_{T\mu}$ (GeV/c)	0.200	0.800	0.250	0.000
Impact parameter of muon (μm)	50	100	100	0
P_{hadron}(GeV/c)	5.000	0.000	0.000	0.000
Impact parameter of hadron (μm)	0.050	0.000	0.000	Failed to fit 1ry
Decay length (mm)	2.000	0.000	0.000	Outside Emulsion
Invariant mass (GeV)	0.250	0.000	0.000	0.000

The above conditions mean the following.

a) Event with secondary muonic vertex:

If the triggered muon came from charm or bottom particles, then its origin is not from the primary vertex but from each decay point (secondary vertex, tertiary vertex). This cut was applied in category 3 sample, and not in other categories.

b) $P_{T\mu}$ cut

Transverse momentum of muon measured with respect to the beam direction is denoted as $P_{T\mu}^{(B)}$. In pion decay, the mass difference between parent π and daughter μ is very small and $P_{T\mu}^{(P)}$ (measured with respect to parent particle) is about 30MeV/c. On the other hand, ($P_{T\mu}^{(P)}$) of charm and bottom particles are several hundreds MeV/c or greater.

We assumed that $P_{T\mu}^{(P)}$ is reflected on $P_{T\mu}^{(B)}$ because secondary particles concentrated in very forward. Then we applied $P_{T\mu}^{(B)}$ cut on events, in particular, category 2 is aiming to select bottom particle.

c) I. P.$_\mu$ cut

The definition of Impact Parameter (I. P.$_\mu$) is illustrated in Figure 3.12. Charm or bottom particle produced in primary vertex decays into daughter muon with an angle with respect to parent θ_{p-d} after traversing length L. The I. P.$_\mu$ is defined as the shortest distance from the primary vertex to the line extrapolated from the direction of the muon emitted. The reason why we chose I. P.$_\mu$ as selection condition is that $P_{T_\mu}^{(P)}$ of pion decay is relatively very small with momentum of parent pion. Since the emission angle θ_{p-d} of $\pi \rightarrow \mu\nu$ decay (ϑ = zenith angle) is nearly equal to zero and its I. P.$_\mu$ is also negligible. On the other hand, $P_{T_\mu}^{(P)}$ in the decay of charm and bottom particles is high, thus the I. P.$_\mu$ is detectable. I. P.is related to ct by using geometrical mean of decay daughter angles of the decay particles; $< \tan\theta_i >$

$$\begin{aligned} < \text{I. P.} > &= < L \cdot \tan\theta_i > \\ &\approx L\gamma^{-1} \\ &= \gamma ct \gamma^{-1} \\ &= ct \ . \end{aligned} \tag{3.7}$$

t is the decay time of parent charm particle. Expected value of I. P.$_\mu$ of charm and bottom particles are an order of 100 μm .

3.4 Emulsion Analysis System

3.4.1 Mini plate method

When events are searched for charm and bottom particles, it is necessary to change emulsion plates so many times in following track toward the downstream if the scanning is done in the conventional method.

Vertical type emulsion module provides easy recognition of individual secondary particles but the disadvantage is the frequent change of emulsion plates. To over come this disadvantage, mini plate method was developed and applied first time into CERN WA75[8].

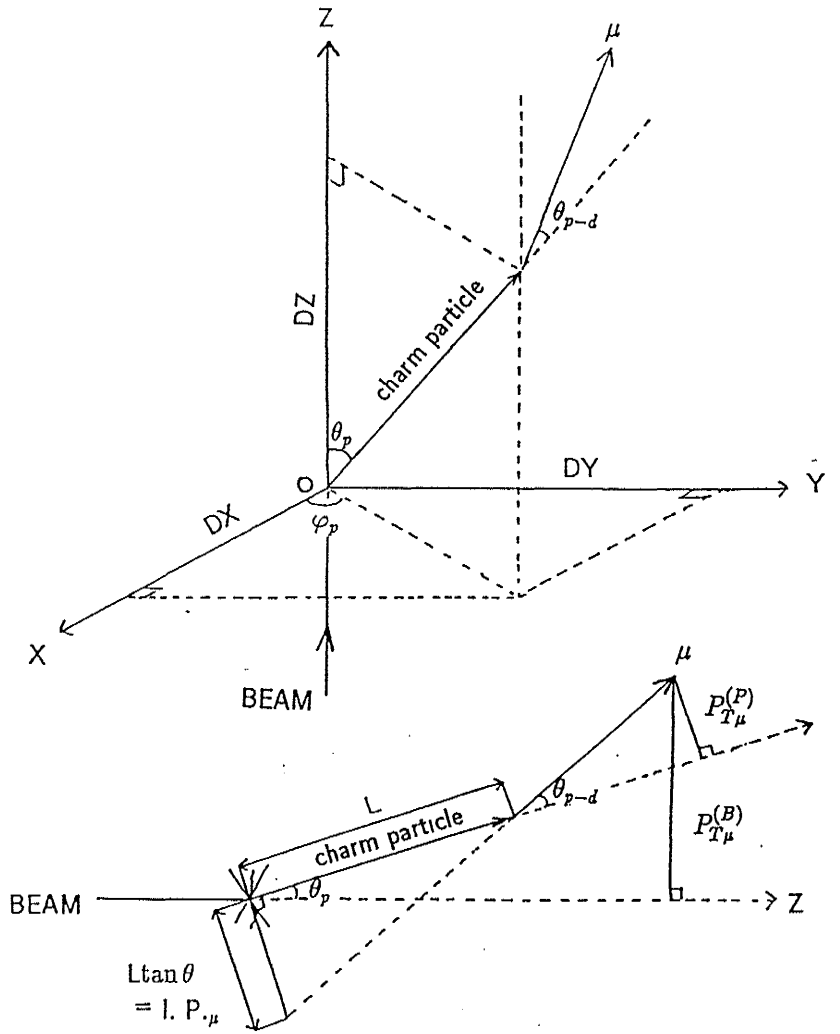

Figure 3.12: Definition of Impact Parameter (I.P.).

When the E653 emulsion target module was exposed to the beam, the each module consisted of 25 plates. The size of each plate was 250mm × 250mm. The mini plate is produced by cutting each emulsion plates into small pieces of 30mm × 30mm after processing them. As shown in Figures 3.13 and 3.14, one section of 24 sheets of mini plates are spread onto an acrylic plate and are fixed by the optically transparent special glue. The 24 mini size plates along the downstream are laid down next to each other so that no change of plate is necessary to move to next plate but just move to right or left from there. In this way the speed of the scanning is greatly improved. The last one plate was used as a interface between the emulsion target and the spectrometer.

Each mini plate after mounted on acrylic plate are calibrated for the absolute coordinates of the apparatus. Prior to the scanning or measurement of events in mini plates, the fiducial marks imprinted on 3 corners of each mini plate are measured for the correction of the stage setting of the mini plate.

Edge part of emulsion plate have much distortion, so 5 mm from the edge of all sides emulsion are discarded before cutting into mini plates. Thus emulsion plates of 24cm× 24cm were cut into 64 mini plates (3cm × 3cm).

3.4.2 Toho on-line measuring system

Figure 3.15 shows the on-line system of our laboratory. One station of Semi automated emulsion scanning and measuring system in our laboratory consisted of electromotive stage with microscope and DOMS (Digitized On-line Microscope System) interface, video camera and CRT monitor. 6 sets of such on-line stations are on work. With this system, the coordinates can be measured very accurately, and the microscope stage move to up to 500mm × 400mm as shown in Figure 3.16. The

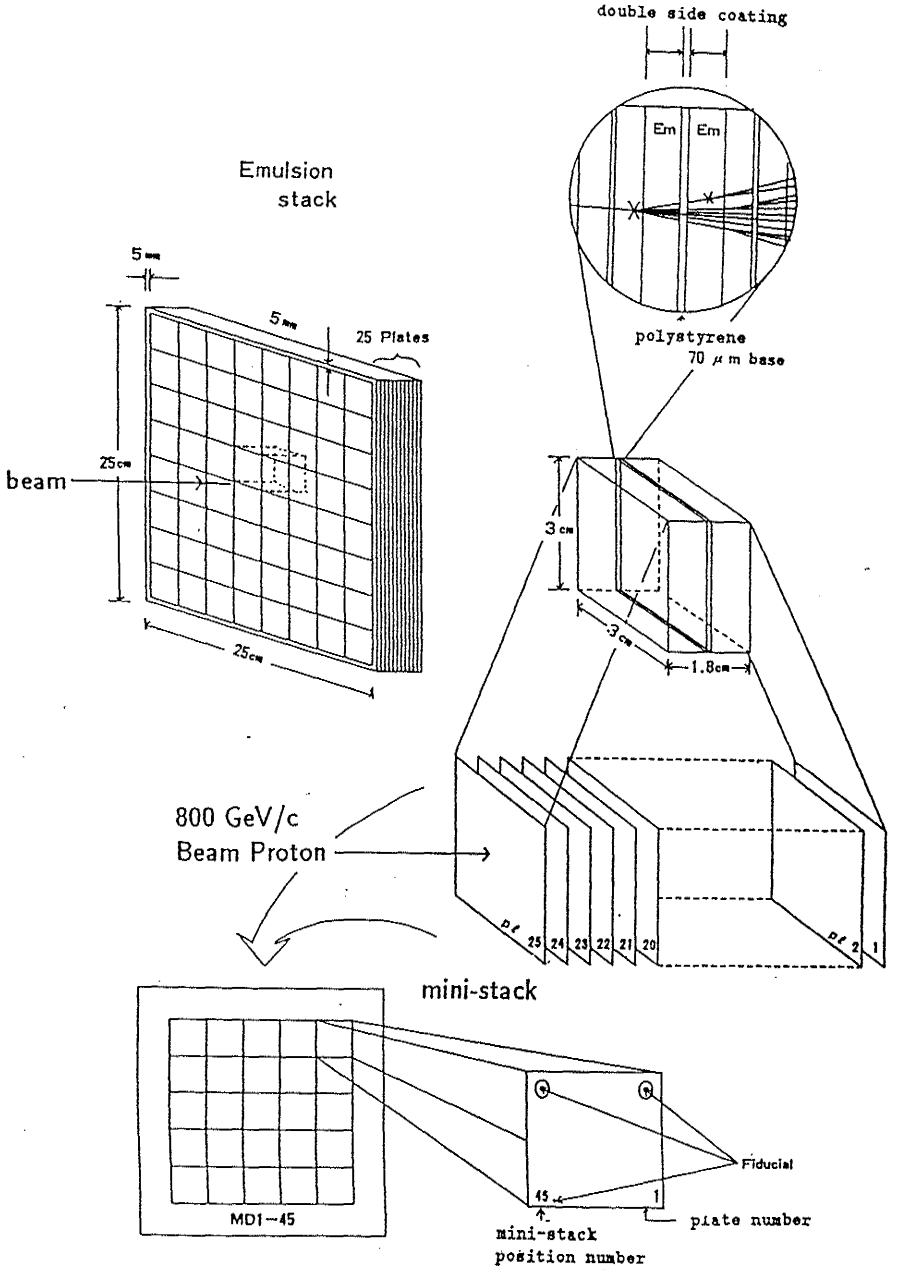

Figure 3.13: Mini plate method.

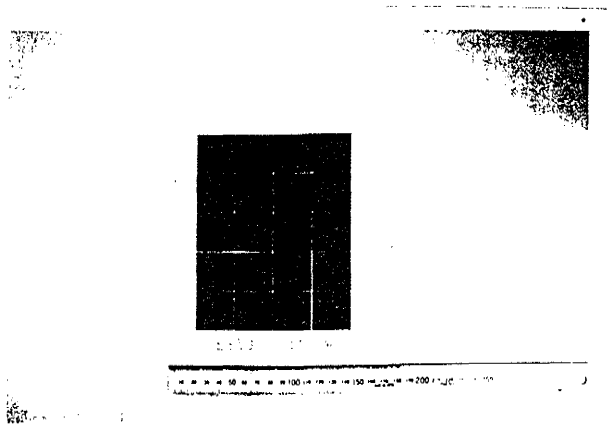

Figure 3.14: Mini plate (photograph).

accuracy of the reproduction of the position by this stage is on average 1 μm .

The system is controlled by a set of big programs which was developed and modified from time to time. The programs are explained in Chapter 4. This system is capable of performing the operation of the measuring instruments, calculation, storage of data, and library control with several tasks at a same time. The operation of the system is done with the interactive mode with a host computer.

The host computer has 32bit CPU, RAM (8Mbytes), hard disk (160Mbytes) and 32 serial lines coupled to the measurement instruments. DOMS interface displays the emulsion image and superimposes graphical guide on CRT. The CRT acts as character display and video monitor. Graphical window (= pointer) on CRT is controlled by control stick on the keyboard. DOMS recognizes a grain of size ~ 1 μm in the video signal and points a most dark spot in a given window.

Graphic display terminal (JCC Japan Computer Co., M1401-III and YAMAHA

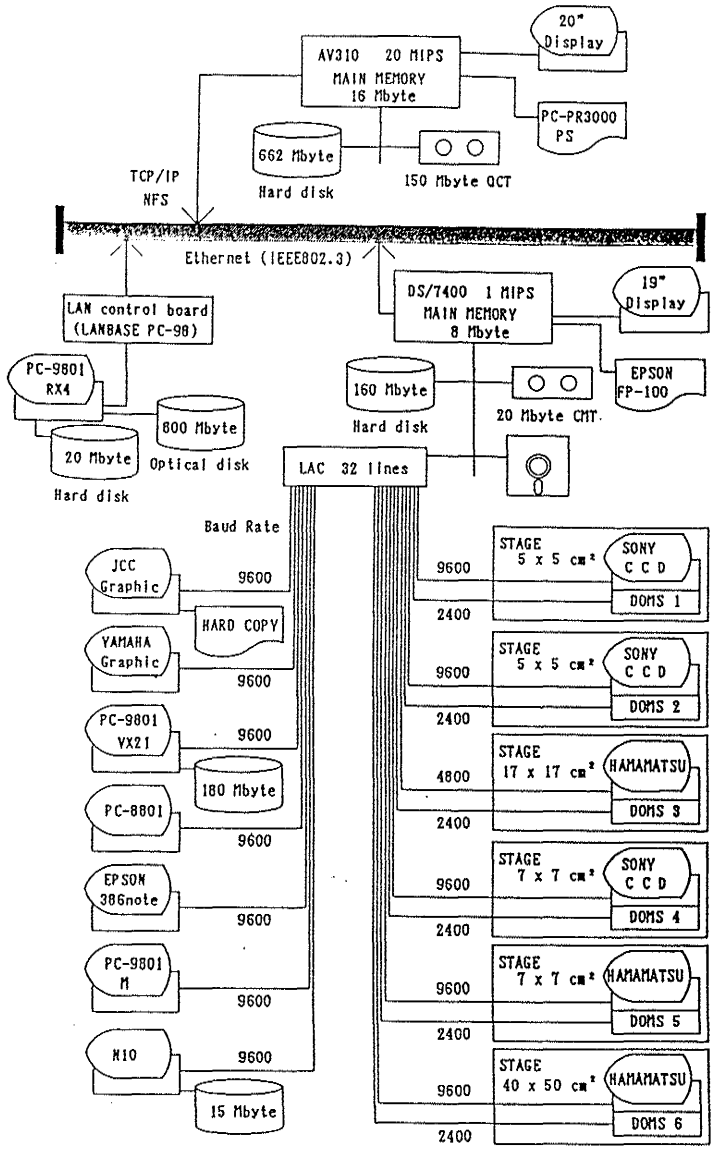

Figure 3.15: Toho on-line system.

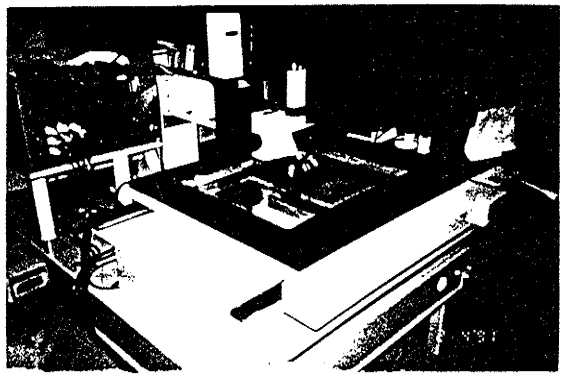

Figure 3.16: Semi-automated analyzing system (photograph).

Co., YGT–GS200S) is a powerful tool when matching the signals of SSD to construct possible vertices for charm or bottom decay. The plotter and emulator terminals (NEC Co., PC–9801) are also at work.

In the following section, the constructions of 7cm× 7cm motor driven microscope stage system and DOMS interface are described.

3.4.3 Production of improved motor driven microscope stage

There were several different experiments running in our laboratory at the time of 1986 when the author began the graduate research. For example, CERN-WA75 (350 GeV/c π-emulsion), Fermilab-E531 (350 GeV/c, ν-emulsion), Fermilab-E758 (800 GeV/c proton-emulsion), and test scanning of our E653 were carried out at same time. Furthermore we planned to take up new experiments CERN-NA34 (Heavy ion beam-emulsion interaction) and KEK-E176 (1.6 GeV/c K^--emulsion, H particle

search) which are in progress now.

Therefore a great demand of additional microscope stages with computer control is raised and the author took the task to produce such stages at the initial phase of the graduate research. Figure 3.17 shows the plan view of the stage produced by the author. A special care was paid for that the all parts of the stage must be produced and assembled within the accuracy of micron order. The interferometer was used to checking the stage movement. To speed up the emulsion scanning, a semi-automated scanning system controlled by Data General host computer was developed. As shown in Figure 3.18, the system consisted of the microscope which has an electromotive stage and a DOMS interface described in Section 3.4.4.

The original microscope was the conventional manual microscope manufactured by Chiyoda Optical Co. The electrical parts provided for the conversion are;

DC motor (escap23HD 11-216E204.4), Liner encoder (HEIDENHAIN LS903, LS403), Stage (Steel material, YH75(JIS 7079T651)) and those are shown in Figure 3.18. Figure 3.19 depicts the Crossed Roller Way (IKO Bearings Co., CRW) which was used as a rail of the stage. The CRW have a liner motion with cylindrical bearing in limited range.

The accuracy of position reproduction of the stage is about 2 μm , and the stage working distance is 70 mm for both X and Y directions of the horizontal plane. The precision of the stage movement was checked by an interferometer and grain measurements were repeated while moving the stage with a long distance.

Two conventional microscopes were converted into the motor driven microscope stages with linear scale to read the position, and the microscopes were connected to the DOMS interface as shown in Figure 3.20 for the system 4 and 5. DOMS controls x,y and z movements of the stage with 4 different speeds. Our microscope has good

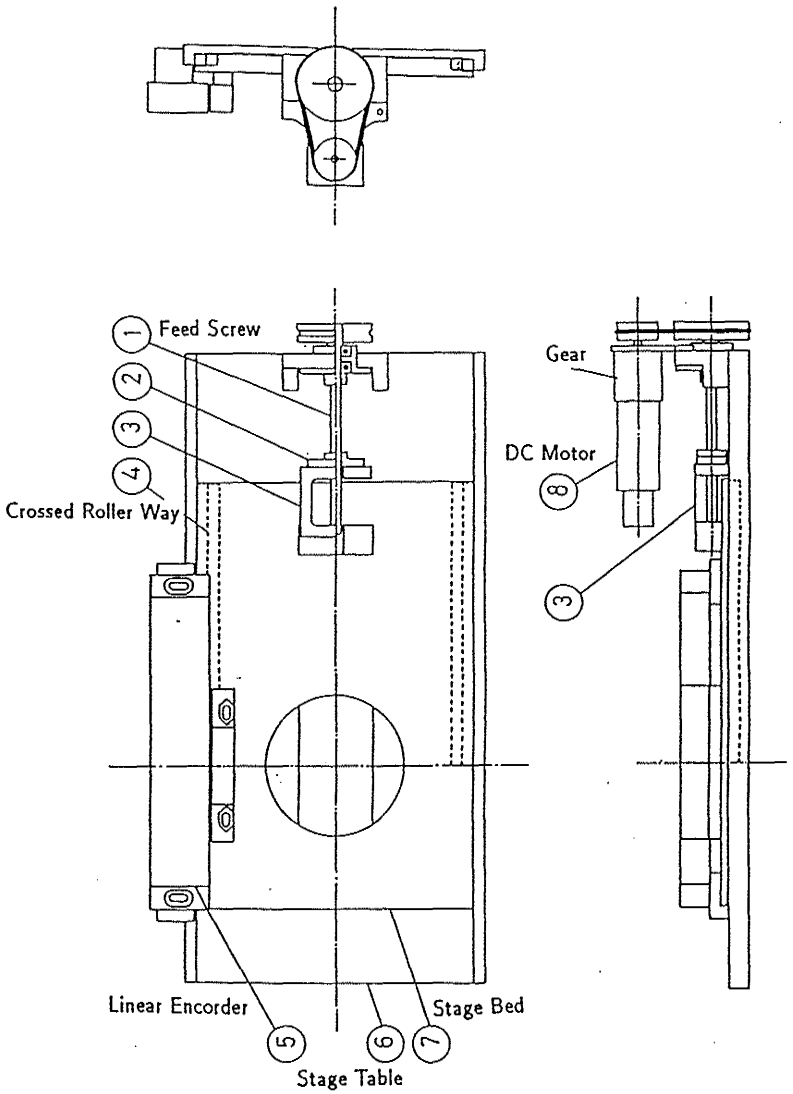

Figure 3.17: Plan view of improved motor drive stage.

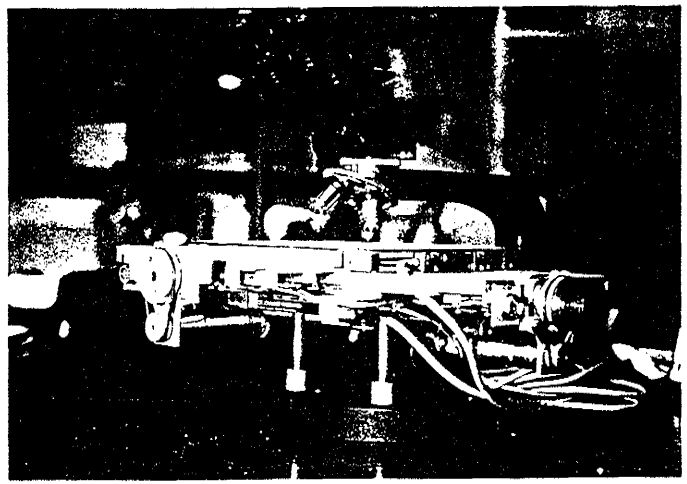

Figure 3.18: Improved motor drive stage(photograph).

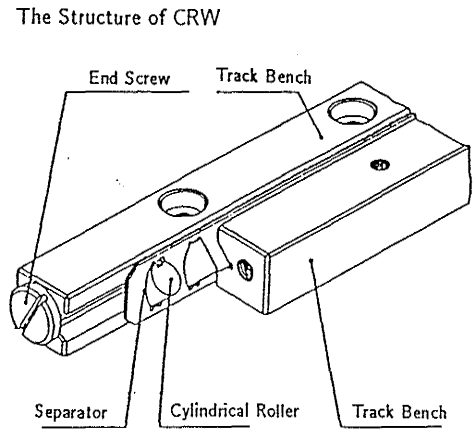

Figure 3.19: Crossed roller way.

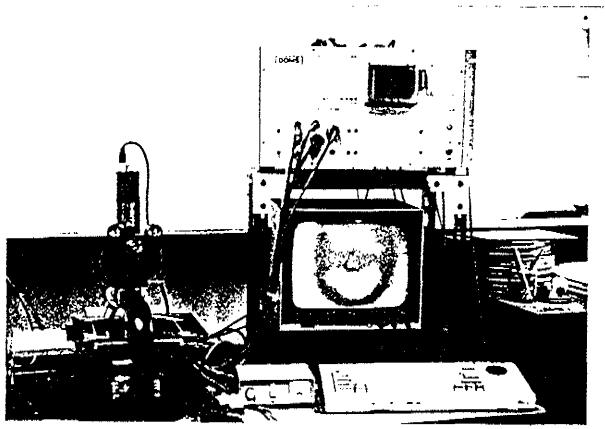

Figure 3.20: Stage and DOMS system (photograph).

cost performance and high precision.

3.4.4 Digitized on-line microscope system (DOMS)

Figure 3.21 shows DOMS controller as photograph, and Figure 3.22 shows the block diagram for data acquisition of DOMS. It was developed as an interface between the host computer and microscope stage. It controlled the microscope stage for real time request. Hardware of DOMS consisted of 12 boards with different functions and keyboard with control stick. These boards can be replaced by other boards with user's need.

Each function of the 12 boards of the DOMS constructed by the author are described in the following.

i) Master CPU Board (Crate Controller).

This CPU board controlled other boards and communicated with host computer.

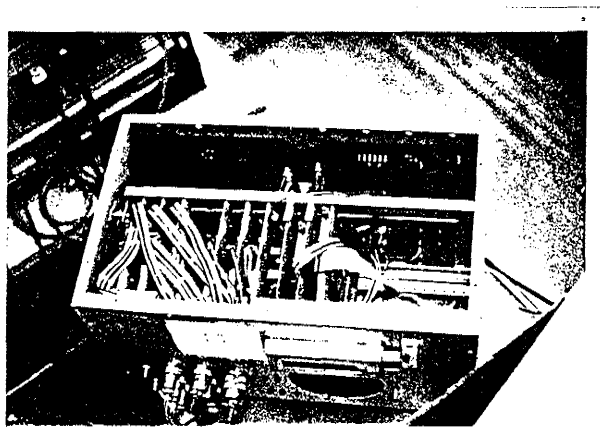

Figure 3.21: DOMS controller(photograph).

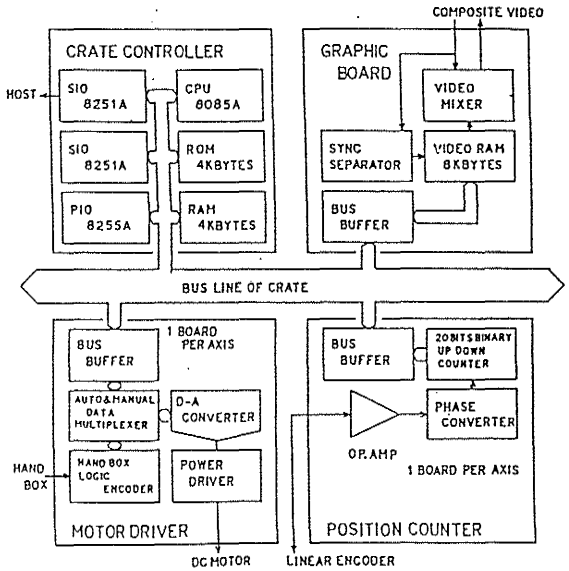

Figure 3.22: Block diagram for data acquisition of DOMS.

The program for CPU board included; the monitor program, the read position of stage, the translation from binary data to decimal data and the stage moving into a specified position.

ii) Motor Driver Board.

This board consisted of 3 boards for X,Y,Z movements and controlled three DC motors of the stage. Each motor is able to move independently. The moving speed of the stage is approximately from minimum 10 μm /sec to maximum 5 mm/sec. The manual control of the stage movement is also accessible with a hand box which change in 4 different speeds.

iii) Position Counter Board.

Output signal of linear encoder is two phases of sinusoidal wave and a operational amplifier divides one cycle of this signal by 20. Then it is transferred binary of 20 figures ($= 10^6$) and the board count up and down. This board transmit position signal to Bus line corresponding with requirements of master CPU.

iv) Display Board.

This board displays the coordinate of position counter. There are three dimensions X, Y, and Z with light emitting diode or liquid crystal. Data was translated from binary to decimal by this board.

v) Graphic Video RAM Board.

This board displays data of Random Access Memory (RAM) as bit image for 256 × 256 on CRT. Graphic signal is superimposed on the composite video signals of CRT, and graphical fonts are displayed on CRT independent of ordinary characters.

vi) ROM Writer Board.

This board write the programs on electrically erasable Read Only Memory or

electrically programmable ROM. It takes 100 seconds per ROM (2Kbytes). The control program for ROM writer was included in Monitor program of the master CPU board.

vii) Charge Coupled Device (CCD) Board.

There are two kind of boards, one is "CCD analog board" and another is "CCD digital board".

The analog board is to pick up the image of grains in nuclear emulsion plate. The window on CRT can be moved by a control stick of the key board (described later) to an objective grain of which position is to be measured. The board catches the peak of signal in the window and separates synchronous signal from composite video signal of CCD. This board send a timing to the CCD digital board. Graphic signal of white dot for the image of grain is superimposed with video signal and sent to the digital board.

The digital board is to measure the position of grains in CRT frame. This board generates horizontal clock and counts it about X axis, counts vertical synchronous clock about Y axis. The digital board keeps the position data of grain in window.

viii) Keyboard with Control stick.

The keyboard box is composed of a keypad (Mitsumi Components Co., KAM-A66YN(R-56-1350)), a character generator (Logic House Co., LH7001N), a power supply (TDK Co., FCP-031 and FMP05-2R0), and a control stick(Sakae Communication Industry, 40JBK-Y0-20).

All the controls of the semi automatic system are done interactively from this keyboard.

CHAPTER 4

METHODS OF EMULSION ANALYSIS

4.1 Outline of Nuclear Emulsion Analysis

Nuclear Emulsion is able to detect the trace of charged particle traversing in the emulsion target as the line, which is called a "track", formed by silver grains. However neutral particle can not be seen since the silver grains are only emerged as a result of the ionization of silver atoms by the traversing charged particle.

The size of silver grains forming a track is about $0.7 \sim 1.0\ \mu m$ after the chemical development, therefore the spatial resolution of the position is far better than those of any other particle detectors. For example, the size of bubbles of most fine rapid cycling bubble chamber is $\sim 17\ \mu m$ [40].

Not only achieving the fine resolution of track positions, a most important feature is to provide a visual examination of events. In particular, when an event is reconstructed by the information of only SSD or other counters, the event happened to be not a genuine one and could be a just crossed background tracks which can be examined visually in the emulsion. However, in the old fashioned emulsion scanning technique, a lot of time and human power are required to search events.

Thus we developed a particle spectrometer by combining emulsion target and counter system. Our semi-automatic emulsion scanning techniques are supported by these electronic counters. These new techniques are described in this chapter.

All the scannings and the measurements of events are done on CRT with programs of interactive mode controlled by the host computer. Many programs for on-line analysis are developed so that all the location, the measurement, and the calculation etc. of events are efficiently done with the same accuracy and quality for all events at any time.

By the counter system at downstream of the apparatus, the 3-dimensional position, charge, track numbers and momentum etc. of each event are recorded. Thus we are able to measure the position of decay vertex of charm particles in the emulsion target very accurately while examining the pulse heights of SSD-raw data on CRT of graphic terminal. The raw data of SSD-pulse heights at the beam exposure has been dumped in the optical disks of our laboratory. Thus we can compare the SSD hits to the actual emulsion events at any time.

This emulsion scanning system consisted of a motor driven microscope stage and an interface box (DOMS). The system was described in the Chapter 3.

4.1.1 Description of charm events

How do we observe heavy mesons decay in nuclear emulsion target ? Figure 4.1 shows a typical topology of an event with multi decay vertices. 800 GeV/c proton beam is injected into the emulsion target and interacts with an emulsion nucleus (for chemical compositions, see Table 3.3).

This first interacting point is called the primary vertex. The position of the incoming beam before interaction was measured by beam SSDs. The produced

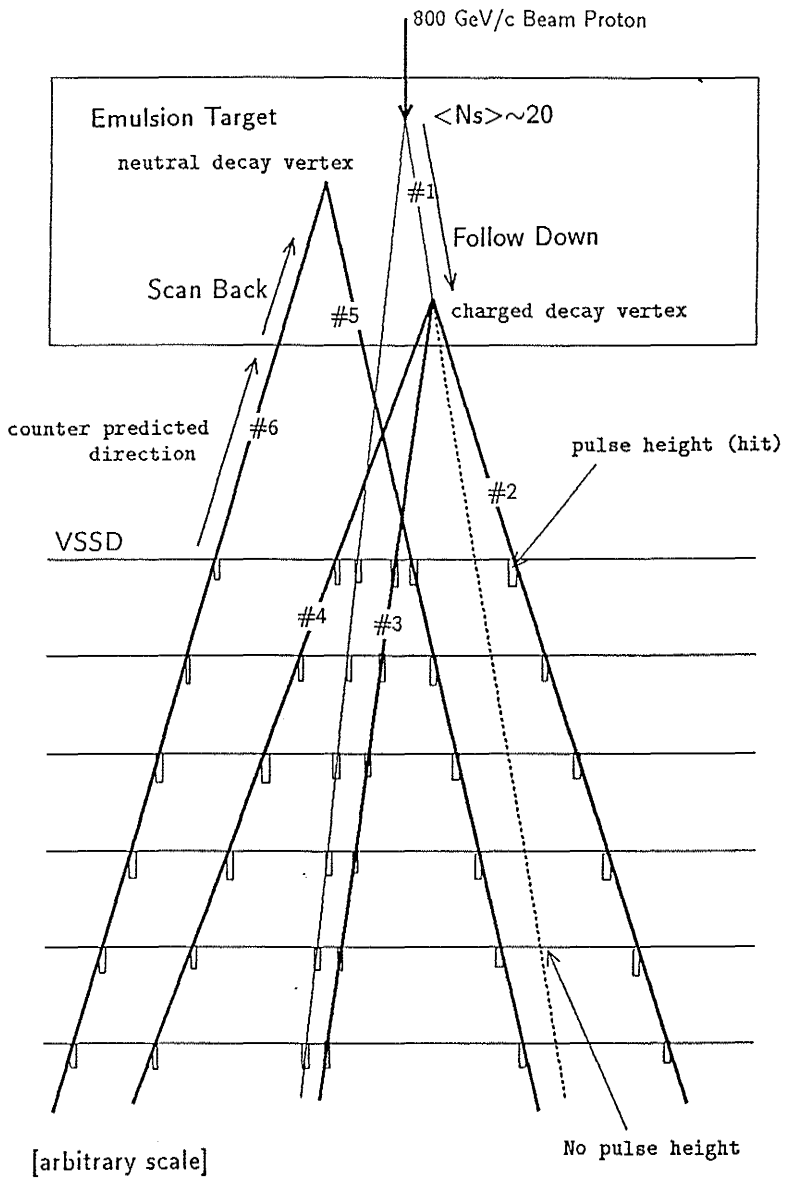

Figure 4.1: Configurations of charm events.

secondary particles by the first interaction are almost light mass mesons such as pions and kaons, but in a rare case heavy (B and D) mesons are produced.

The production rate, the structure of emulsion target, and mini plate method have been described in Chapter 3.

The produced secondary particles are classified into three types, namely:

a) MTK (matching track)

The track slope in the spectrometer matches to that of a track from the primary vertex in the emulsion target.

b) ETK (emulsion only track)

The track exists at the primary vertex in the emulsion target but a track with same slope can not be measured in the spectrometer.

c) CTK (counter only track)

The track slope is measured in the spectrometer but the corresponding track doesn't come from the primary vertex in the emulsion target.

The ETK and the CTK could not be found at one side (emulsion target or spectrometer) hence some possibility of decay is expected and they could be the candidate tracks of a heavy meson and its daughter, respectively.

Figure 4.1 illustrates a parent particle ETK #1 decays into 3 daughters tracks #2, #3, and #4. There is no counter hit at the extrapolated direction of track #1. On the other hand, CTKs #2, #3, and #4 have hits on the counters but these are not found at the primary vertex. And the tracks #5 and #6 are also not observed at the primary vertex and they could be possible decay daughter tracks of a neutral charm particle produced at the primary vertex.

4.2 Flow Chart of Emulsion Scanning Procedures

Figure 4.2 shows a flow chart of emulsion scanning procedures and Table 4.1 summarizes a brief explanation of the on-line programs used for the scanning. The outline of the flow is as follows.

1. Locate the primary vertex in the emulsion target.
2. Check the origin of the predicted muon track at the primary vertex.
3. If the predicted muon track matches to a track come from the primary vertex, then stop the decay search. Since such muons are from pion decays.
4. If the predicted muon track does not match to a track in the primary vertex, then start the decay search for the event.

The event is located in the emulsion target, when the counter information of slope and momentum are predicted and a reconstructed vertex point is in the emulsion bulk (i.e. in the emulsion target). When a candidate event is found in the predicted position, the track pattern of the candidate event is checked by comparing with that of the counter prediction track pattern by the "Graphic Matching". The graphic matching method will be explained in Section 4.3.1. When the track pattern of candidate event agrees with that of the prediction and the muon is unmatched track, then the event is stored for the decay search.

There are mainly two procedures for the decay search in the emulsion target and one procedure for outside of the emulsion target. The procedures are;

· Follow down method

This procedure is mainly applied for searching charged particle decays by

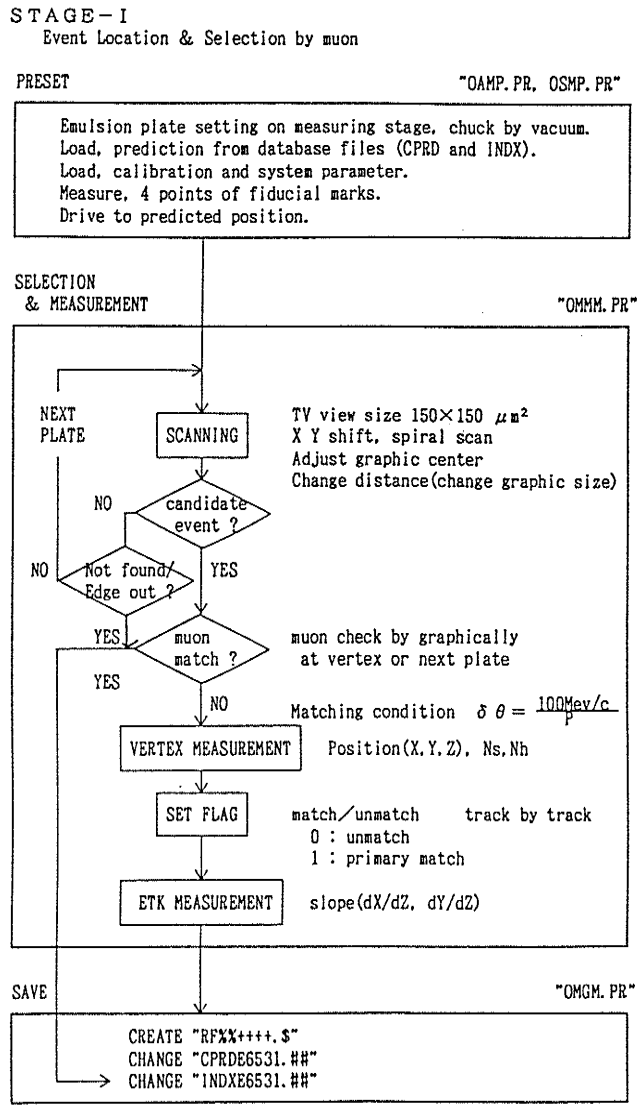

Figure 4.2: Measurement method of events.

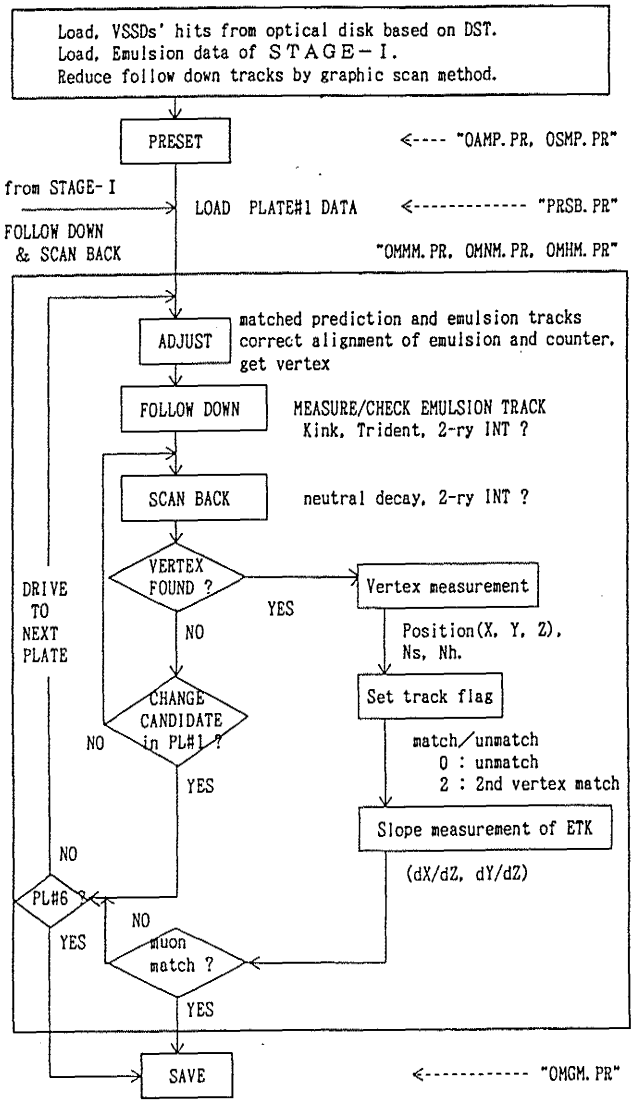

Figure 4.2: Measurement method of events(continued).

Table 4.1: On-line programs for emulsion analysis.

OAMP	Master program for on line analysis · For miniplate setting and reading fiducials, · Correction of the coordineates among the systems.
OSMP	Event location with graphic matching · Location and spiral scanning for primary interaction, · Graphic matching of interaction.
OMMM	Scan back and follow down procedures · Measurements of slopes of ETK and referance tracks.
OMGM	Main program for event quality test and decay search · Store the measured track data in the file "RF−−++++.#", · Check the quality of ETK slope.
PRSB	Preparation for scan back mode · Check the flag of tracks based on the data read by OSMP, · Load the measured data of pl#1 .
OMPM	Load file of previous measurement ("RF−−++++.#") · Displays measured emulsion track by cross mark, · Produce temporary file including emulsion track and vertex data.
OMNM	Vertex measurement procedure for secondary vertex · Decay vertex analysis with graphic matching method, · Position measurement of secondary vertex.
OMHM	Track slope measurement · CTK search with measured reference beam track.

following ETKs from the primary vertex toward to the downstream emulsion plates (see the Section 4.4.1 for details).

- Scan back method

  This procedure applies mainly for searching neutral particle decays. That is, a specified CTK is scanned back toward to the upstream and find decay vertex (see the Section 4.4.2 for details).

- Graphic scan method

  Mainly this procedure is applied for searching charged- and neutral-particle-decay vertices at the outside region of the emulsion target, and also for the check of track reliability by looking at the hits of the downstream VSSDs. To look out for the decay vertex, we optimized the track data of the spectrometer together with the data newly measured in the emulsion (see the Section 4.4.4 for details).

All measurement data in the emulsion target such as position, slope and flag for the tracks were stored in the hard disk unit of the host computer through DOMS interface. We can always read these data for the graphic scanning.

4.3 Event Location

Event location is the procedure for searching primary vertex produced by the interaction of 800 GeV/c proton beam with an emulsion nucleus, thus the vertex must be found in the emulsion target. The primary vertex position is predicted by reconstructing tracks with the information of slope and momentum.

First of all, a mini plate is fixed on the microscope stage with the vacuum chuck so that the mini plate is securely fixed in the stage. As described in Chapter 3, four

fiducial marks are measured at the beginning of the location so that the calibration is made automatically for the rotation and the shift of the mini plate setting against the absolute coordinates.

Then the microscope stage was driven automatically to the predicted position of the primary vertex when the event number is fed. Scanning area for primary-vertex-search is done within the predicted plate and the adjoining $\pm$ 2 plates in the upstream and the down stream of the predicted plate. For each plate, a search is made within a volume equivalent to a circle of 250 μm diameter times the thickness of each emulsion plate. The volume is just corresponding to one view of the microscope with the magnification of 10 *times* 50. In general, the emulsion scanning is done on CRT except when a close examination is needed.

The location efficiency of primary vertex in the emulsion is on average 94% after the fiducial volume cuts.

4.3.1 Graphic matching method

The event with muon matched to the primary vertex are rejected from the scanning list as the event is not worth to search for charm or bottom decay. When a primary vertex candidate is found in the view of the microscope, the vertex is compared with the track pattern of counter predicted event displayed on CRT. Figure 4.3 illustrates a typical graphic matching of vertex. The track pattern is displayed with vectors or points so that both the predicted event and the located candidate event are compared for their agreement.

We can determine when the candidate vertex has at least 3 matched tracks, the vertex is considered as real one. Then the predicted muon track in the spectrometer is examined whether it matches to one of the tracks come from the primary vertex.

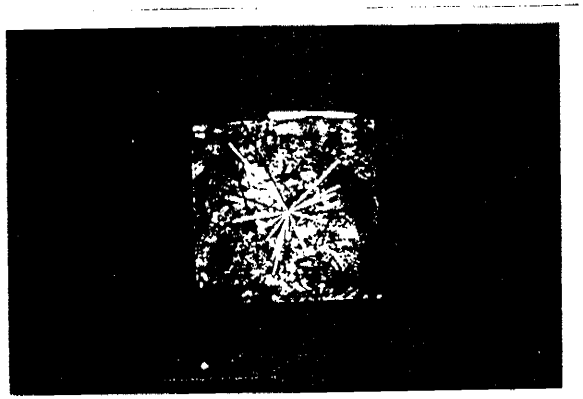

Figure 4.3: Graphic matching method (photograph).

If it is matched, then the event is discarded. The reason for the event discarded for the further decay search is that the muon track associated with the primary vertex is most likely due to the background muons come from the decay of pions or kaons produced in the first interaction. Thus the muon of $\pi \rightarrow \mu\nu$ decay have a small transverse momentum and succeed the direction of the parent pions or kaons. All these check may be done in a few minutes.

The criterion of muon matching with primary vertex is $\delta P_{T\mu} = 0.1$ GeV/c and most of background muons have smaller than this $P_{T\mu}$. However the muons from real charm decay will have much larger transverse momentum. The correction of the loss of charm events by this criterion was done by Monte Carlo simulation[41, 42].

Events with muon unmatched were kept for further decay search. The procedures are described in the following.

4.4 Decay Search

The main part of decay search in the emulsion target is carried out by the follow down method and by the scan back method. Together with these decay search procedures, the graphic scanning method was applied repeatedly during the course of decay search.

4.4.1 Follow down method

The follow down method is applied for searching charged particle decay in the emulsion target. The ETK, a track only found at the primary vertex and not in the spectrometer, has a possibility of something happened between the primary vertex and the spectrometer such as a decay of bottom, charm, or background interactions. First we choose a reference track which has a high momentum so that the low possibility of scattering while traversing in the emulsion target. The reference track is measured at the bottom surface of the mini plate before measure ETKs. The error of the position measurement is about 1.0 μm and is comparable to the grain size. ETK is followed from the primary vertex to the downstream plates. When a decay vertex is found, the graphic matching is made, just like the one applied to locate the primary vertex. The agreement is checked between counter reconstructed tracks and emulsion tracks on CRT.

4.4.2 Scan back method

The scan back method is really a powerful method to find the decay vertex with minimizing the scanning bias. The method is at first developed in our previous E531[43] neutrino experiment in 1979. The scan back method is adapted for searching neutral particle decay in the emulsion target.

Neutral particles can not be recorded as the tracks in nuclear emulsion. Therefore if a neutral bottom or charmed particle is emitted from the primary vertex, we could not observe them at the primary vertex. In this case, the search of the decay from such neutral particle is performed the scan back method by using CTKs, a track only found in the spectrometer, starting from the last plate of the emulsion bulk.

In the E653, the improved "Scan Back Method" provided the track vector which is the reproduced graphic image of the track to be followed. The track vector is displayed in the CRT view and is very helpful to find the real track-segment in a plate by comparing the angle and the projected length of the track with the predicted graphic track vector during the following. The scan back is performed through the CRT view area of 120 $\mu m \times 100\ \mu m$.

When a decay vertex is found, the agreement between the emulsion vertex and the counter predicted vertex is checked by the graphic matching method (see Section 4.3.1). Whole procedure of this decay search is done with the semi-automatic scanning system.

4.4.3 Heavy track check at decay vertex

The heavy track if attached at the found vertex is a low energy proton or a recoil fragment of target nucleus. In baryon number conservation, D meson cannot decay into baryon final state and therefore if heavy track associated with the vertex, which means it is an inelastic interaction.

In the emulsion, the track which has $I/I_0 > 1.4$ called heavy track, where I is the grain density of the track and I_0 is the grain density of the minimum ionization track. In our experiment $I_0 = 30.65 \pm 0.53$[42] and is the number of grains per 100 μm .

If heavy tracks come from the secondary vertex, this vertex is flagged as inelastic interaction because it is not meson (D or B) decay candidate.

The emulsion information played crucial role in this analysis, because it provides us the high resolution of the vertex positions and clarify the structure of decay vertex. With the counter experiment, the vertex of the decay is not seen directly therefore if there is a short track such as less than 10 μm attached at the vertex, no way to know the existence.

We have also checked very carefully near the decay vertex for grains (blobs) and very short heavy tracks to remove the background events from inelastic interactions. Blob check at vertex is described in Chapter 5.

4.4.4 Graphic scan method

The decay vertex are initially predicted with a conversing point formed with a few tracks through counter information alone and are sometime failed to be detected in emulsion. In such a case, new information of tracks measured in emulsion during the decay search is added to the existing counter information and try reconstructing tracks again with the VSSDs hits to see new prediction of the vertex.

The graphic scan method is the procedure to obtain a possible decay vertex based on VSSDs hits.

For events with muon unmatched at primary vertex and the origin of CTKs was not found in the emulsion bulk, we tried to look for a possible decay vertex outside emulsion bulk, by adding the data of newly measured emulsion track slopes. New reconstruction of tracks are attempted when unreconstructed hits remained. The emulsion information is very important to reconstruct tracks with new slopes measured in the emulsion.

Figure 4.4 shows a hard copy of CRT output for a typical event in X view. For each event, three plane views U, V, and X from VSSDs, are available. To look out for a decay vertex, we optimized the track measured in the emulsion (blue line) and the track in the spectrometer (red line) as shown in Figure 4.4.

The quality of hits in VSSDs of both hadronic tracks and muon tracks is examined in order to exclude nonsense tracks. These tracks had no pulse height of VSSD's in a certain view. We also checked unreconstructed VSSD hits and tried a new reconstruction for a possible track formation.

The Graphic scanning system consists of an optical disk driver unit (RICOH Co., RS-9200F), an optical disk cartridge (RICOH RD520), a color graphic terminal (YAMAHA Co., YGT-GS200S), and a personal computer (NEC Co., PC-9801). This system linked with the host computer (Data General Co., DS/7400) and exchange the data with LAN. The optical disk cartridge can record 800 Mbytes, its size is 5 $\frac{1}{4}$ inch, and double side type.

When a proton beam is exposed to the emulsion target, each counter data of the interactions are recorded in MTs. The memory capacity of one MT is about 2400 ft ($\sim$ 800 m) $\times$ 6500 bpi equals $\sim$ 180 Mbytes, thus the data of 4 MTs may be dumped in one optical disk. In the E653 first run, altogether we used about 1300 MTs. Similarly 2000 MTs were used in the second run. One module emulsion target contains $\sim$ 1500 useful events to be located in the first run.

When the decay search for all ETKs and CTKs are done, whole the measurements for this event are finished.

The measured data files of the candidate events with charm decay are transmitted by the electronic mail to the collaborators of the counter side so that the candidate events are again tried fitting for new tracks to determine the momentum. We called

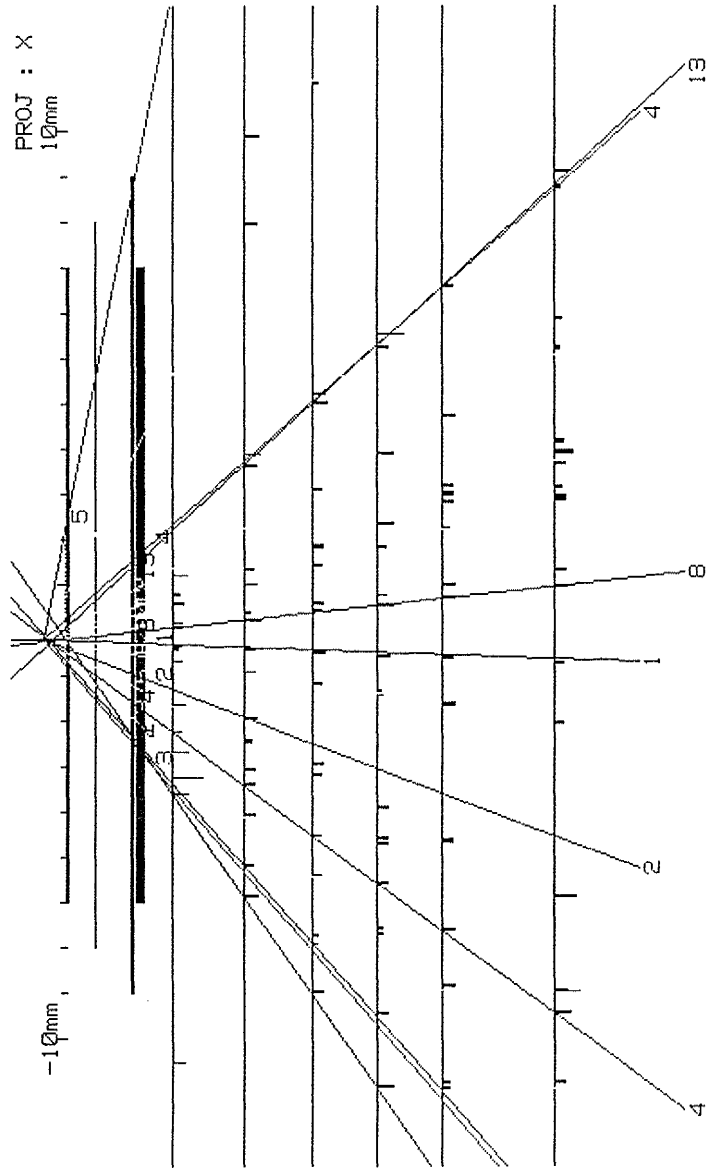

Figure 4.4: Decay search event by graphic scan system.

this process as "refitting". Then the refitting information are sent back to this side. After the refitting, the momentum data for new tracks may be obtained in most cases. Most of the new tracks were resulted as the daughter tracks of charm particles.

4.4.5 Measurement of the bottom emulsion plate

In the scan back procedure, the human judgment required is only concerned with the identification of track-segment which is the candidate track to be followed. However in reality, it is very heavy task to do, because there are many similar background tracks recorded in scanning area.

In the E531 experiment, the "Changeable Sheet" is used in the scan back method. The changeable sheet is a thin emulsion plate and is placed between the bulk emulsion target and the counter system as the interface of tracks in both sides. This sheet is changed every three days during the beam exposure to suppress the background tracks. This low-track-density-plate helps to locate a particular track to be found easily among the background tracks. A specified track found in the changeable sheet and is connected to the pl # 1 of the emulsion target.

Thus the changeable sheet must be processed (chemically developed) soon after the removal from the exposure so that no accumulation of background tracks. However changing the sheets frequently was the additional work.

In E653, the idea of the changeable sheet was substituted by the bottom plate (pl # 1) of the emulsion target. Thus the pl # 1 had a thin emulsion layer, but the plate was not changed during the exposure since the exposure time for each module was rather short as compared to the neutrino exposure. The track scan in the plate # 1 was carried out by the device called "Track Selector", a fully automated track scanning device[44].

Figure 4.4.5 shows the box diagram of the track selector. The track selector provides a limited scanning area of the counter tracks and about $\pm$ 20 μm , about 1/8 of the ordinary scanning area, thus it saved the scanning time.

4.4.6 Emulsion tape

In the second run of E653, the idea of the changeable sheet is further developed in a form of the emulsion tape[45]. The emulsion tape is a new invention introduced in this experiment for the first time.

The function of the emulsion tape is the interface which provide reliable tracking and control the density of tracks recorded in the emulsion target.

Figure 4.6 shows the cross section of the emulsion tape. The emulsion tape is made of 200 μm base with 60 μm thickness of Fuji ET-7B emulsion coated on both sides of the base. Total of 150 meters of 35 mm wide tape was used. The amount of emulsion volume in the tape is only 1.5 % of total interaction length. The emulsion tape was placed just behind the emulsion target module and before the vertex silicon strip detector. Figure 4.7 illustrates the setup around emulsion target of the second run.

The track density become higher as the emulsion target accumulates interactions, then the tracks of produced secondary particles become congested. This makes track matching between VSSDs and the emulsion module very difficult. To solve this problem, the emulsion tape was changed to new one every module exposure to keep the track density low. The emulsion tape is drew out with a constant speed during the beam exposure and is under the control of a micro computer (in which DOMS acts as a host computer).

The emulsion tape keeps low track density and $\sim$ 1/10 of that of emulsion

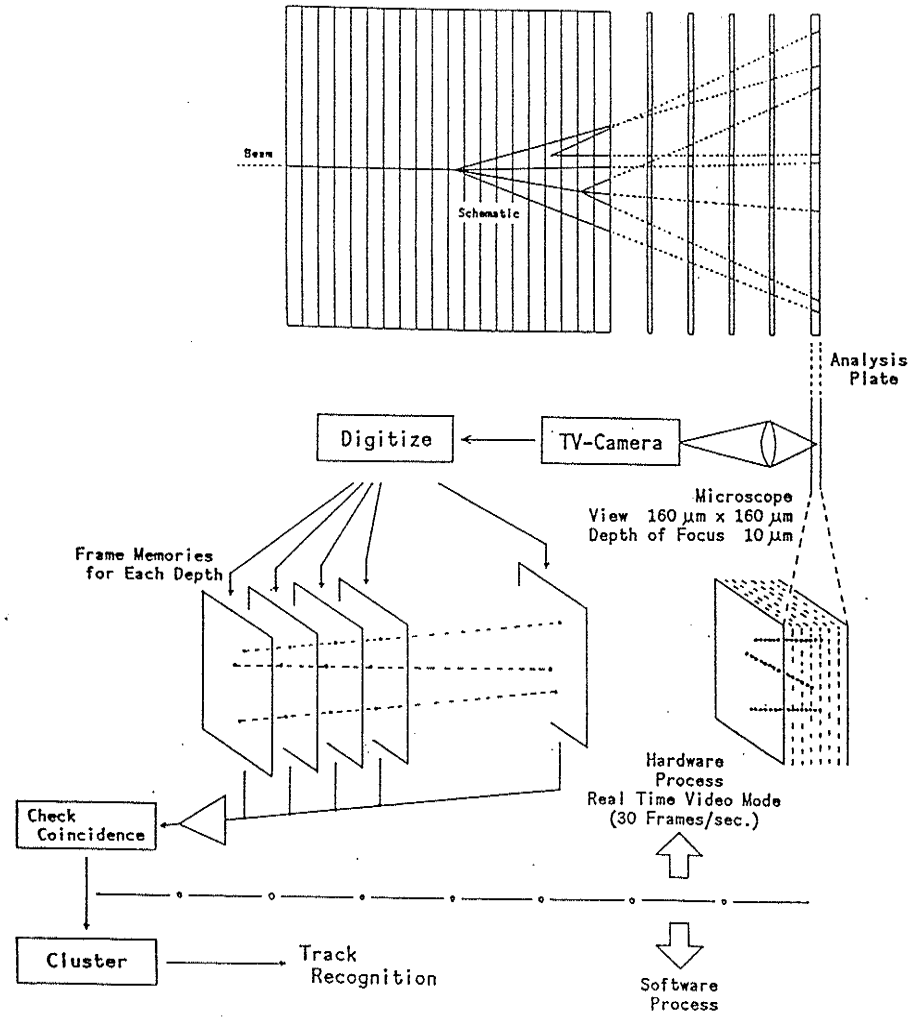

Figure 4.5: Box diagram of track selector.

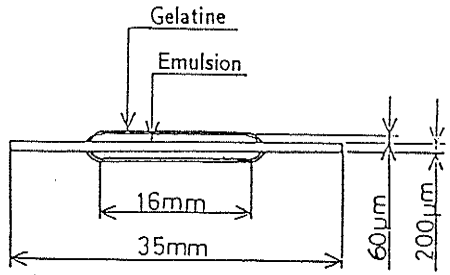

Figure 4.6: Emulsion tape.

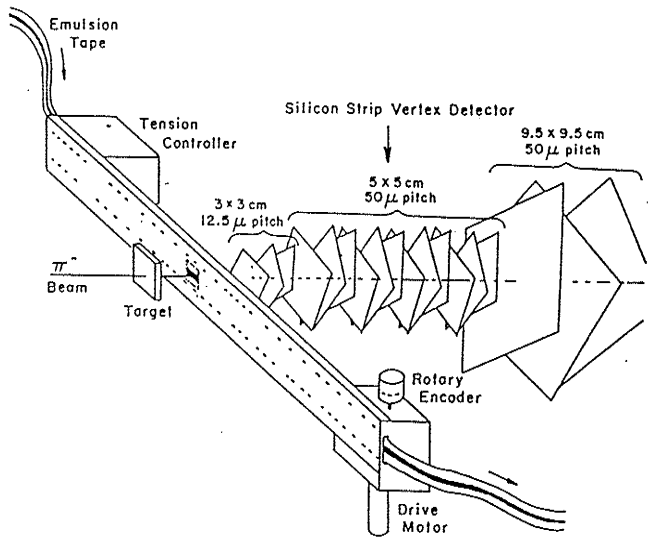

Figure 4.7: E653 2nd run target system with emulsion tape.

target. Accuracies for the position and the slope of emulsion track are ~ 1 μm and $1/(200 + 60 \times 2) \approx 3$ mrad in emulsion tape, respectively. Hence this emulsion tape is used to find tracks to connecting the corresponding track in the last plate of emulsion target and in the VSSDs. The tape is also useful to determine the decay vertex position outside of emulsion target.

The use of the emulsion tape has brought a new potential functions into the emulsion techniques. That is, the time resolution of emulsion target is added as well as high spatial resolution.

By introducing the emulsion tape, many advantages are brought out. For example;

1. It was able to control the track density independent of emulsion target. Emulsion target may be exposed to high density beam as high as $10^5/cm^2$, while emulsion tape will complement the emulsion target with easy identification of tracks in the low track density tape.

2. It removed the work such as the replacing changeable sheet frequently. The new emulsion surface is supplied continuously during the beam exposure by winding up the emulsion tape.

CHAPTER 5

SUMMARY OF DATA

5.1 Event Summary

5.1.1 Summary of emulsion scanning

After scanning events in the emulsion target, we found altogether 1084 charm decay candidate events by the direct observation. This is a world largest collection in the direct observation which is the most reliable method.

Table 5.1 shows the summary of the status of events in each location process for all collaboration group.

The notations in Table 5.1 are explained in the following. V-MOD and H-MOD represent the target modules in which the beam is injected vertically and horizontally with respect to the emulsion plane. The Categories 1, 2 and 3 indicate the grouping of the events as regard to the values of the transverse momentum or the I.P. of tagged muons and of some hadrons. The detailed descriptions for the categories of the events are found in Chapter 3. "Three vertices with muon" implies that the event which accompanies three decay vertices and a tagged muon. "Pair with muon" or "Single with muon" implies that the event accompany two or one decay like vertex with a tagged muon.

Table 5.2 shows summary of scanning results in Toho university.

Table 5.1: Summary of location of events.

INSTITUTE	AUE	GIFU	NGY	OCU	TOHO	UU	KOBE	
Module Type	V-MOD						H-MOD	TOTAL
Muon Triggered Events $\times 10^3$	3050						2200	5250
Category 1,2 and 3	2331						1681	4012
As for Category 1, 2, and 3 Number of events was listed below.								
Events in fiducial	1032	1677	10126	4181	1637	2376	2200	23229
Tried to find 1ry	881	1487	9800	2967	1415	2303	1257	20110
Found 1ry	801	1368	9351	2718	1363	2031	1256	18888
No muon from 1ry	248	392	3459	945	512	633	338	6527
Tried to search decay (include graphic scanning)	248	392	3459	945	507	623	338	6512
— Charm Candidates — (Vertices of decay candidates exist in main block of Emulsion)								
Three Vertex with Muon	1 (0)	1 (0)	14 (2)	2 (0)	1 (0)	1 (0)	2 (2)	22 (4)
Three Vertex without Muon	0 (0)	0 (0)	2 (0)	0 (0)	0 (0)	0 (0)	0 (0)	2 (0)
Pair with Muon	3 (1)	11 (1)	139 (45)	22 (9)	18 (7)	22 (4)	9 (6)	224 (73)
Pair without Muon	1 (0)	6 (1)	36 (4)	3 (2)	5 (1)	1 (0)	2 (0)	54 (8)
Single with Muon	10 (6)	23 (14)	228 (113)	54 (34)	28 (18)	42 (22)	14 (13)	399 (220)
Single without Muon	15 (10)	29 (15)	232 (91)	49 (25)	34 (14)	20 (9)	4 (3)	383 (167)
TOTAL CANDIDATES	30 (17)	70 (31)	651 (255)	130 (70)	86 (40)	86 (35)	31 (24)	1084 (472)

[events]

( ) means a multi-prong + multi-prong.

AUE : Aichi University of Education
GIFU : Gifu University
NGY : Nagoya University
OCU : Osaka City University and Science Education Institute of Osaka Prefecture
TOHO : Toho University
UU : Utsunomiya University
KOBE : Kobe University

V-MOD : Vertical Module.
H-MOD : Horizontal Module.

Table 5.2: Summary of scanning in Toho Univ.

Module# (module)	12 (3/8)	15 (1/4)	18 (1/4)	22 (1/16)	23 (1/4)	TOTAL
Events of DST <Category 1,2 & 3>	392	304	402	84	455	1637
Tried to Search 1ry	340	276	340	74	385	1415
Found (Found/Tried)	322 (94.7%)	269 (97.5%)	331 (97.4%)	68 (91.9%)	373 (96.9%)	1363 (96.3%)
Muon not Seen at 1ry (Muon not Seen/Found)	114 (35.4%)	90 (33.5%)	150 (45.3%)	35 (51.5%)	123 (33.0%)	512 (37.6%)
Tried to Search Decay	114	87	148	35	123	507
After Graphic Check	78	82	119	27	104	410
Decay Candidates in Main Block						
Pair with Muon	3(2)	5(2)	4(1)	2(0)	4(2)	18(7)
Pair without Muon	1(1)	2(0)	1(0)	0	1(0)	5(1)
Single with Muon	9(6)	5(3)	6(3)	3(1)	5(5)	28(18)
Single without Muon	5(0)	5(3)	14(8)	1(0)	9(3)	34(14)
Others	1(0)	0	0	0	0	1(0)
Charm Candidate Total	19(9)	17(8)	25(12)	6(1)	19(10)	86(40)
( )→ multi-multi						
Candidates/Found	(5.9%)	(6.3%)	(7.6%)	(8.8%)	(5.1%)	(6.3%)

Some notations in Table 5.2 are explained in the following. DST is the abbreviation of "Data Summary Tape" where the all events located in the emulsion target are stored separately with the module number. "Found/ Tried" is the ratio of number of events found to that of the location tried with the help of counter information. Sometime, events are so happened to be expected right on the edge or just in the beam spots. Such events can not be found and are removed from the statistics of the ratio of "Found/Tried". This process is called the fiducial volume cut.

5.1.2 Events sample for $\Gamma(D^0 \to K^-\mu^+\nu_\mu)$ analysis

As stated in Chapter 1, the main research in this thesis is the investigation of the weak interaction, in particular, the properties of semi-muonic D^0 charm decay. We made a careful selection on the decay sample of events in order to get sample as pure as possible for the study of $D^0 \to K^-\mu^+\nu_\mu$ which required the following conditions.

5.1.2.1 Blob check at decay vertex

To select pure charm decay sample, the vertices of decay candidates were carefully examined under the microscope with high magnification for mainly Auger electron, a recoiled heavy nucleus or nuclear-breakup.

The decay like vertices sometime have a slow electron forming with a few grains. Such an electron is Auger electron which is emitted as the result of nuclear excitation.

If such a signal attached at the vertex of event, the event is not a charm decay. Such events are thus removed from the candidates of the charm decay.

The vertex check was done with a few people independently. This careful check with 0.5 μm resolution in space is only possible with nuclear emulsion target, and

bring us a strong confidence of pure event selection. Table 5.3 shows the result of checking the decay vertices with high magnification in Toho laboratory.

5.1.2.2 Physical requirements for charm vertex

The decay vertex must be found in the emulsion target in order to eliminate fake vertex by counter reconstruction. And all daughter tracks must be matched with the corresponding counter tracks and further their momenta must have been analyzed.

All vertices were required to have one track identified as a muon, and to have an emulsion-measured decay length $>$ 1mm.

After passing all requirements, the sample for the study of $D^0 \to K^-\mu^+\nu_\mu$ survived was altogether 121 two-prong decay and 3 four-prong decay candidates.

5.2 List of Background in Decay Candidates

In the decay search process, we observed decay like topology vertices, but some vertices are not real charm decay. Thus all the vertices must be studied carefully. Components of background in charm decay topology are listed in the following.

1. In neutral decay topologies:
   (a) N2 topology background events are from;
      i. Electron pair.
      ii. Strange particle decay.
      iii. Inelastic scattering (with Nh=0,Ns=2), caused by a neutral hadron.
   (b) N4 topology background events are from;

Table 5.3: Result of blob check at decay vertex.

1) Number of charm vertices at different places.

	Total # of vertices
A) In upper layer on the base (330 microns).	42
B) In polystyrene base (70 microns thickness).	16
C) In lower layer on the base (330 micron).	49
D) Very near the emulsion surface.	11
	118 vertices
	93 events

2) Result of blob check under *100 objective lens to type C, *50 objective lens to others.

	(a)	(b)	(c)	sub total	(d)	(e)	(f)	total
A)	37	1	1	39	2	1	0	42
B)	15	0	0	15	0	0	1	16
C)	44	2	0	46	2	0	1	49
D)	10	1	0	11	0	0	0	11

Figures indicate the number of decay candidate vertices.
(a): clear.
(b): almost clear, but uncertain.
(c): very near primary interaction.
(d): with Auger electrons.
(e): with blob.
(f): not a decay vertex.

3) 7 events rejected from charm candidates list.

EVENT #	TYPE	REASON
R1815E3061	C3 with muon	with Auger electrons
R1825E0611	N2 without muon	with Auger electrons
R2006E2418	C1 with muon	with Auger electrons
R2011E0466	C1 without muon	not decay vertex (scattering)
R2249E0972	N2 without muon	with Auger electrons
R2251E0611	C1 without muon	not decay vertex
R2263E4531	C3 with muon	with blob

i. Inelastic scattering (with Nh=0,Ns=4),

caused by a neutral hadron.

2. In charged decay topologies:

(a) C1 topology background events are from;

i. Inelastic scattering (with Nh=0,Ns=1).

ii. Strange particle decay.

iii. Elastic scattering.

(b) C3 topology background events are from;

i. Inelastic interaction (with Nh=0,Ns=3).

ii. Strange particle decay.

iii. Diffractive dissociation.

Here Nh and Ns mean the numbers of heavy tracks and of shower tracks, respectively. In this analysis, only neutral decay candidate samples are used for the analysis. The evaluations of the decay rate and the decay width critically depend on the contamination of events. Thus the elimination of backgrounds is essential. The neutral backgrounds will be discussed in the below. The estimation and the discussion on the charged backgrounds has been given in the author's Master thesis[46] and elsewhere[47, 48].

5.3 Estimation of Neutral Backgrounds

5.3.1 Electron pair

For electron pair, almost in all cases, the pair was discriminated easily from the genuine charm decay since the opening angle of electron pair is very small as compared

to that of D^0 decay. Typical opening angle of electron pair is a few mrad and that of charm decay is some ten mrad. This is because the transverse momentum reflect the mass of the particle which is decaying. In some cases the opening angle of electron pair is large when energy disparity between the two electrons is large. However one of electron in such pair is of low energy and soon suffers a typical multiple scattering.

5.3.2 Strange particle decay

For strange particle such as K^0, Λ, the decays are observed as N2 topology, so they can be the D^0 backgrounds. We required at least one track of the daughters to have a transverse momentum P_T relative to the parent direction (decay P_T) greater than 0.25 GeV/c.

Decay P_T of strange particle is smaller than 0.25 GeV/c , since the maximal momentum of the daughter of the strange particle in the rest flame is at most 0.25 GeV/c[1].

This cut eliminated all decays of strange particles.

5.3.3 Inelastic interaction

Most of inelastic interactions were eliminated by the requirement of the vertex with no heavy track. However in the special case, inelastic neutral interactions with no heavy track may appear as same topology as the D^0 meson decay. In obvious case, if the vertex has odd number of tracks, the charge conservation is incorrect. Neutral charm decay candidates must have even number of daughter tracks. It is very difficult to eliminate the inelastic neutral interactions with Nh=0 and even number of daughter tracks.

The number of N2 backgrounds without heavy track or blob is estimated from

the present experiment by the measured number of two-prong secondary inelastic interactions which have nuclear breakup tracks and an identified muon track. The measured number is 14 $\pm$ 6 events. This number must be multiplied by the known fraction of low multiplicity events with Nh=0. By using the fraction (21 $\pm$ 8 %)[49, 50] of events with Ns=3 and Nh=0 in the high energy interactions with nuclear emulsion, and by considering 1/2 for the requirement of charge conservation, the number of inelastic backgrounds is estimated as 1.5 $\pm$ 0.9 interactions in the two-prong sample of 121 decays.

Similarly the estimated background interactions in the four-prong sample is 3 and is comparable to the number of the decay candidates.

5.3.4 Backgrounds from hadronic feedthrough

In semi-muonic charm decay sample, there is another background from hadronic feedthrough (contamination of hadronic D^0 decays) which occurs as false muon identification. The contamination from two-prong hadronic decays of charm originated from decay muon of $K^{\pm}$ and $\pi^{\pm}$ mesons was estimated to be 3 $\pm$ 1 %. This fraction was estimated by using non-muonic two-prong decays of D^0 as input data to the Monte Carlo program.

A second potential source of hadronic feedthrough is that, track mismatches between the emulsion and the spectrometer. It was estimated to be (3$\pm$3)% from the number of decay candidates which have sum of the charge $\pm$ 2.

The methods of data analysis are described in Chapter 6, and the result of the analysis and the discussion are described in Chapter 7.

CHAPTER 6

ANALYSIS OF CHARM DECAYS

6.1 Introduction

The significance of investigating the relative branching fraction and the width of semi-leptonic decay of charm particles has been described in Chapter 2.

How do we know the decay width of charmed semi-leptonic decay mode? If we know the relative branching fraction of the decay mode in the semi-muonic decay of charm particles, it would give a very useful information for $\Gamma(D^0 \to K^-\mu^+\nu_\mu)$.

The most difficult point in semi-leptonic decay physics is the lack of particle identification. Because semi-leptonic decay mode involves at least one neutrino particle which is extremely difficult to detect because it has no charge, no mass and interact with matter only through the weak interaction. Thus the parent mass calculation (in Section 6.3.1)is too difficult. This is reason why the experimental report of semi-leptonic charm decay is very scarce although very interesting physics is involved in.

The most of high energy experimental groups could not have a reliable particle identifications for pions and kaons. Because the masses of pion and kaon are rather

close to each other and they are produced with high momentum in these experiments, the velocity βc of these particles become similar. This fact makes the mass separation between pion and kaon very difficult. In general, the identification of hadron tracks with high momentum are very hard even with magnets. Therefore the identification of decay mode of the semi-leptonic decays is very difficult.

As described in the above, the analysis of decay mode; $D \to K\mu\nu$ has the difficulty of the lack of track information. That is why no one yet reported the branching fraction of the above decay mode before this analysis.

Now, a new method and technique[51] developed by the author for the determination of the relative branching fractions and of $\Gamma(D^0 \to K^-\mu^+\nu_\mu)$ will be described in the following.

6.2 Analysis of Muon Transverse Momentum Distribution

Theoretically, the lepton energy spectrum for D meson decay is calculable mainly through weak current part of Weak interaction. Figure 6.1 [52] shows theoretical lepton energy spectrum for semi-leptonic decay in D meson rest frame. The present attempt is to extract the relative branching ratio of $D \to K\mu\nu$ to $D \to X\mu\nu$ from the experimental data. If the lepton energy spectrum is obtained from this experimental data, the relative branching fraction may be estimated by comparing the spectrum shown in Figure 6.1. However transformation of the energy momentum of the daughter lepton from the lab system to D meson rest system is only possible when the slopes and momenta of all daughter tracks are known. As described in Section 6.1, the daughter neutrino is not observed hence the transformation is impossible. Furthermore the momentum of the daughter K meson has not been evaluated at the

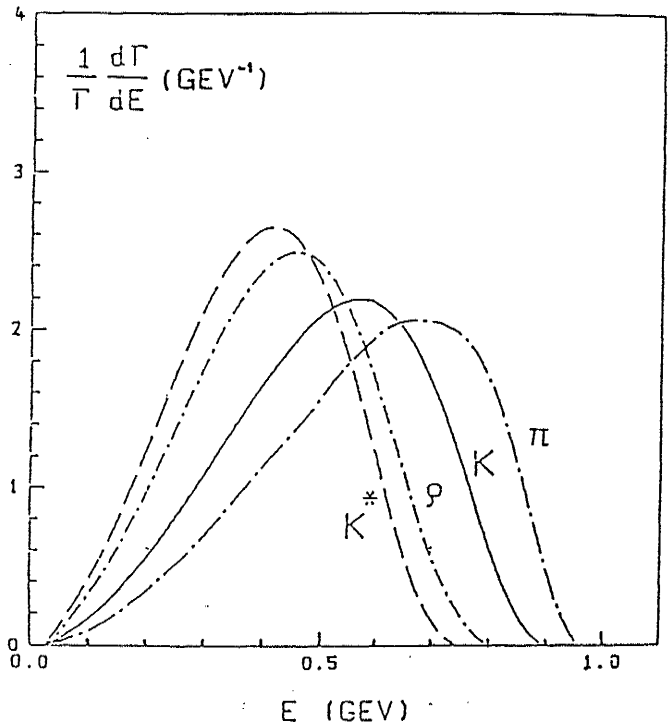

Figure 6.1: Theoretical energy spectra for semi-leptonic decays.

time. We have the observed momentum and slope of the muon in lab system.

In this analysis the main idea is to look at the kinematics of this decay mode. It is to take the distribution of transverse momentum of decay muon, $P_{T\mu}$, with respect to the parent charm particle, this was only available data at the time.

With the above situation, the determination of the branching fraction of semi-muonic charm decay mode mainly $D^0 \rightarrow K^-\mu^+\nu_\mu$ and $D^0 \rightarrow K^*(892)^-\mu^+\nu_\mu$ is attempted.

Transverse momentum of muon $P_{T\mu}$ is a Lorentz invariant variable between lab system and D meson rest system. $P_{T\mu}$ distribution for semi-leptonic charm decay must be analyzed with the Monte Carlo simulation as follows.

The outline of the Monte Carlo simulation performed for the D meson is:

1. Generation of charm particle in the interaction of 800 GeV/c proton.
2. Decay of charm particle into semi-muonic mode.
3. $P_{T\mu}$ correction for E653 experimental conditions.

6.2.1 Generation of charm particle

Charm particle is generated through the following Equation (6.1). The equation is somewhat phenomenological but widely accepted among the experimentalists who are working on the production properties of charm particles at high energy.

$$\frac{d^2\sigma}{dx_F dP_{TD}^2} = (1 - |x_F|)^n \exp(-bP_{TD}^2) \ , \tag{6.1}$$

in which $n = 8.6$ and $b = 0.847$[53] are applied for this energy region.

x_F (Feynman-x) is defined as

$$x_F \equiv \frac{P_{LD}^*}{P_{LmaxD}^*} \ , \tag{6.2}$$

where P_{TD}, P^*_{LD}, and P^*_{LmaxD} are

P_{TD} ; transverse momentum

P^*_{LD} ; longitudinal momentum

P^*_{LmaxD} ; maximum longitudinal momentum

of charm particle with respect to the beam direction and the asterisk "$*$ " indicates for the center of mass system about the incident beam and target.

6.2.1.1 Feynman-x distribution

At first, x_F distribution is generated through the probability density function as following equation

$$\frac{dN}{dx_F} = K(1-|x_F|)^n \qquad (-1 \le x_F \le 1)\ . \tag{6.3}$$

The coefficient K is able to be calculated through the integration of Equation (6.3), then the equation become

$$\frac{dN}{dx_F} = \frac{n+1}{2}(1-|x_F|)^n \qquad (-1 \le x_F \le 1)\ . \tag{6.4}$$

The probability variable has been calculated by rejection method [54].

6.2.1.2 P_T^2 distribution

P_T^2 distribution is generated according to probability density function,

$$\frac{dN}{dP_T^2} = K' \exp(-bP_{TD}^2)\ , \tag{6.5}$$

where coefficient K' is also able to be calculated by the integration of Equation (6.5), then

$$\frac{dN}{dP_{TD}^2} = b\exp(-bP_{TD}^2), \tag{6.6}$$

and P_{TD}^2 was calculated by direct method[54],

$$P_{TD}^2 = -\frac{1}{b}\ln\xi\ , \tag{6.7}$$

where ξ is uniformed random number in [0,1].

Thus we have obtained x_F and P_{TD}^2 according to Equation (6.1).

6.2.1.3 Longitudinal momentum

Maximal longitudinal momentum may be expressed as

$$P^*_{LmaxD} = \frac{\sqrt{s}}{2}\ , \tag{6.8}$$

where s is the square of the C.M.S. of the interaction. Thus P^*_{LD} is calculated based on the definition of x_F in Equation (6.2),

$$P^*_{LD} = \frac{\sqrt{s}}{2} \times x_F\ . \tag{6.9}$$

6.2.1.4 Emission angle

The emission angle of charm particle ϑ_D is expressed as

$$\vartheta_D = \tan^{-1}\left(\frac{\sqrt{P_{TD}^2}}{P_{LD}}\right)\ , \tag{6.10}$$

in which the longitudinal momentum is obtained by

$$P_{LD} = \gamma_B\left(P^*_{LD} + \beta_B\sqrt{P^{*2}_{LD} + P^{*2}_{TD} + M_D^2}\right)\ , \tag{6.11}$$

where γ_B is Lorentz γ-factor from the rest frame of charm particle to the C.M.S. of incident beam and target.

$$\gamma_B = \frac{E^*}{M_p}\ , \tag{6.12}$$

and β_B is calculated from definition of γ-factor

$$\beta_B = \sqrt{1 - \frac{1}{\gamma_B^2}}\ , \tag{6.13}$$

with energy in the center of mass system, as

$$E^* = \frac{\sqrt{s}}{2} \tag{6.14}$$

$$= \frac{\sqrt{2M_p^2 + 2M_p E_p}}{2}\ , \tag{6.15}$$

where

M_p ; mass of proton = 0.938 [GeV/c^2][1]

E_p ; energy of proton = 800 [GeV] .

From the above equations, P_D (the momentum of charm particle in lab system) can be calculated by,

$$P_D = \sqrt{P_{TD}^2 + P_{LD}^2}\ . \tag{6.16}$$

6.2.2 Semi-muonic decay of D meson

6.2.2.1 Generations of variables of decay time and decay length

The next step of the simulation is decay part of charm particle. Charm particle decays according to

$$\frac{dN}{dt} = \frac{1}{\tau}\exp\left(\frac{-t}{\tau}\right), \tag{6.17}$$

where τ is the lifetime of D meson [1],

$$\tau(D^+, D^-) = 10.7 \times 10^{-13}[sec], \qquad \tau(D^0, \bar{D}^0) = 4.28 \times 10^{-13}[sec].$$

and t is decay time variable, and is the flight time of each charm particle before decay. The decay time t was calculated by direct method using following equation,

$$t = -\tau \ln \xi\ . \tag{6.18}$$

Decay length L of each charm particle was calculated by using this t and P_D which was calculated in Equation (6.16),thus

$$L = vt\gamma = c\beta t\gamma = ct\,\frac{P_D}{M_D\,c}\ , \tag{6.19}$$

where c is velocity of light, and M_D is mass of D meson[1],

$$M_{D^\pm} = 1.869[GeV/c^2], \qquad M_{D^0,\bar{D}^0} = 1.864[GeV/c^2].$$

6.2.2.2 Emission angle of muon particle

Here, muon is assumed to be emitted isotropically in the rest frame of charm particle. In Figure 6.2.2.2, $d\omega$ is differential solid angle in polar coordinates,

$$d\omega = \sin\vartheta\, d\vartheta\, d\varphi\ . \tag{6.20}$$

Integral calculation is

$$4\pi = \int_0^\pi \sin\vartheta\, d\vartheta \int_0^{2\pi} d\varphi\ , \tag{6.21}$$

where 4π is integrated solid angle and normalized to unity in this analysis. Probability density function $f(\vartheta)$ was calculated from Equation (6.21),

$$f(\vartheta) = \frac{1}{2}\sin\vartheta \qquad (0 \le \vartheta < \pi). \tag{6.22}$$

because

$$\int_0^{2\pi} \varphi = 2\pi\ . \tag{6.23}$$

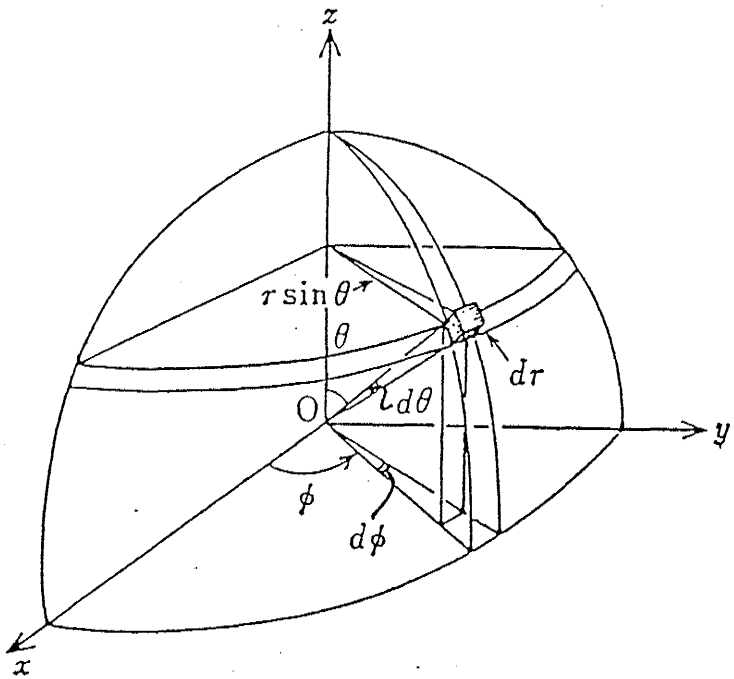

Figure 6.2: Differential solid angle in polar coordinates.

The zenith angle ϑ was calculated by the direct method,

$$\int_0^\eta f(\vartheta)\,d\vartheta \equiv \xi\,, \tag{6.24}$$

$$= \frac{1}{2}[-\cos\vartheta]_0^\eta$$

$$= \frac{1}{2}(-\cos\eta+1)\,, \tag{6.25}$$

with ξ is uniformed random number in [0,1],

$$\cos\eta = -2\xi+1\,. \tag{6.26}$$

Then ϑ is obtained by substituting ϑ for η

$$\vartheta = cos^{-1}(-2\xi+1) \qquad (0\le\vartheta<\pi). \tag{6.27}$$

Probability density function $g(\varphi)$ of azimuthal angle φ is

$$g(\varphi) = \frac{1}{2\pi} \qquad (0\le\varphi<2\pi). \tag{6.28}$$

The azimuthal angle φ was also calculated by direct method,

$$\int_0^\eta g(\varphi)\,d\varphi \equiv \xi\,, \tag{6.29}$$

$$= \frac{1}{2\pi}[\varphi]_0^\eta$$

$$= \frac{\eta}{2\pi}\,. \tag{6.30}$$

Then φ is obtained by substituting φ for η

$$\varphi = 2\pi\xi \qquad (0\le\varphi<2\pi). \tag{6.31}$$

In semi-muonic decay of charm, ϑ and φ are regarded as ϑ^*_μ, φ^*_μ that the emission angles in the rest frame of charm particle. Momentum P^*_μ was calculated by E^*_μ which was obtained from E^*_{lepton} distribution in Figure 6.1.

$$P^* = \sqrt{E^{*2}-M_\mu^2}\,, \tag{6.32}$$

where M_μ is mass of muon, 0.106 GeV/c^2.

The longitudinal momentum of muon with respect to parent (charm particle) direction; $P_{L_\mu}^{(P)\ *}$, and transverse momentum of it; $P_{T_\mu}^{(P)\ *}$ (= $P_{T_\mu}^{(P)}$ in lab system) were calculated as,

$$P_{L_\mu}^{(P)} = P_\mu^* \cos\vartheta_\mu^* , \tag{6.33}$$

$$P_{T_\mu}^{(P)} = P_\mu^* \sin\vartheta_\mu^* = P_{T_\mu}^{(P)} , \tag{6.34}$$

and $P_{L_\mu}^{(P)}$ in lab system is

$$P_{L_\mu}^{(P)} = \gamma_D \sqrt{P_{L_\mu}{}^{*} + \beta_D (P_{L_\mu}{}^{*2} + P_{T_\mu}{}^{2} + M_\mu^2)} , \tag{6.35}$$

where γ_D is a Lorentz factor between C.M.S. and lab system of charm meson

$$\gamma_D = \frac{\sqrt{P_D^2 + M_D^2}}{M_D} . \tag{6.36}$$

β_D is,

$$\beta_D = \sqrt{1 - \frac{1}{\gamma_D^2}} . \tag{6.37}$$

Momentum of muon P_μ in lab system was calculated from $P_{L_\mu}^{(P)}$ and $P_{T_\mu}^{(P)}$,

$$P_\mu = \sqrt{(P_{L_\mu}^{(P)\ 2} + P_{T_\mu}^{(P)\ 2})} . \tag{6.38}$$

And $\tan\vartheta_\mu^{(P)}$ was also calculated by,

$$\tan\vartheta_\mu^{(P)} = \frac{P_{T_\mu}^{(P)}}{P_{L_\mu}^{(P)}} . \tag{6.39}$$

6.2.2.3 Coordinate transformation

To estimate the effects of off-line P_{T_μ} cut, the calculation was performed for the transverse momentum of muon $P_{T_\mu}^{(B)}$ (with respect to beam) by the coordinate transformation.

Firstly, the direction of charm particle is regarded as Z axis and the momentum components of muon $(P_X, P_Y, P_Z)_\mu^{(P)}$ are expressed as;

$$P_X^{(P)} = P_{T_\mu}^{(P)} \cos\varphi_\mu^{(P)} , \tag{6.40}$$

$$P_Y^{(P)} = P_{T_\mu}^{(P)} \sin\varphi_\mu^{(P)} , \tag{6.41}$$

$$P_Z^{(P)} = P_{L_\mu}^{(P)} . \tag{6.42}$$

Secondly, when the beam direction is regarded as Z axis, the momentum components of muon $(P_X, P_Y, P_Z)_\mu^{(B)}$ are

$$\begin{pmatrix} P_X \\ P_Y \\ P_Z \end{pmatrix}_\mu^{(B)} = \begin{pmatrix} \cos\vartheta\cos\varphi & -\sin\varphi & \sin\vartheta\cos\varphi \\ \cos\vartheta\sin\varphi & \cos\varphi & \sin\vartheta\sin\varphi \\ -\sin\vartheta & 0 & \cos\vartheta \end{pmatrix}_\mu^{(B)} \times \begin{pmatrix} P_X \\ P_Y \\ P_Z \end{pmatrix}_\mu^{(P)} \tag{6.43}$$

$P_{T_\mu}^{(B)}$ was then calculated as,

$$P_{T_\mu}^{(B)} = \sqrt{(P_X^{(B)2} + P_Y^{(B)2})} . \tag{6.44}$$

Now, the effect due to the off-line cuts of P_μ, P_{T_μ}, and I. P.$_\mu$ on the P_{T_μ} distribution was evaluated from the relations as mentioned the above. Figure 6.3 shows $P_{T_\mu}^{(P)}$ distribution calculated in various decay modes.

6.2.3 P_{T_μ} correction for experimental conditions

The various theoretical curves described in the above need to be corrected for the actual E653 experimental conditions such as the acceptance and the off-line selections to enrich charm particles.

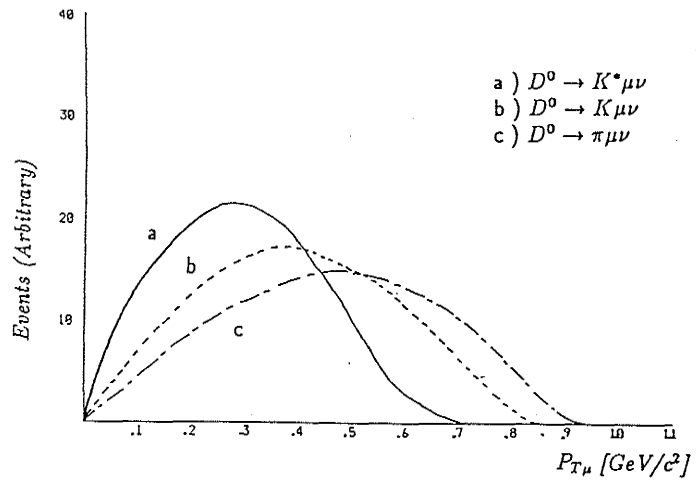

Figure 6.3: $P_{T\mu}$ distribution in various decay modes.

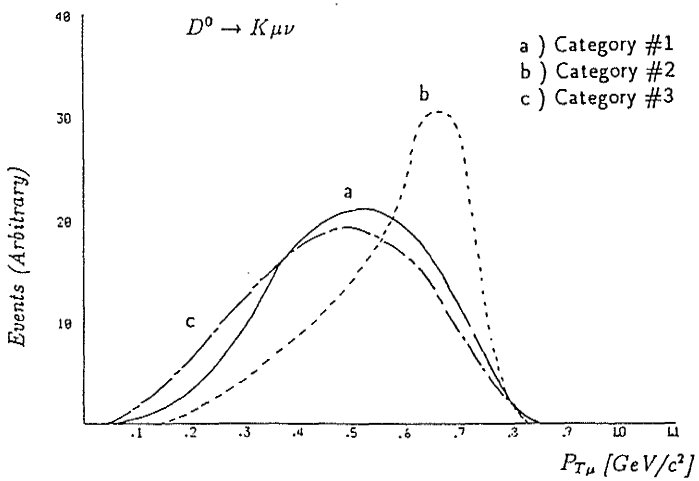

Figure 6.4: $P_{T\mu}$ distribution in various categories cut.

The off-line selection was applied on the transverse momentum of muon evaluated with respect to the beam direction; $P_{T\mu}^{(B)}$. Therefore this selection affects to the distribution of $P_{T\mu}^{(P)}$; with respect to the parent direction.

Figure 6.4 shows the $P_{T\mu}^{(P)}$ distributions for various categories (see Chapter 3)including the effects of the off-line selections of P_μ, $P_{T\mu}$, I. P.$_\mu$.

6.3 Analysis of Mass Distribution

6.3.1 Invariant mass

Invariant mass analysis is performed with the energy and the momentum conservation of the charm decay system. The momentum of the particle is expressed as

$$\vec{P}_i = (P_{iX}, P_{iY}, P_{iZ}) \ , \tag{6.45}$$

and the invariant mass M_0 of three body decay case has been calculated by

$$\begin{aligned} M_0^2 &= E_0^2 - P_0^2 \ , \qquad (6.46) \\ &= \left(\sqrt{m_1^2+P_1^2}+\sqrt{m_2^2+P_2^2}+\sqrt{m_3^2+P_3^2}\right)^2 - (\vec{P}_1+\vec{P}_2+\vec{P}_3)^2 \\ &= m_1^2+m_2^2+m_3^2 \\ &\quad + 2\left(\sqrt{m_1^2+P_1^2}\sqrt{m_2^2+P_2^2} - \vec{P}_1\cdot\vec{P}_2\right) \\ &\quad + 2\left(\sqrt{m_2^2+P_2^2}\sqrt{m_3^2+P_3^2} - \vec{P}_2\cdot\vec{P}_3\right) \\ &\quad + 2\left(\sqrt{m_3^2+P_3^2}\sqrt{m_1^2+P_1^2} - \vec{P}_3\cdot\vec{P}_1\right) \ , \qquad (6.47) \end{aligned}$$

where suffix "$_0$" indicates for the parent particle, and $\vec{P}_i \cdot \vec{P}_j$ is inner products,

$$\vec{P}_1 \cdot \vec{P}_2 = P_{1X}P_{2X} + P_{1Y}P_{2Y} + P_{1Z}P_{2Z}. \tag{6.48}$$

General expression of invariant mass is written as

$$\begin{aligned} M_0^2 &= E_0^2 - P_0^2 \\ &= \sum_i^n m_i^2 + \sum_{i \neq j}(E_i E_j - \vec{P}_i \cdot \vec{P}_j) \\ &= \sum_i^n m_i^2 + 2\sum_{i<j}(E_i E_j - \vec{P}_i \cdot \vec{P}_j)\ . \end{aligned} \tag{6.49}$$

6.3.2 Momentum balance

In semi-muonic decay mode of $D^0 \to K^- \mu^+ \nu_\mu$, at least one neutrino is missing. Neutrino carried some unknown momentum but its transverse component can be estimated from the imbalance of the transverse momentum of the charm rest frame. This imbalance is called the missing P_T. Figure 6.5 shows the total momentum vectors in the laboratory system.

P_{Tvis} is the sum of perpendicular components of the visible momenta of the charged daughter tracks to the parent direction, in which the visible momenta were measured and recorded in the spectrometer.

$$P_{Tvis(X)} = \sum_{i=1}^{n} P_{Xi}, \tag{6.50}$$

$$P_{Tvis(Y)} = \sum_{i=1}^{n} P_{Yi}. \tag{6.51}$$

This P_{Tvis} is equal to the missing P_T. In general,

$$P_{Tneut(X)} = -P_{Tvis(X)}, \tag{6.52}$$

$$P_{Tneut(Y)} = -P_{Tvis(Y)}. \tag{6.53}$$

where P_{Tneut} equals to the sum of P_T of missing neutral particles. Thus when the missing particle is only one neutrino, the P_{Tneut} is equal to $P_{Tneutrino}$.

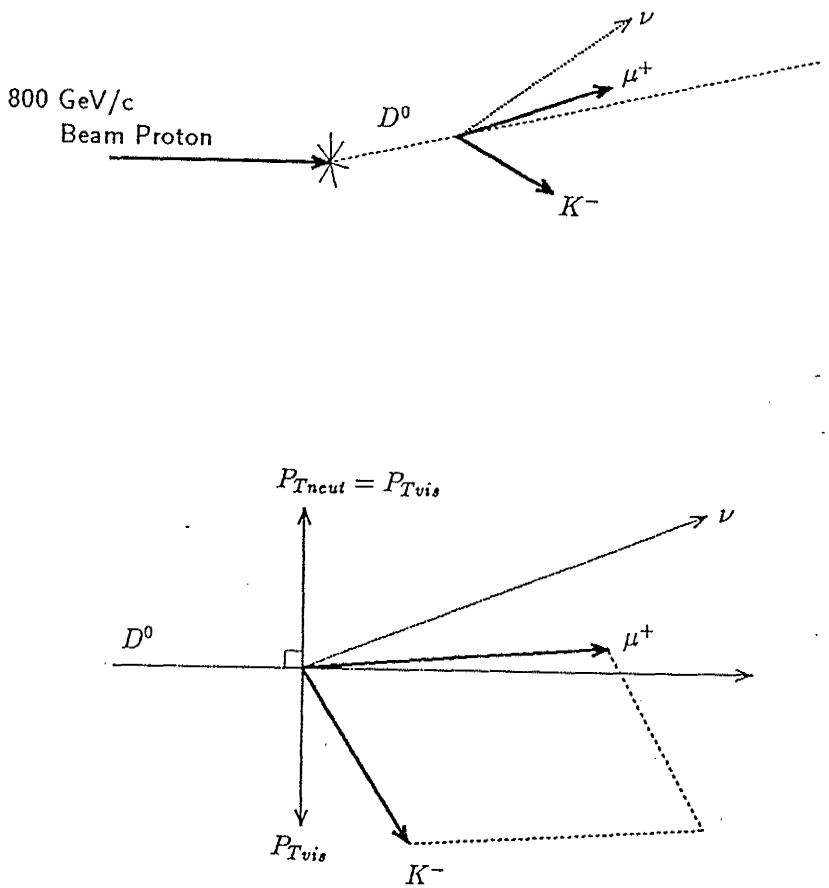

Figure 6.5: Total momentum vectors in the laboratory frame.

On the other hand, the missing longitudinal momentum P_{Lneut} was not constrained. The parent mass was calculated by assuming various P_{Lneut} values. Figure 6.6 shows a example of –1C fit in semi-muonic two-prong decay with assumption for decay mode of $D^0 \rightarrow K^-\mu^+\nu_\mu$. The horizontal axis represents P_{Lneut} and the vertical axis expresses the calculated parent mass. The missing neutrino was assumed to be massless.

6.3.3 Minimum mass distribution

In Figure 6.6, the minimum parent mass;M_{min} is the value at the lowest point of –1C fitting curve. This point corresponds to where P_{Lneut} is equal to zero in the center of mass system of charm. In other words,

$$M_{min} = \sqrt{m_{vis}{}^2 + P_t^2} + \sqrt{m_{neut}{}^2 + P_t^2}. \tag{6.54}$$

where m_{vis} is the invariant mass calculated from the visible (charged) tracks, and m_{neut} is equal to zero if the decay mode was assumed to emit one neutrino.

The fraction f for the semi-muonic decay $K\mu\nu$ is determined from the shape of the M_{min} distribution. In this case, the charged hadron track from decay vertex was assumed to be a kaon particle.

To apply the M_{min} method in the above decay mode, the kinematic information of both charged daughter tracks of two-prong decay is necessary. Therefore the decay sample used for this analysis was required to have both the charged decay tracks matched with the counter tracks.

M_{min} distribution has a peak, in particular $D^0 \rightarrow K^-\mu^+\nu_\mu$ would have a very narrow peak. In this regard, M_{min} distribution is different from $P_{T\mu}$ distribution. The M_{min} distribution will become broader for multi neutral decay mode and shift the peak to lower M_{min} value.

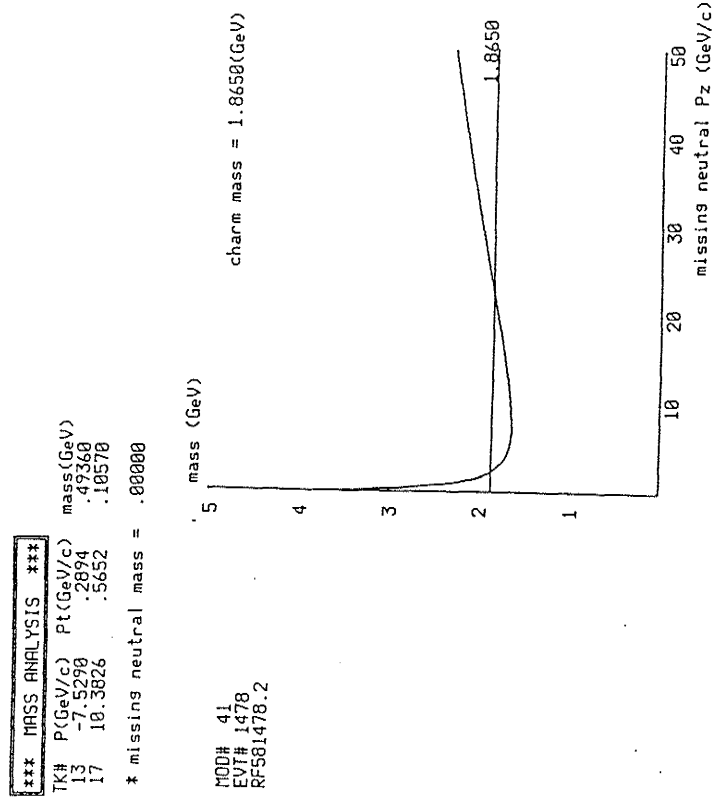

Figure 6.6: -1C fit in semi-muonic two-prong decay.

The M_{min} method could separate between one neutral missing decay mode and multi neutral missing decay mode. Figure 6.7 shows the Monte Carlo simulation of M_{min} distributions in which the hadron track is assigned as kaon. The solid line represents the true decay mode $D^0 \rightarrow K^-\mu^+\nu_\mu$ and the dashed line for $D^0 \rightarrow \pi^-\mu^+\nu_\mu$ and the dotted line for $D^0 \rightarrow K^*(892)^-\mu^+\nu_\mu$.

We had identification for muon but not for hadron track. In this $D^0 \rightarrow K^-\mu^+\nu_\mu$ analysis the M_{min} was calculated by assuming the mass of charged hadron as a kaon mass.

In the M_{min} distribution for $D^0 \rightarrow K^-\mu^+\nu_\mu$, if the hadron mass is assigned as kaon mass, then the M_{min} distribution exhibits a sharp peak at the D^0 mass. However if the decay mode is $D^0 \rightarrow \pi^-\mu^+\nu_\mu$, and the hadron mass is assigned as kaon mass, then the peak of M_{min} distribution will be shifted to the larger side and the tail extending beyond the D^0 mass.

If the decay includes one or more neutral hadrons in addition to the neutrino, the M_{min} distribution becomes broader and its maximum shifts to lower mass.

Figure 6.7 was assumed that the vertex resolution is perfect. The histograms depict Monte Carlo M_{min} distributions for the two prong decays $D^0 \rightarrow K^-\mu^+\nu_\mu$ (solid), $D^0 \rightarrow K^*(892)^-\mu^+\nu_\mu$ (dots), and $D^0 \rightarrow \pi^-\mu^+\nu_\mu$ (dashes). However in reality the measurement includes error. In this experiment, the knowledge of M_{min} is affected mainly by the measurement of the charm direction in the emulsion and the typical error for this measurements is $\sim$ 1.0 mrad.

Figure 6.8 exhibits M_{min} distribution for the decay mode $D^0 \rightarrow K^-\mu^+\nu_\mu$, taking into account the vertex resolution. Histograms depict $D^0 \rightarrow K^-\mu^+\nu_\mu$ (solid), $D^0 \rightarrow K^*(892)^-\mu^+\nu_\mu$ (heavy dashes),$D^0 \rightarrow \pi^-\mu^+\nu_\mu$ (dots).

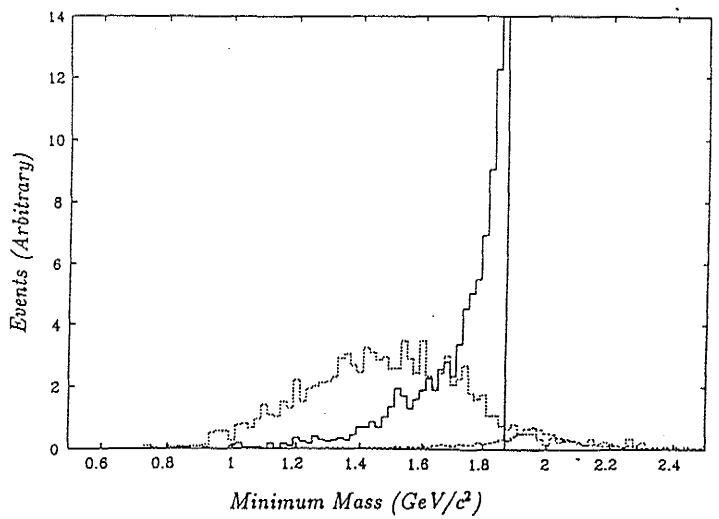

Figure 6.7: M_{min} distribution with perfect vertex resolution.

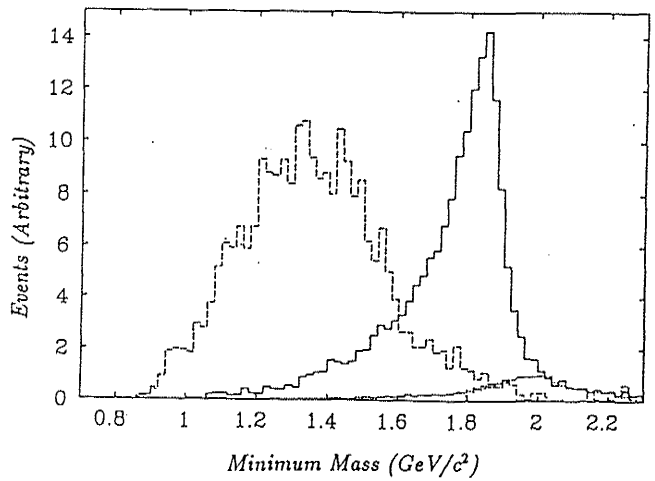

Figure 6.8: M_{min} distribution with 1 mrad vertex resolution.

CHAPTER 7

EXPERIMENTAL RESULTS AND DISCUSSION

7.1 The Fraction f

The decay branching fraction f of $D^0 \to K^-\mu^+\nu_\mu$ is defined as :

$$f \equiv \frac{\Gamma(D^0 \to K^-\mu^+\nu_\mu)}{\Gamma(D^0 \to X^-\mu^+\nu_\mu)}. \tag{7.1}$$

There are two methods to determine the value of f, namely from the differential frequency distributions of $P_{T\mu}$ and of M_{min} . The actual procedures are described in the following section.

7.1.1 Fitting for $P_{T\mu}$ distribution

Figure 7.1 shows the comparison of the experimental $P_{T\mu}$ distribution (histogram) with fitted Monte Carlo $P_{T\mu}$ distributions (curves). The solid curve depicts $P_{T\mu}$ distribution for $D^0 \to K^-\mu^+\nu_\mu$ and dashed curve for $D^0 \to K^*(892)^-\mu^+\nu_\mu$. The fraction f was obtained from χ^2 and maximum likelihood fits.

7.1.1.1 χ^2 fit for $P_{T\mu}$ distribution

Here, f is evaluated from the experimental data of $P_{T\mu}$ of all events with two prong semi-muonic decay modes. In fitting the experimental distribution of $P_{T\mu}$ and

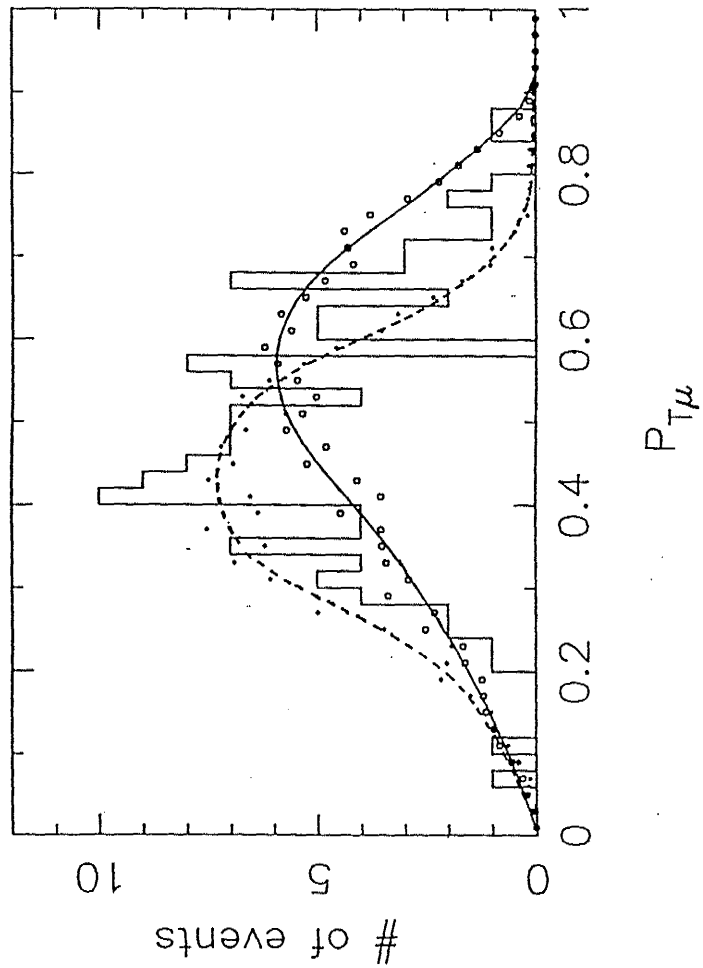

Figure 7.1: Comparison of the experimental $P_{T\mu}$ distribution with Monte Carlo $P_{T\mu}$ distributions.

of M_{min} , the single parameter f_{raw} is obtained at first as a raw value for $K\mu\nu$ fraction.

χ^2 is defined as,

$$\chi^2 = \sum_{i=1}^{N} \frac{(x_i - \bar{x}_i)^2}{\sigma_i^2} \ . \tag{7.2}$$

For the sample of this analysis contains 121 two-prong decays, f_{raw} has been obtained from $P_{T\mu}$ distribution,

$$f_{raw} = 0.43 \qquad \frac{\chi^2}{N.D.F.} = 0.70 \ , \tag{7.3}$$

where N.D.F. is number of degrees of freedom, and the fitting region is $(0.3 \leq P_{T\mu} < 0.8)$ GeV/c.

7.1.1.2 Maximum likelihood fit for $P_{T\mu}$ distribution

The f_{raw} has been obtained also by maximum likelihood fit from $P_{T\mu}$ distribution,

$$f_{raw} = 0.42 \pm 0.13 \ . \tag{7.4}$$

This rate is in good agreement with the one from M_{min} distribution in Equation (7.6) as described in the next section. Figure 7.2 shows the fitting curve and experimental data (histogram).

The error of this value is a little larger than the error of M_{min} method. This effect is mainly attributed to the shape of the distribution curve. The M_{min} distribution has a narrow peak while the $P_{T\mu}$ distribution has no such narrow one because the input information is less than the former. However a estimation of f still can be made even if no information on the hadron decay product of the $K\mu\nu$ is available.

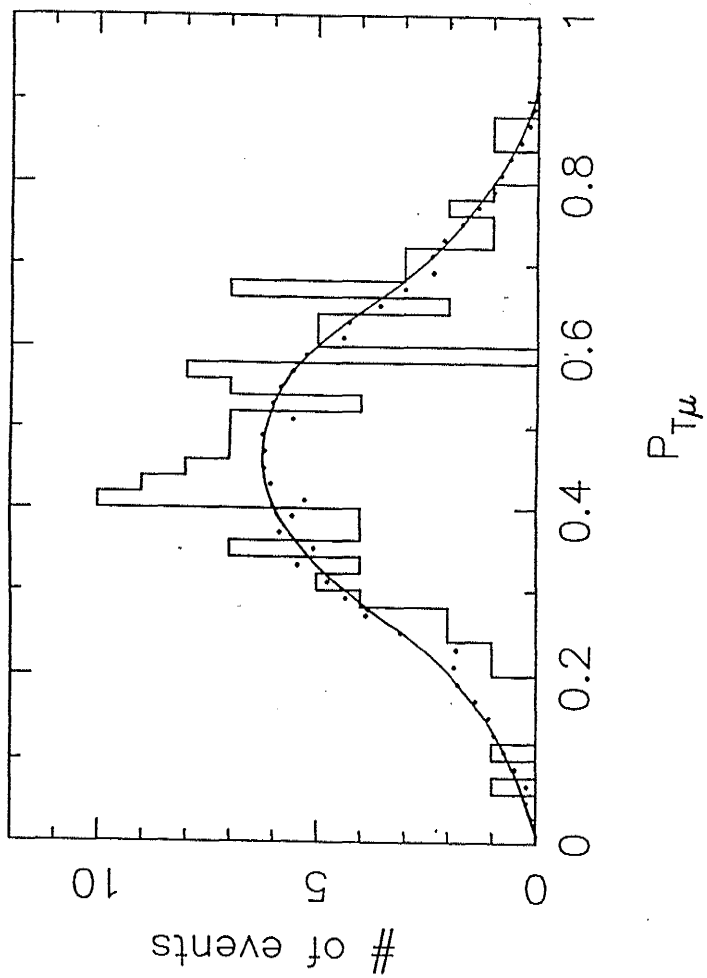

Figure 7.2: Experimental $P_{T\mu}$ distribution with fitted Monte Carlo $P_{T\mu}$ distributions.

7.1.2 Maximum likelihood fit for M_{min} distribution

In this section f is evaluated from the distribution of M_{min}. Figure 7.3 shows the comparison of the experimental M_{min} distribution (error flags) with fitted Monte Carlo M_{min} distributions (histograms).

The f_{raw} evaluation from M_{min} distribution has been obtained by maximum likelihood fit

$$\ln L = \sum_{events} \ln\{0.97[f_{raw}(I_{K\mu\nu}+0.11I_{K\mu\nu})+(1-1.11f_{raw})I_{k\mu\nu X}]+0.03I_{had}\} \ , \quad (7.5)$$

where the I_i are Monte Carlo M_{min} distributions (normalized to unity) for $D^0 \to K^-\mu^+\nu_\mu$, for $D^0 \to \pi^-\mu^+\nu_\mu$ (fixed at 11 % of $K\mu\nu$) , for $D^0 \to K^-\mu^+\nu_\mu$ X, and for the 3% contamination from feedthrough of hadronic decays.

If $I_{K\mu\nu}$ is assumed to contain only $K^{*-}\mu^+\nu$, f_{raw} is obtained as

$$f_{raw} = 0.42 \pm 0.07 \ . \quad (7.6)$$

Full E653 Monte Carlo program which is based on GEANT Monte Carlo program[55], simulated charge deposit in the silicon detectors, drift time over the threshold in the drift chambers, acceptances, reconstruction efficiencies, and resolution for the spectrometer. The charm pairs were generated with the Equation (6.1) with n=8.0 for Feynman x distribution and b=1.0 for the transverse momentum P_T distribution,the both values are consistent with those measured in the charm production at 800 GeV proton-proton interaction[53]. Those values are also estimated in this experiment[47]. The charm pairs have been superimposed as uncorrelated charm particles to the proton-emulsion interactions generated by the FRITIOF program[56].

These simulated data were processed by the same routines used for the real data, and thus it provided a test for the analysis procedure as well as the determination

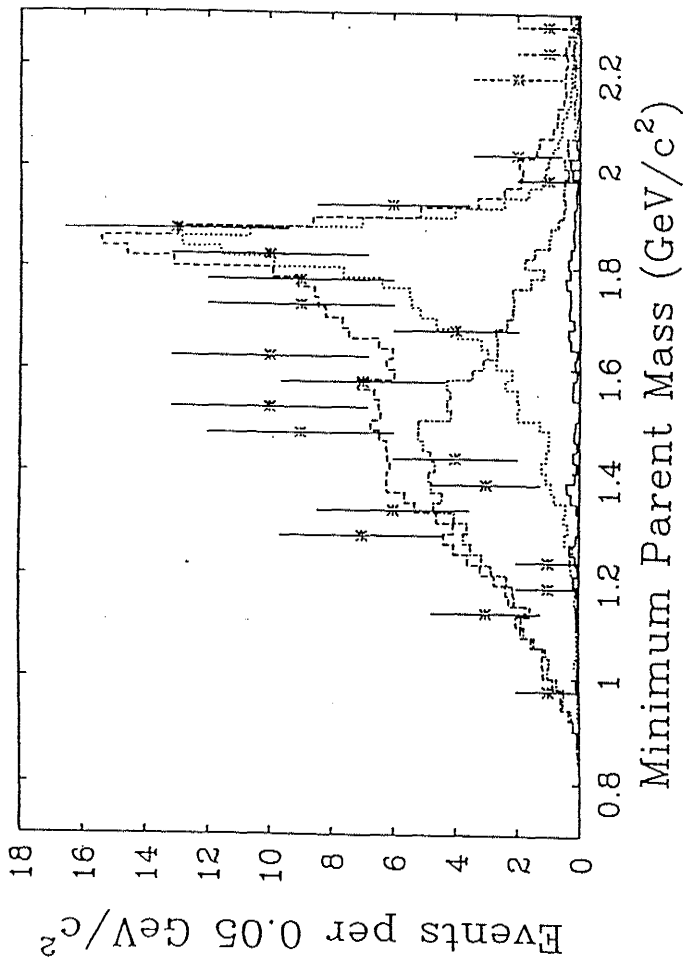

Figure 7.3: Comparison of the experimental M_{min} distribution with fitted Monte Carlo M_{min} distributions.

Table 7.1: Detection efficiencies for various decay modes.

$K\mu\nu$	0.072
$\pi\mu\nu$	0.061
$K^*\mu\nu$	0.046
$K^*\pi^0\mu\nu$	0.027
$K\rho\mu\nu$	0.021
$K\eta\mu\nu$	0.031

Table 7.2: The fraction f for multi-neutral decay modes.

Mix of multineutral decay modes	f_{raw}	f_{corr}	Conf. Lev.
100% $K^*\mu\nu$	0.42±0.07	0.32±0.06	44%
50% $K^*\mu\nu$ +25% $K\rho\mu\nu$ +25% $K\eta\mu\nu$	0.48±0.07	0.32±0.05	58%
50% $K^*\mu\nu$ +50% $K\rho\mu\nu$	0.46±0.07	0.29±0.04	24%
60% $K^*\mu\nu$ +40% $K\eta\mu\nu$	0.48±0.07	0.34±0.05	22%
80% $K^*\mu\nu$ +20% $K^*\pi^0\mu\nu$	0.44±0.07	0.31±0.05	13%

of the decay vertex detection efficiency. The efficiencies for the various decay modes, which are shown in Table 7.1, have been determined in full E653 Monte Carlo simulation.

As seen in the Table 7.2, if $I_{K\mu\nu}$ is assumed to contain only $K^{*-}\mu^+\nu$, the corrected fraction f_{corr} has been obtained as

$$f_{corr} = 0.32 \pm 0.05 \ , \tag{7.7}$$

with a confidence level of 44%.

The confidence level for each multi-neutral fitting hypothesis has been obtained by generating 100 Monte Carlo 'experiments', each having f_{raw} equal to the fitted value of f_{raw} for the data. We then fitted each of these Monte Carlo samples as if it were data, and obtained the fitted f_{raw} and value of likelihood function for each Monte Carlo 'experiment'.

The confidence level has been obtained by asking how many of these Monte Carlo experiments have a better value of likelihood than the data.

For example, if 40 out of the 100 Monte Carlo experiments have better value of likelihood than the data, the confidence level is

$$C.L. = 100\% \times (1. - \frac{40}{100}) \ , \tag{7.8}$$

$$= 60\% \ . \tag{7.9}$$

The width of the distribution of these 100 values of fitted f_{raw} has also been checked with the estimated error on f_{raw} from the fit to the data.

7.1.3 Multi-neutral decay mode

The value of f evaluated from the fits are not very sensitive to the choice of multi-neutral decay modes ($I_{K\mu\nu X}$). The fraction f was evaluated with mixtures of the two-neutral mode $K^{*-}\mu^+\nu$ and the multi-neutral modes $K^{*-}\pi^0\mu^+\nu$, $K^0\rho^-\mu^+\nu$ and $K^-\eta^0\mu^+\nu$. Table 7.2 shows the fraction f for the multi-neutral decay modes of all allowed mixtures for $I_{K\mu\nu X}$. The maximum contribution of the multi-neutral modes is constrained by the observed number of four-prong candidates, which was three. For example, every assumed two-prong decay $D^0 \to K^-\eta^0\mu^+\nu$ with $\eta \to \gamma\gamma$ or $\to 3\pi^0$ implies[1] 0.41 four-prong decay with $\eta \to \pi^+\pi^-\pi^0$ or $\to \pi^+\pi^-\gamma$.

We have not allowed multi-neutral mixtures which would contribute more than

three observed four-prong events. This restricts the sum of the multi-neutral branching fractions to be comparable or less than that for $K^{*-}\mu^+\nu$.

7.1.4 Effect of Systematic errors

A systematic error from uncertainty of vertex resolution estimate has been checked by changing the assumed vertex resolution. The larger resolution is assumed, the larger f value is obtained. Thus it is very important to measure the vertices accurately and to estimate the errors on them properly.

The typical error of (X,Y) direction was obtained 1 μm by measuring the position of five reference beam tracks. The error of beam direction has been obtained by the measurements of the thickness of emulsion plates.

Emulsion thickness were measured at arbitrary 4 points. Data of the thickness of emulsion plates for modules from #9 to #20 of E653 Run 1, were measured directly by the thickness-gauge at 4 points in each plate.

Table 7.3 shows the data of the thickness of emulsion plates for module #18 as an example. Sheet number equal to plate number. Plate # 1 is the thickness of 70 μm emulsion was coated in both sides of 300 μm polystyrene base. Plate #2 $\sim$ #5 are 70 μm emulsion thickness on both sides of 100 μm base, and plate #6 $\sim$ # 25 are 330μm emulsion on both sides of 70 μm base. Average value was calculated with removing maximum and minimum values.

Using the data of module #9 $\sim$ #20, the mean value (+ include gap between plates) of the emulsion thickness with standard deviation is found to be 741(+10) $\pm$ 15 μm . The variation of plate thickness among the modules ranges from 716(+10) to 756(+10) μm , and the variation is larger than the variation within a plate, which is less than 20 micron. Taking the variation among modules into the consideration,

Table 7.3: Measurements data of emulsion plate thickness.

MOD#18	E653-1					
sheet#	1	2	3	4	average	comment
01	465	450	435	475		300μm base
02	225	250	240	230		100μm base
03	240	210	215	250		
04	250	245	230	230		
05	225	220	260	230		
06	750	750	745	735	748	70μm base
07	765	755	750	740	753	
08	745	760	755	740	750	
09	770	765	760	745	763	
10	770	765	755	745	760	
11	760	760	755	750	758	
12	760	755	770	735	758	
13	760	760	760	745	760	
14	765	750	755	740	753	
15	765	755	745	745	750	
16	760	750	750	740	750	
17	770	750	750	740	750	
18	750	750	750	740	750	
19	755	750	750	735	750	
20	760	765	750	740	755	
21	755	750	755	750	753	
22	760	755	755	750	755	
23	760	755	740	730	748	
24	750	750	760	745	750	
25	755	760	750	740	753	

the average thickness was obtained to be 740(+10) ± 25 μm .

Thus we may have the following formula for the error of Z direction (i.e., the beam direction).

$$dZ = \sqrt{5^2 + \frac{Z}{(740+10)} \times 25^2} \quad \mu m \ , \tag{7.10}$$

where the first term, 5 micron, is the error of measurement at the vertex plate by optical focusing and the second term is from uncertainty of the thickness of emulsion plate with Z direction which is the component of measured flight length of charm meson.

Combining error of (X,Y) and that of Z, a typical error of charm direction was obtained as ±1.0 mrad. This error mainly contributes to the M_{min} resolution. There are some other uncertainties which affect the result.

As the result, the systematic error included contributions come from uncertainties in multi-neutral composition (± 0.030), in M_{min} resolution (± 0.016), in the number of real four-prong events (± 0.016), in Monte Carlo statistics and parametrization (± 0.016), in the treatment of backgrounds (± 0.010), in the fraction of $\pi\mu\nu$ (± 0.016) and in the X_F and P_T dependence (± 0.006). These contributions are combined in the quadrature.

The fraction f is quite stable to assumed production parameters n and b. It is changed by ± 2 % when n is replaced by $n \pm 3$. It is stable within 1 σ statistical standard deviation for cuts on decay length larger than 4 mm (which removes about a half of the data sample), and stable to 0.67 σ for cuts on the lowest allowed M_{min} from 0.8 to 1.3 GeV.

Finally, the fraction f has been obtained from f_{raw} by correcting each contribution of the experimental acceptance and efficiency,

$$f = 0.32 \pm 0.05 \pm 0.05 \ . \tag{7.11}$$

7.2 Decay Width of $D^0 \to K^-\mu^+\nu_\mu$

Once the value of f was obtained, the decay width $\Gamma(D^0 \to K^-\mu^+\nu_\mu)$ is evaluated.

The branching fraction and the partial decay rate for $D^0 \to K^-\mu^+\nu_\mu$ is calculated by combining our value of f with the world-average value of semi-electronic branching fraction [1],

$$BR(D^0 \to e^+X) = (7.7 \pm 1.2)\% \ , \tag{7.12}$$

and for D^0 lifetime[1]

$$\tau_{D^0} = (4.21 \pm 0.10) \times 10^{-13} sec. \tag{7.13}$$

Total decay width for D^0 is

$$\Gamma_{total} = \frac{\hbar}{\tau_{D^0}} \ , \tag{7.14}$$

and the total semi-electronic decay width is given by

$$\Gamma_{eX} = \Gamma_{total} \times BR(D^0 \to e^+X) \ . \tag{7.15}$$

Semi-muonic branching fraction $BR(D^0 \to \mu^+X)$ is derived from

$$\omega = \frac{G_\pi^2}{30\pi^2}\Delta^5 r \left(\frac{m_e}{\Delta}\right), \tag{7.16}$$

where Δ and $r(x)$ are

$$\Delta = M_{D^0} - M_{K^+} \ , \tag{7.17}$$

$$r(x) = \sqrt{1-x^2}\left(1 - \frac{9}{2}x^2 + 4x^4\right) + \frac{15}{2}x^4 \ln\left(1 + \frac{\sqrt{1+x^2}}{x}\right) \ . \tag{7.18}$$

Since the universality between electron and muon is hold, the ratio between electronic and muonic decay modes is

$$\frac{r(x_\mu)}{r(x_e)} = 0.96 \ , \tag{7.19}$$

and that is purely due to the mass difference between electron and muon.

Then total semi-muonic branching fraction is expressed as

$$BR(D^0 \to \mu^+ X) = 0.96 \times BR(D^0 \to e^+ X) \ . \tag{7.20}$$

And semi-muonic branching fraction therefore is obtained as

$$BR(D^0 \to K^- \mu^+ \nu_\mu \ ) = (2.4 \pm 0.4 \pm 0.5)\% \ , \tag{7.21}$$

and partial decay width for $D^0 \to K^- \mu^+ \nu_\mu$ can be obtained as

$$\Gamma\,(D^0 \to K^- \mu^+ \nu_\mu) \ = (5.6 \pm 0.9 \pm 1.2) \times 10^{10} s^{-1} \ , \tag{7.22}$$

Once the decay width is evaluated, either the form factor or C-K-M matrix element $|V_{cs}|$ can be estimated.

7.3 V_{cs} ; C-K-M Matrix Element

The C-K-M matrix element $|V_{cs}|$ is related with the decay width as

$$\Gamma\,(D^0 \to K^- \mu^+ \nu_\mu) \ = \ |f_+(0)|^2 \cdot |V_{cs}|^2 \cdot (1.54 \times 10^{11}) s^{-1} \ , \tag{7.23}$$

$$= \ (5.6 \pm 0.9 \pm 1.2) \times 10^{10} s^{-1} \ , \tag{7.24}$$

where $|f_+(0)|$ is the form factor, then we get

$$|f_+(0)|^2 \cdot |V_{cs}|^2 = 0.36 \pm 0.06 \pm 0.08 \ . \tag{7.25}$$

If $|f_+(0)|$ is known, this measurement can be translated directly into a measurement of $|V_{cs}|$. If we take

$$|f_+(0)| = 0.7 \pm 0.1 \ , \tag{7.26}$$

then $|V_{cs}|$ can be obtained as the model-dependent result

$$|V_{cs}| = 0.86 \pm 0.14 \pm 0.16 \ . \tag{7.27}$$

7.4 Form Factor

In contrast with the preceding section, now we evaluate the form factor by assuming the value of V_{cs}. Also we assumed three generation of quarks and leptons and used the value of $|V_{cs}|$ as

$$|V_{cs}| = 0.974 \pm 0.001 \ , \tag{7.28}$$

then the form factor is obtained as

$$|f_+(0)| = 0.62 \pm 0.05 \pm 0.07 \ . \tag{7.29}$$

7.5 Semi-electronic Decay Mode

If μ-e universality is assumed, we can compare our result of the decay width to the electronic decay data obtained in the experiment E691 and Mark III.

E691 is the experiment of tagged photon spectrometer with fixed target [22]. They reported that

$$\Gamma(D^0 \to K^- e^+ \nu) \ = (9.1 \pm 0.7 \pm 1.7) \times 10^{10} s^{-1}, \tag{7.30}$$

which is somewhat larger than our value. However in May 1991, E691 collaboration has obtained new result [57]

$$\Gamma(D^+ \to \overline{K}^0 e \nu) \ = (5.6 \pm 0.8 \pm 1.5) \times 10^{10} s^{-1}. \tag{7.31}$$

This value should be equal to the transition rate $\Gamma(D^0 \to K^-\mu^+\nu_\mu)$ by isospin invariance. Thus our result is in good agreement with the new result of E691. The weighted average of E691 results is

$$\Gamma(D \to Ke\nu) = (7.3 \pm 1.3) \times 10^{10} s^{-1}. \quad (7.32)$$

Mark III is the e^+e^- collider experiment and by using the peak of the Ψ (3770). The Mark III collaboration has obtained[23]

$$\Gamma(D^0 \to K^-e^+\nu) = (8.1 \pm 1.2 \pm 0.9) \times 10^{10} s^{-1}, \quad (7.33)$$

$$\Gamma(D^+ \to \overline{K}^0 e\nu) = (6.1^{+1.5}_{-1.0} \pm 0.7) \times 10^{10} s^{-1}. \quad (7.34)$$

The weighted average of Mark III results is

$$\Gamma(D \to Ke\nu) = (7.0 \pm 1.0) \times 10^{10} s^{-1}. \quad (7.35)$$

Our result is consistent with these results for $\Gamma(D \to Ke\nu)$ of the other experiments within the errors.

CHAPTER 8

CONCLUSIONS

The experimental study of exclusive semi-leptonic decays is particularly interesting because the phenomena are clear to be interpreted than those of the non-leptonic decays. Also there is a number of the theoretical investigations regarding the weak interaction, and for some aspects the quantitative predictions have been suggested. However the data of experimental evaluations for those aspects are very rare because of the difficulty to carry out such evaluation with experiments.

The author had developed a method to evaluate the relative fraction (=relative branching fraction) of the semi-muonic decay of D^0 charm meson with only muon information. Then the quantitative evaluations of the Cabibbo-Kobayashi-Maskawa Matrix element and the form factor were made for the first time after International seminar in 1989[51]. At the time no such experimental data were reported in the world.

To accomplish the present research work in E653 experiment, the author's graduate study was devoted to working on a number of tasks as summarized in the following.

8.1 Beam Exposure and Target Mover Control

For this research, the author had been to the United States of America in order to carry out the E653 experiment with international collaborators, in particular, the beam exposure to the emulsion target, the control of target mover and the target processing. The beam intensity and the uniformity were achieved for 49 independent emulsion target modules. The exposure condition is one of the most crucial things to accomplish the successful research (see Section 3.1).

8.2 Constructions of Semi-automated Microscope Stage and its Interface

8.2.1 Semi-automated stage

In the emulsion-counter hybrid experiment, the most concerned matter was the accuracy of the mechanical control of the microscope stage. The accuracy must be in the order of 1.0 μm and is the same order of the spatial resolution of emulsion target. Also the position-reproduction-accuracy of the stage after long distance movement must be within a few μm since an event must be located out of 100 million events. Both requirements were achieved by the careful production and the assemble with use of the interferometer (see Section 3.4).

8.2.2 DOMS interface

The motor driven microscope stage is controlled by the host computer with number of programs. Therefore a device ,DOMS, was constructed to interface between the host computer and the stage, which consisted of 12 circuit boards (see Section 3.4).

8.3 Evaluation of Relative Branching Fraction of $D^0 \to K^-\mu^+\nu_\mu$

Semi-muonic branching fraction has been evaluated through two analyses, one of which is with '$P_{T\mu}$ distribution analysis' and the other is with 'M_{min} distribution analysis'.

8.3.1 $P_{T\mu}$ distribution analysis

The $P_{T\mu}$ analysis is simple and effective method when the information of the decay hadron is not available (see Section 6.2). With this method, the author presented quantitative evaluations on the branching fraction of $D^0 \to K^-\mu^+\nu_\mu$, C-K-M etc. for the first time at the International seminar in 1989. Until that time no such result has been reported, thus the impact accelerated the researches on semi-muonic decay modes. The method is stable to the accuracy of vertex measurements. $P_{T\mu}$ distribution had been separated into the fractions for different decay modes. The fraction f obtained from $P_{T\mu}$ distribution analysis is consistent with the value from M_{min} distribution analysis. However this method provided rather loose separations of decay modes.

8.3.2 M_{min} distribution analysis

A different approach to evaluate the relative fraction of $D^0 \to K^-\mu^+\nu_\mu$ is made with the analysis of M_{min} distribution which has a narrow peak for $D^0 \to K^-\mu^+\nu_\mu$ (see Section 6.3). The analysis used the momentum information of all decay hadrons. The information became available when the on-line data were fully processed. Then the M_{min} method gave better separation between one neutral decay mode and multi neutral decay modes than the $P_{T\mu}$ method. By using M_{min} method,

the decay width of $D^0 \to K^-\mu^+\nu_\mu$ has been obtained as

$$\Gamma(D^0 \to K^-\mu^+\nu_\mu) = (5.6 \pm 0.9 \pm 1.2) \times 10^{10} sec^{-1},$$

in Fermilab-E653 which is the 'emulsion-counter hybrid experiment'. This rate is consistent with E691 and Mark III results within the error where the lepton is an electron instead of a muon.

8.4 C-K-M Matrix Element and Form Factor

Once the relative branching fraction f or the decay width $\Gamma(D^0 \to K^-\mu^+\nu_\mu)$ was evaluated, the form factor of $D^0 \to K^-\mu^+\nu_\mu$ was estimated by the relation described in the Chapter 7 assuming either the value of V_{cs} or $|f_+(0)|$ and the three generations of lepton and quark family (see Sections 7.3 and 7.4).

First, the evaluation of the form factor is presented,

$$|f_+(0)| = 0.62 \pm 0.05 \pm 0.07 .$$

On the other hand, when the form factor was assumed as

$$|f_+(0)| = 0.7 \pm 0.1 ,$$

then model-dependent value of V_{cs} has been evaluated as

$$|V_{cs}| = 0.86 \pm 0.14 \pm 0.16 .$$

The above value may be compared with the theoretical predictions.

8.5 Future Prospects

As demonstrated in the above, the physics of semi-leptonic decays provides deep insights of the standard theory and now the research becomes more active but still a few reports are available. The author evaluated the decay mode of $D^0 \to K^-\mu^+\nu_\mu$.

However study of another Cabibbo favored decay mode $D^0 \to K^*(892)^-\mu^+\nu_\mu$, more complicated than $D^0 \to K^-\mu^+\nu_\mu$, is also very important because this physics of semi-leptonic decays could not be discussed by one decay mode only.

To date, the second run data of our experiment E653 has been analyzed in each laboratory of the collaboration and about thousand of charm candidates will be accumulated in the nuclear emulsion targets. Therefore with the accurate vertex measurement of charm decays, the relative fraction of exclusive decay modes of unsolved semi-leptonic or pure leptonic charm decays can be investigated in the near future.

APPENDIX

SUMMARY OF EVENT SAMPLE

In this appendix, the event-data sample are summarized for the analysis of $\Gamma(D^0 \to K\mu\nu)$ in Chapter 6 and 7.

- $M_{min}\ \pi\mu\nu$: M_{min} value in assumption of decay mode $D^0 \to \pi\mu\nu$.
- $M_{min}\ K\mu\nu$: M_{min} value in assumption of decay mode $D^0 \to K\mu\nu$.
- P_{Tvis} : Sum of the visible P_T, which equal to missing P_T.
- δP_{Tvis} : Error of P_{Tvis}.
- P_T Trk1 : P_T of a daughter track.
- P_T Trk2 : P_T of another daughter track.
- μ Trk : Track number of muon.
- V/H : Vertex at the emulsion in Vertical module or in Horizontal module.

SEMI-MUONIC D^0 EVENT

Run	Event	M_{min}		P_{Tvis}	δP_{Tvis}	P_T		μ	V/H
		$\pi\mu\nu$	$K\mu\nu$			Trk 1	Trk 2	Trk	
1249	1437	1.309	1.525	0.124	0.038	0.525	0.592	1	VE
1477	3914	1.488	2.255	0.560	0.025	0.686	0.126	1	VE
1478	4640	0.894	1.133	0.029	0.011	0.405	0.423	2	VE
1489	3156	1.716	1.841	0.213	0.099	0.762	0.711	2	VE
1491	65	1.564	1.837	0.743	0.019	0.307	0.472	2	VE
1493	5014	1.105	1.351	0.387	0.013	0.416	0.205	1	VE
1495	442	1.225	1.509	0.474	0.024	0.146	0.503	2	VE
1504	2935	1.734	1.872	0.252	0.020	0.779	0.672	1	VE
1506	2435	1.472	1.706	0.471	0.012	0.457	0.506	2	VE
1511	4467	1.582	1.699	0.400	0.113	0.410	0.670	1	VE
1514	1232	1.623	1.911	0.430	0.044	0.645	0.469	1	VE
1515	2674	1.573	1.766	0.293	0.016	0.663	0.585	1	VE
1548	1093	1.245	1.439	0.305	0.051	0.259	0.558	2	VE
1550	1582	1.279	1.689	0.362	0.089	0.525	0.305	1	VE
1550	5106	1.617	1.732	0.336	0.089	0.778	0.450	2	VE
1551	2305	0.934	1.296	0.257	0.020	0.235	0.386	2	VE
1553	3108	1.947	3.001	0.858	0.311	0.074	0.860	2	VE
1557	2212	1.178	1.696	0.510	0.031	0.229	0.308	2	VE
1562	775	1.498	1.675	0.373	0.037	0.338	0.710	1	VE
1569	393	1.022	1.275	0.378	0.026	0.220	0.371	1	VE
1570	1139	1.133	1.308	0.247	0.009	0.385	0.412	2	VE
1574	5418	1.172	1.321	0.172	0.040	0.349	0.478	2	VE
1576	1781	0.893	1.797	0.349	0.108	0.033	0.320	2	VE
1576	2911	1.006	1.481	0.236	0.059	0.456	0.229	1	VE
1578	3450	0.961	1.270	0.342	0.026	0.348	0.209	1	VE
1580	4375	1.250	1.465	0.029	0.027	0.593	0.566	2	VE
1580	4915	1.726	1.817	0.442	0.197	0.293	0.454	1	VE
1582	1889	1.526	1.629	0.127	0.044	0.666	0.568	2	VE
1584	396	1.616	1.855	0.699	0.019	0.476	0.388	2	VE
1586	2596	1.643	1.770	0.186	0.482	0.780	0.595	1	VE
1587	444	1.223	1.488	0.243	0.019	0.476	0.429	2	VE
1595	1315	1.305	1.547	0.426	0.022	0.488	0.324	2	VE
1597	2914	1.671	1.838	0.403	0.041	0.671	0.569	1	VE
1599	4711	1.070	1.301	0.469	0.038	0.189	0.281	2	VE
1601	994	1.734	1.842	0.588	0.081	0.736	0.285	2	VE

Run	Event	M_{min}		P_{Tvis}	δP_{Tvis}	P_T		μ	V/H
		$\pi\mu\nu$	$K\mu\nu$			Trk 1	Trk 2	Trk	
1616	2542	1.275	1.693	0.084	0.009	0.394	0.460	1	VE
1617	552	1.604	1.695	0.072	0.138	0.613	0.679	1	VE
1624	4853	0.868	1.209	0.126	0.023	0.287	0.401	2	VE
1626	2233	1.648	1.776	0.576	0.032	0.319	0.462	2	VE
1631	1186	1.845	1.962	0.658	0.046	0.898	0.258	2	VE
1637	3461	1.516	1.916	0.692	0.028	0.284	0.464	2	VE
1645	2984	1.277	1.611	0.489	0.037	0.123	0.572	2	VE
1647	4992	1.881	1.968	0.147	0.118	0.829	0.740	2	VE
1650	4729	1.213	1.432	0.448	0.042	0.466	0.018	1	VE
1651	2583	1.825	1.928	0.293	0.058	0.605	0.871	1	VE
1660	2092	1.157	1.378	0.231	0.057	0.537	0.325	2	VE
1660	3692	1.608	1.752	0.378	0.035	0.704	0.501	2	VE
1661	115	1.345	1.481	0.389	0.079	0.287	0.373	2	VE
1671	5059	1.556	1.732	0.563	0.056	0.556	0.320	1	VE
1673	2873	1.472	1.694	0.318	0.030	0.439	0.624	1	VE
1675	1447	1.366	1.794	0.517	0.023	0.453	0.294	1	VE
1708	4028	1.707	1.987	0.803	0.111	0.297	0.565	2	HE
1715	156	1.292	1.572	0.576	0.013	0.478	0.098	1	HE
1715	183	1.284	1.484	0.552	0.027	0.369	0.196	1	HE
1720	913	1.751	1.892	0.406	0.046	0.682	0.622	1	HE
1724	3784	1.233	1.520	0.438	0.019	0.120	0.557	2	HE
1743	3918	1.416	1.554	0.125	0.023	0.609	0.629	2	VE
1745	4701	1.062	1.277	0.240	0.036	0.435	0.321	1	VE
1747	3849	1.802	1.905	0.256	0.022	0.760	0.591	1	VE
1747	4000	1.617	1.705	0.231	1.628	0.387	0.573	1	VE
1748	375	1.656	1.857	0.344	0.062	0.724	0.443	2	VE
1749	4644	1.790	1.912	0.427	0.032	0.489	0.851	1	VE
1752	733	1.448	1.593	0.301	0.033	0.709	0.411	2	VE
1753	2393	0.821	1.498	0.012	0.013	0.248	0.260	2	VE
1754	140	0.844	1.292	0.350	0.012	0.087	0.312	2	VE
1759	2267	1.016	1.204	0.116	0.063	0.441	0.396	1	VE
1762	1278	1.623	1.760	0.482	0.383	0.235	0.611	2	VE
1769	2377	0.921	1.112	0.100	0.052	0.382	0.365	1	VE
1774	1782	1.786	1.889	0.301	0.108	0.670	0.661	1	VE
1782	1476	1.528	1.796	0.467	0.056	0.479	0.496	1	VE

Run	Event	M_{min}		P_{Tvis}	δP_{Tvis}	P_T		μ	V/H
		$\pi\mu\nu$	$K\mu\nu$			Trk 1	Trk 2	Trk	
1782	2932	1.395	1.564	0.263	0.055	0.660	0.439	2	VE
1787	3151	1.603	1.701	0.148	0.090	0.574	0.714	1	VE
1800	1716	1.494	1.913	0.596	0.014	0.688	0.145	1	VE
1830	3981	1.787	1.892	0.385	0.023	0.806	0.520	2	VE
1833	282	1.059	1.429	0.251	0.023	0.263	0.491	2	VE
1852	4225	1.529	1.638	0.341	0.088	0.368	0.677	1	VE
1864	2992	1.634	1.807	0.305	0.033	0.772	0.468	2	VE
1865	4963	1.638	1.942	0.592	0.009	0.675	0.331	1	VE
1869	907	1.293	1.465	0.319	0.053	0.258	0.547	2	VE
1874	2309	0.876	1.809	0.283	0.038	0.082	0.307	2	VE
1882	925	1.581	1.794	0.317	0.033	0.482	0.665	1	VE
1889	2466	1.532	1.721	0.448	0.011	0.259	0.702	1	HE
1931	5234	1.606	1.782	0.686	0.027	0.299	0.486	2	VE
1932	953	1.378	1.579	0.295	0.013	0.535	0.516	2	VE
1946	3428	1.440	1.726	0.529	0.043	0.343	0.462	1	VE
1947	2930	1.529	1.909	0.485	0.010	0.414	0.450	2	VE
1989	4783	1.190	1.480	0.372	0.040	0.195	0.551	2	VE
1990	3448	1.494	2.349	0.485	0.027	0.232	0.416	2	VE
1993	1857	1.443	1.695	0.355	0.033	0.436	0.613	2	VE
1997	502	1.275	1.868	0.413	0.128	0.430	0.252	1	VE
1997	2587	0.674	0.973	0.071	0.014	0.237	0.308	2	VE
2001	4401	1.403	1.556	0.060	0.082	0.642	0.676	2	VE
2014	347	1.275	1.469	0.250	0.041	0.579	0.405	2	VE
2016	22	1.435	1.633	0.559	0.017	0.185	0.521	2	VE
2028	3915	1.474	1.656	0.368	0.035	0.342	0.675	2	VE
2029	2732	1.396	1.545	0.439	0.186	0.678	0.243	2	VE
2033	3827	1.505	1.639	0.476	0.107	0.162	0.474	2	VE
2035	1333	1.605	1.926	0.627	0.029	0.443	0.402	2	VE
2037	3923	0.904	1.473	0.270	0.342	0.024	0.252	1	VE
2041	4969	1.214	1.507	0.057	0.074	0.516	0.497	2	VE
2044	438	1.012	1.408	0.301	0.020	0.359	0.098	2	VE
2056	618	1.376	2.234	0.544	0.061	0.440	0.167	1	VE
2058	2408	1.437	1.701	0.178	0.019	0.542	0.574	1	VE
2059	4569	1.564	1.732	0.123	0.030	0.638	0.750	1	VE
2069	2311	1.679	1.875	0.186	0.043	0.603	0.756	1	VE

Run	Event	M_{min}		P_{Tvis}	δP_{Tvis}	P_T		μ	V/H
		$\pi\mu\nu$	$K\mu\nu$			Trk 1	Trk 2	Trk	
2070	1978	1.571	1.757	0.455	0.030	0.393	0.661	2	VE
2097	1569	1.672	1.763	0.267	0.152	0.665	0.452	2	VE
2103	1889	0.935	1.166	0.248	0.045	0.292	0.327	2	VE
2107	2631	1.735	1.865	0.025	0.051	0.851	0.841	1	VE
2107	4481	0.724	1.409	0.259	0.009	0.038	0.280	2	VE
2108	1636	1.462	1.702	0.279	0.038	0.537	0.578	2	VE
2110	2432	1.720	1.841	0.517	0.035	0.622	0.476	2	VE
2127	4890	1.082	1.259	0.170	0.020	0.427	0.415	1	VE
2132	3632	1.151	1.411	0.237	0.030	0.355	0.479	1	VE
2136	3095	1.079	1.211	0.037	0.181	0.447	0.420	2	VE
2150	1213	1.191	1.582	0.379	0.020	0.564	0.192	1	HE
2211	1631	1.702	1.820	0.211	0.216	0.679	0.772	1	VE
2212	4048	1.161	1.318	0.310	0.026	0.362	0.333	2	VE
2224	5003	1.026	1.693	0.433	0.030	0.372	0.105	1	VE
2227	4855	0.894	1.484	0.380	0.018	0.034	0.352	2	VE
2234	870	1.488	1.660	0.171	0.241	0.608	0.675	1	VE
2236	2784	1.306	1.582	0.541	0.034	0.260	0.453	2	VE
2239	768	1.791	2.077	0.195	0.198	0.785	0.610	1	VE
2250	423	1.197	1.796	0.389	0.041	0.503	0.192	1	VE
2250	2967	0.925	1.449	0.291	0.026	0.041	0.285	1	VE
2261	329	1.487	1.804	0.289	0.031	0.526	0.456	2	VE
2263	2764	1.351	1.500	0.351	0.371	0.517	0.190	1	VE
2270	4549	1.450	1.564	0.247	0.066	0.515	0.349	1	VE
2272	2966	1.609	1.800	0.509	0.034	0.653	0.391	1	VE
2275	2221	1.262	1.422	0.388	0.021	0.416	0.349	2	VE
2287	3798	1.357	1.537	0.457	0.035	0.233	0.615	1	HE
2321	715	1.584	1.826	0.568	0.230	0.413	0.526	1	VE
2321	3540	1.266	1.534	0.272	0.041	0.577	0.380	1	VE
2333	613	1.086	1.438	0.511	0.020	0.313	0.201	1	VE
2333	840	1.500	1.634	0.132	0.063	0.597	0.706	2	VE
2334	3427	1.602	1.713	0.243	0.040	0.638	0.512	1	VE

References

[1] Particle Data Group, J. J. Hernández *et al.*, Phys. Lett. B239(1990)1.

[2] K. Kodama *et al.*, Nucl. Instr. & Meth. A289(1990)146.

[3] K. Niu, E. Mikumo, and Y. Maeda, Prog. Theor. Phys. 46(1971)1644.

[4] T. Hayashi *et al.*, Prog. Theor. Phys. 47(1972)280,1998.

[5] N. Ushida *et al.*, Nucl. Instr. & Meth. 224(1984)50.

[6] N. Ushida *et al.*, Phys. Rev. Lett. 56(1986)1771.

[7] N. Ushida *et al.*, Phys. Rev. Lett. 56(1986)1767.

[8] S. Aoki *et al.*, Nucl. Instr. & Meth. A274(1989)64.

[9] J. P. Albanese *et al.*, Phys. Lett. 158B(1985)186.

[10] S. Aoki *et al.*, Phys. Lett., B209(1988)113.

[11] S. Weinberg, Phys. Rev. Lett. 19(1967)1264.

[12] M. Kobayashi and T. Maskawa, Prog. Theor. Phys. 49(1973)652.

[13] G. S. Abrams *et al.*, Phys. Rev. Lett. 63(1989)2173.

[14] D. Decamp *et al.*, to be published in Phys. Lett. B(1990).

[15] P. Abreu *et al.*, CERN-EP/90-32, to be published in Phys. Lett. B(1990).

[16] B. Adeva *et al.*, submitted to Phys. Lett. B(1990).

[17] M. Z. Akrawy *et al.*, to be published in Phys. Lett. B(1990).

[18] N. Cabibbo, Phys. Rev. Lett. 10(1963)531.

[19] L.-L. Chau and W.-Y. Keung, Phys. Rev. Lett. 53(1984)1802.

[20] L. Wolfenstein, Phys. Rev. Lett. 51(1983)1945.

[21] V. Barger, T. Gottschalk and R. J. N. Phillips Phys. Rev. D16(1977)746.

[22] J. C. Anjos *et al.*, Phys. Rev. Lett. 62(1989)1587.

[23] Z. Bai *et al.*, Phys. Rev. Lett. 66(1991)1011.

[24] M. Wirbel, B. Stech and M. Bauer, Z. Phys. C34(1987)103; M. Bauer and M. Wirbel, Z. Phys. C42(1989)671.

[25] N. Isgur *et al.*, Phys. Rev. D39(1989)799; D. Score and N. Isgur, Phys. Rev. D40(1989)1491.

[26] F. J. Gilman and R. L. Singleton, Phys. Rev. D41(1990)142; T. Altomari and L. Wolfenstein, Phys. RevD37(1988)681.

[27] J. G. Körner and G. A. Schuler, Z. Phys. C38(1988)511; Z. Phys. C46(1990)93.

[28] K.G.Wilson, Phys. Rev. D10(1974)2445

[29] V. Lubicz, G. Martinelli and C. T. Sachrajda, Nucl. Phys. B356(1991)301.

[30] M. Crisafulli *et al.*, Phys. Lett. 223(1989)90.

[31] C. W. Bernard, A. X. El-Khadra and A. Soni, U. C. Santa Barbara preprint NSF-ITP-90-215, and Fermilab preprint Fermilab-Pub-91/242-T, 1991; Phys. Rev. D 43(1991)2140

[32] P. Ball, V. M. Braun and H. G. Dosch, Heidelberg University preprint, HD-THEP-91-16, 1991; Phys. Rev. D 44(1991)3567

[33] C. A. Dominguez and N. Paver, Phys. Lett. 207(1988)499.

[34] T. M. Aliev, A. A. Ovchinnikov and V. A. Slobodenyuk, Trieste preprint, IC/89/382, 1989.

[35] D. M. Potter, Carnegie-Mellon University preprint, CMU-HEP91-19(1991)

[36] P. Nason, S. Dawson, and R. K. Ellis, Nucl. Phys. B327(1989)49.

[37] Gene A. Oleynik, Ph. D. thesis, The Ohio State University, (1987).

[38] James M Dunlea, Ph. D. thesis, The Ohio State University, (1987).

[39] Akbar Mokhtarani, Ph. D. theses, Univ. of California at Davis, (1988).

[40] M. Aguilar-Benitez *et al.*, Z. Phys. C36(1987)559.

[41] Arne P. Freyberger, Ph. D. thesis, Carnegie Mellon University, (1990).

[42] Takeo Watanabe, Ph. D. thesis, Osaka City University, (1990).

[43] H. Fuchi *et al.*, J. Phys. Soc. Japan 47(1979)687.

[44] S. Aoki *et al.*, Nucl. Tracks 12(1986)249.

[45] Hiroyasu Tajima, M. Sc. thesis, Nagoya University, (1988).

[46] Shoji Watanabe, M. Sc. thesis, Toho University(1989).

[47] K. Kodama *et al.*, Phys. Lett. B263(1991)573.

[48] K. Kodama *et al.*, Phys. Lett. B263(1991)579.

[49] H. Winzeler, Nucl. Phys. 69(1965)661.

[50] S. Hasegawa *et al.*, Suppl. Prog. Theor. Phys. 47(1971)126.

[51] S. Watanabe, in Proceedings of the Japan-U.S. Seminar on Present and Future of Experimental Particle Physics by Hybrid Emulsion-Electronic Detectors p.215.

[52] M. Wirbel, B. Stech and M. Bauer, Z. Phys. C29(1985)637.

[53] R. Ammar *et al.*, Phys. Rev. Lett. 61(1988)2185.

[54] T. Tsuda, "Monte Carlo Method and Simulation", Baifukan, 1985(Japanese)

[55] R. Brun *et al.*, GEANT Long Writeup, CERN Program Library W5103(1989).

[56] B. N. Almqvist and E. Stelund, Comput. Phys. Commun. 43(1987)387.

[57] J. C. Anjos *et al.*, Phys. Rev. Lett. 67(1991)1507.

HIGH ENERGY PHYSICS Fermilab-E653

Measurement of the Semi-leptonic Decay Width $\Gamma(D^0 \to K^- \mu^+ \nu_\mu)$

1. Originality (and Introduction)
2. Theoretical Description
3. Experimental Apparatus
4. Methods of Bottom & Charm Searching
5. Analysis of the Branching Fraction
6. Results and Discussions

Shoji WATANABE
TOHO University

1. Originality

Jan 1989, **No Experimental Data of**

$\Gamma(D \to K \ell \nu)$ Semileptonic Decay $c \to s$

$D^0 (c\bar{u})$, $K^-(s\bar{u})$, ℓ (lepton; e, μ)

$\begin{pmatrix} u \\ d \end{pmatrix} \begin{pmatrix} c \\ s \end{pmatrix} \begin{pmatrix} t \\ b \end{pmatrix}$ $\begin{pmatrix} \nu_e \\ e^- \end{pmatrix} \begin{pmatrix} \nu_\mu \\ \mu^- \end{pmatrix} \begin{pmatrix} \nu_\tau \\ \tau^- \end{pmatrix}$

Preliminary Results of
the Relative Branching Fraction
etc.

" Present and Future of Experimental Particle Physics by Hybrid Emulsion - Electronic Detectors "

" Master thesis "

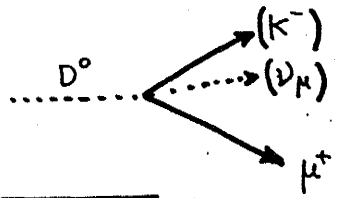

Dec 1991.

$\Gamma(D \to K\mu\nu)$	$\Gamma(D \to Ke\nu)$
E653	E691
Mark III	Mark III
CLEO	CLEO

Partial Decay Width

$$P_i(p_i) \to X_f(p_f)\, l(p_l)\, \nu(p_\nu)$$

$$D^0 \to K^- \quad \mu^+ \quad \nu_\mu$$

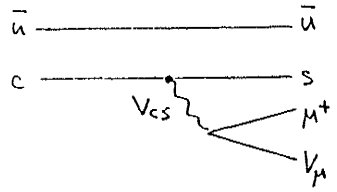

Lorentz invariant matrix element $\mathcal{M}$

$$\mathcal{M} = \sqrt{2E_i}\sqrt{2E_f}\sqrt{2E_l}\sqrt{2E_\nu}\,\langle X_f(p_f)\, l(p_l)\, \nu(p_\nu) \mid H_{weak} \mid P_i(p_i)\rangle$$

$$d\Gamma = \frac{2\pi}{2\pi i}\,|\mathcal{M}^2|\,d\Psi \qquad d\Psi = \delta^4(p_i - p_f - p_l - p_\nu)\,\frac{1}{(2\pi)^3}\,\frac{d^3p_f}{2E_f}\,\frac{d^3p_l}{2E_l}\,\frac{d^3p_\nu}{2E_\nu}$$

$$\mathcal{M} = h_\mu\, l^\mu$$

$$l_\mu = \sqrt{2E_l}\sqrt{2E_\nu}\,\langle l^+(p_l)\, \nu(p_\nu) \mid j_\mu \mid 0\rangle$$

$$h_\mu = \sqrt{2E_i}\sqrt{2E_f}\,\langle X_f(p_f) \mid j_\mu^+ \mid P_i(p_i)\rangle$$

$$h_\mu = f_+(q^2)(p_i + p_f)_\mu + f_-(q^2)(p_i - p_f)_\mu$$

f: form factor

D^0 ≠ point like

$$f_+(q^2) \approx f_+(0)\,\frac{1}{1 - q^2/m_V^2} \qquad m_l^2 = m_\nu^2 = 0$$

$$\frac{d^2\Gamma}{dx\,dy} = |V_{fi}|^2\,\frac{G_F^2}{16\pi^3}\,m_i^5\,|f_+(m_i^2 y)|^2\,A(x, y, \varepsilon)$$

$$A(x, y, \varepsilon) = 2x(1 - \varepsilon^2 + y) - 4x^2 - y$$

$$x \equiv \frac{E_l}{m_i}, \quad y \equiv \frac{q^2}{m_i^2}, \quad \varepsilon \equiv \frac{m_f}{m_i}$$

$$\Gamma(D^0 \to K\, l\, \nu) = |V_{cs}|^2\,|f_+(0)|^2\,(1.54 \times 10^{11})\ \text{sec}^{-1}$$

$|V_{cs}|$: CKM matrix element

$f_+(0)$: formfactor strong interaction

3. Experimental Apparatus

E653

Japan - U.S.A. - Korea

(11univ) (5) (5)

- $c\bar{c}$ ~ small
- scanning time
- S/N ratio

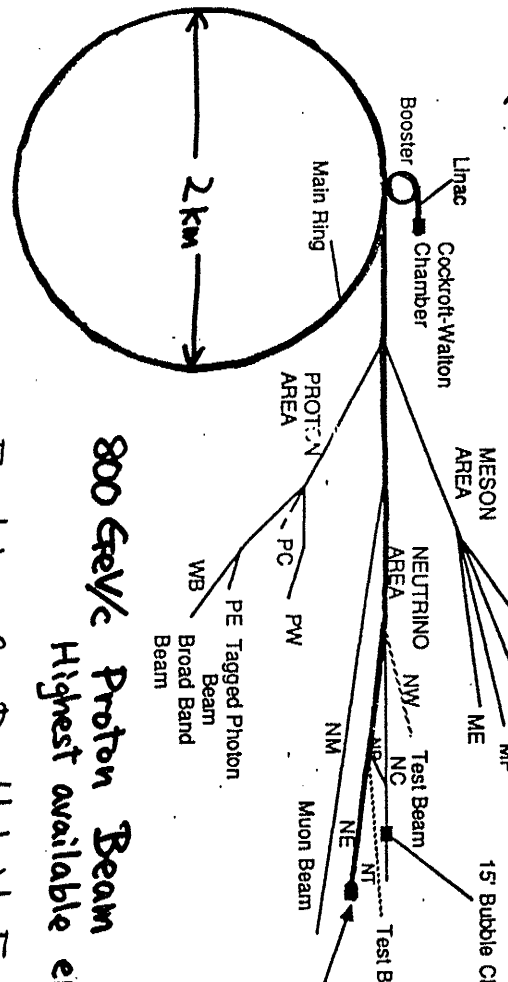

800 GeV/c Proton Beam

Highest available energy

Emulsion - Counter Hybrid Experiment

Fermi National Accelerator Laboratory

2. Theoretical Description

n $\tau(n) = 8.9 \times 10^{2}$ [sec] $\left(\tau(p) > 10^{25}\ \text{year}\right)$

$\pi^+(u\bar{d})$ $(2.6030 \pm 0.0024) \times 10^{-8}$

$K^+(u\bar{s})$ $(1.2371 \pm 0.0029) \times 10^{-8}$

$D^0(c\bar{u})$ $(4.21 \pm 0.10) \times 10^{-13}$

$\tau(B^0)/\tau(B^+) = 0.44 \sim 2.05$

$D^0 \to K^-\pi^+$

$\to \overline{K^0}\pi^+\pi^-$

$\to K^-\pi^+\pi^0$

$\to K^-\mu^+\nu_\mu$

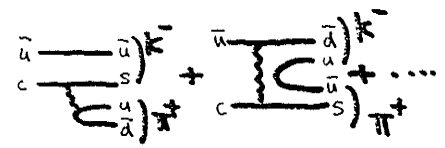

1 Feynman diagram → 1 partial decay width

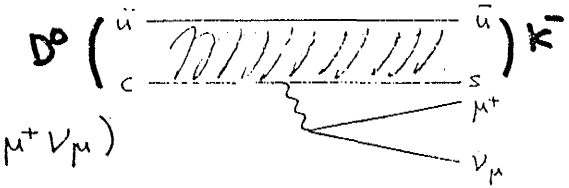

$\Gamma(D^0 \to K^-\mu^+\nu_\mu)$

→ Weak interaction V_{cs} ; C-K-M matrix element

→ Strong interaction f : form factor

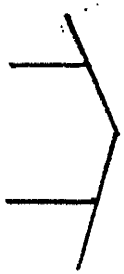

- Non leptonic decay
- $D\bar{D}$, $B\bar{B}$ mixing
- CP violation
- JLC
- SSC

⋮

C-K-M matrix

Weak interaction Hamiltonian,

$$H^{\text{eff}}_{\text{weak}} = \frac{G_F}{\sqrt{2}} (j_\mu + J_\mu)(j_\mu^\dagger + J_\mu^\dagger)$$

$G_F \sim 1.17 \times 10^{5}\ \text{GeV}^{-2}$

j_μ : lepton current

J_μ : quark current

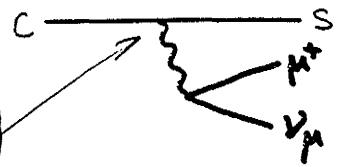

$$J^\mu = (\bar{u}\ \bar{c}\ \bar{t}) \frac{\gamma^\mu(1-\gamma^5)}{2} \begin{pmatrix} d' \\ s' \\ b' \end{pmatrix}$$

$$\begin{pmatrix} d' \\ s' \\ b' \end{pmatrix} = \begin{pmatrix} V_{ud} & V_{us} & V_{ub} \\ V_{cd} & V_{cs} & V_{cb} \\ V_{td} & V_{ts} & V_{tb} \end{pmatrix} \begin{pmatrix} d \\ s \\ b \end{pmatrix}$$

Cabibbo - Kobayashi - Maskawa matrix

t ?

b △

$$\begin{bmatrix} V_{ud} & V_{us} & V_{ub} \\ V_{cd} & V_{cs} & V_{cb} \\ V_{td} & V_{ts} & V_{tb} \end{bmatrix}$$

$$= \begin{pmatrix} 0.9747\ to\ 0.9759 & 0.218\ to\ 0.224 & 0.001\ to\ 0.007 \\ 0.218\ to\ 0.224 & 0.9734\ to\ 0.9752 & 0.030\ to\ 0.058 \\ 0.003\ to\ 0.019 & 0.029\ to\ 0.058 & 0.9983\ to\ 0.9996 \end{pmatrix}$$

- three generations
- $|V_{cd}| \approx |V_{us}|$

$\to |V_{cs}| = 1 - (|V_{us}|^2 + |V_{cb}|^2)$

① first run '85 May ~ Aug.

② second run '87 Aug. ~ Oct.

$\tau \sim 10^{-13}$ sec → 1 μm space resolution

Vertex SSD's
- ① 50μm pitch × 18
- ② 25μm pitch × 3
  50μm × 12
  50μm (10cm × 10cm) × 3

Emulsion

$b \to c\,\mu\nu$

$\hookrightarrow s\,\mu\nu$

↓ Muon trigger

E-653

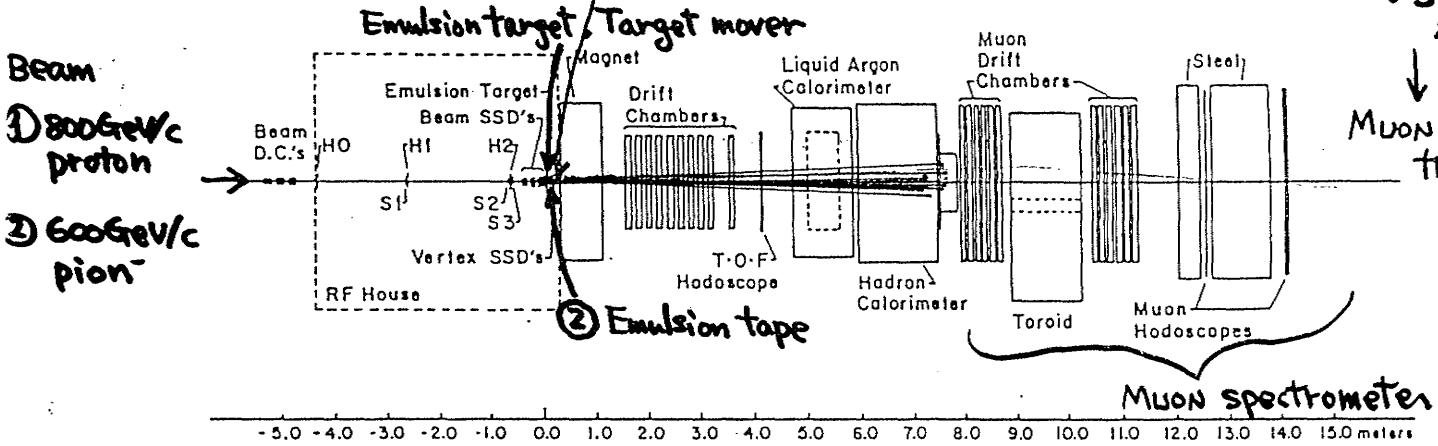

Muon trigger

Event

①	32 ℓ emulsion	5.4×10^6 trigger	$\sim 1 \times 10^8$ ints.	$\frac{\sigma_{B\bar{B}}}{\sigma_{PP}} \sim 10^{-6}$
②	36 ℓ emulsion	9.8×10^6 trigger	$\sim 3 \times 10^8$	$\frac{\sigma_{c\bar{c}}}{\sigma_{PP}} \sim 10^{-3}$ OK

Graphic Match

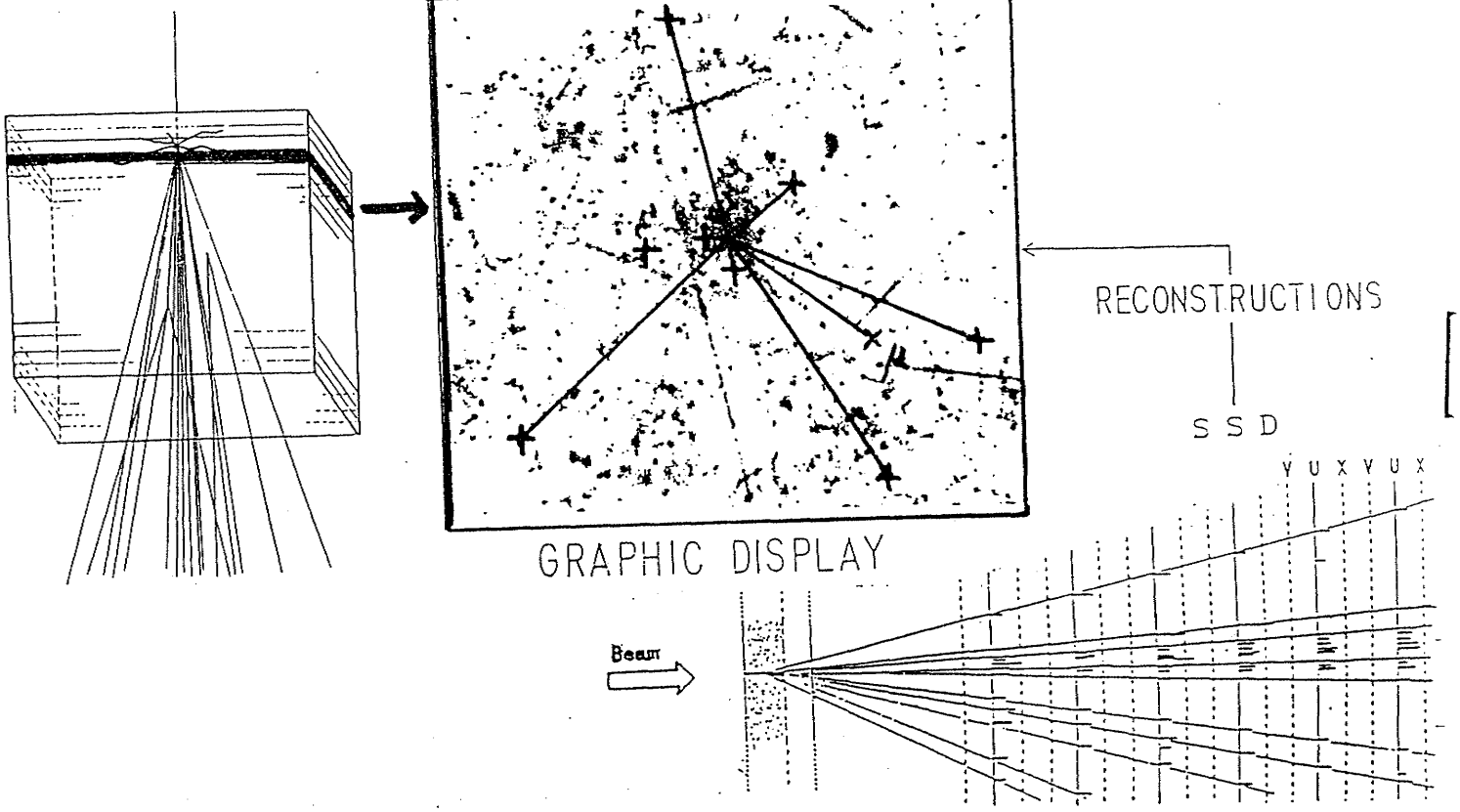

Silicon Strip Detector

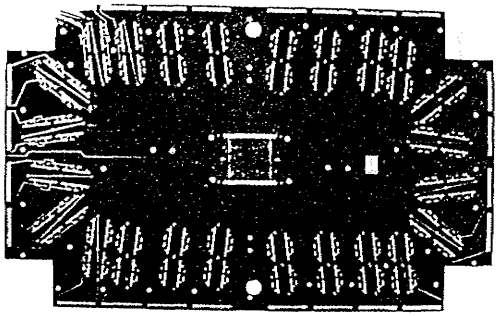

On line Microscope Stage System

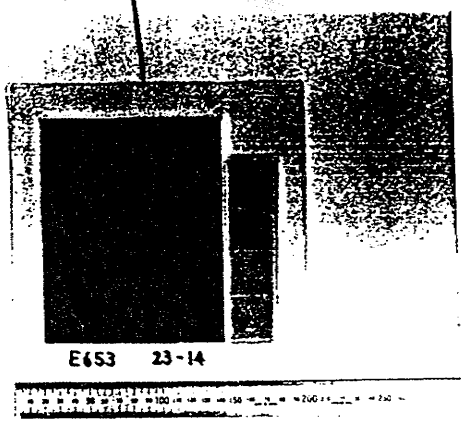

Emulsion Plate

Reconstruction of Counter Tracks

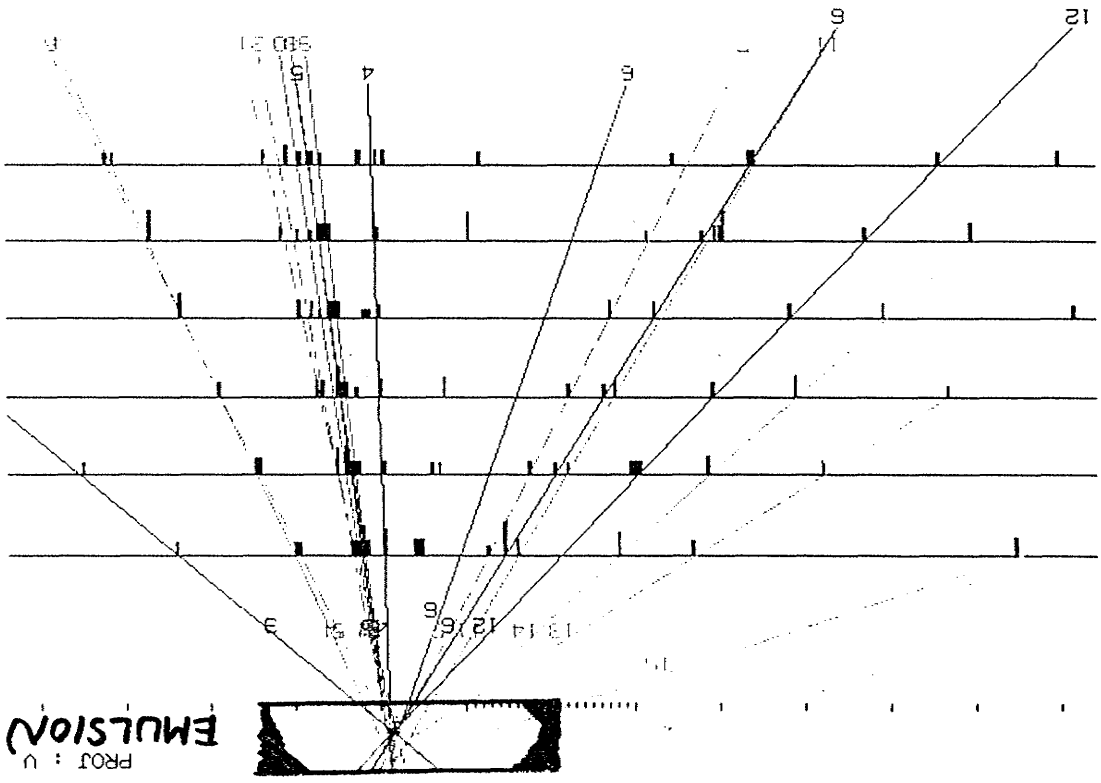

4. Emulsion Scanning Methods

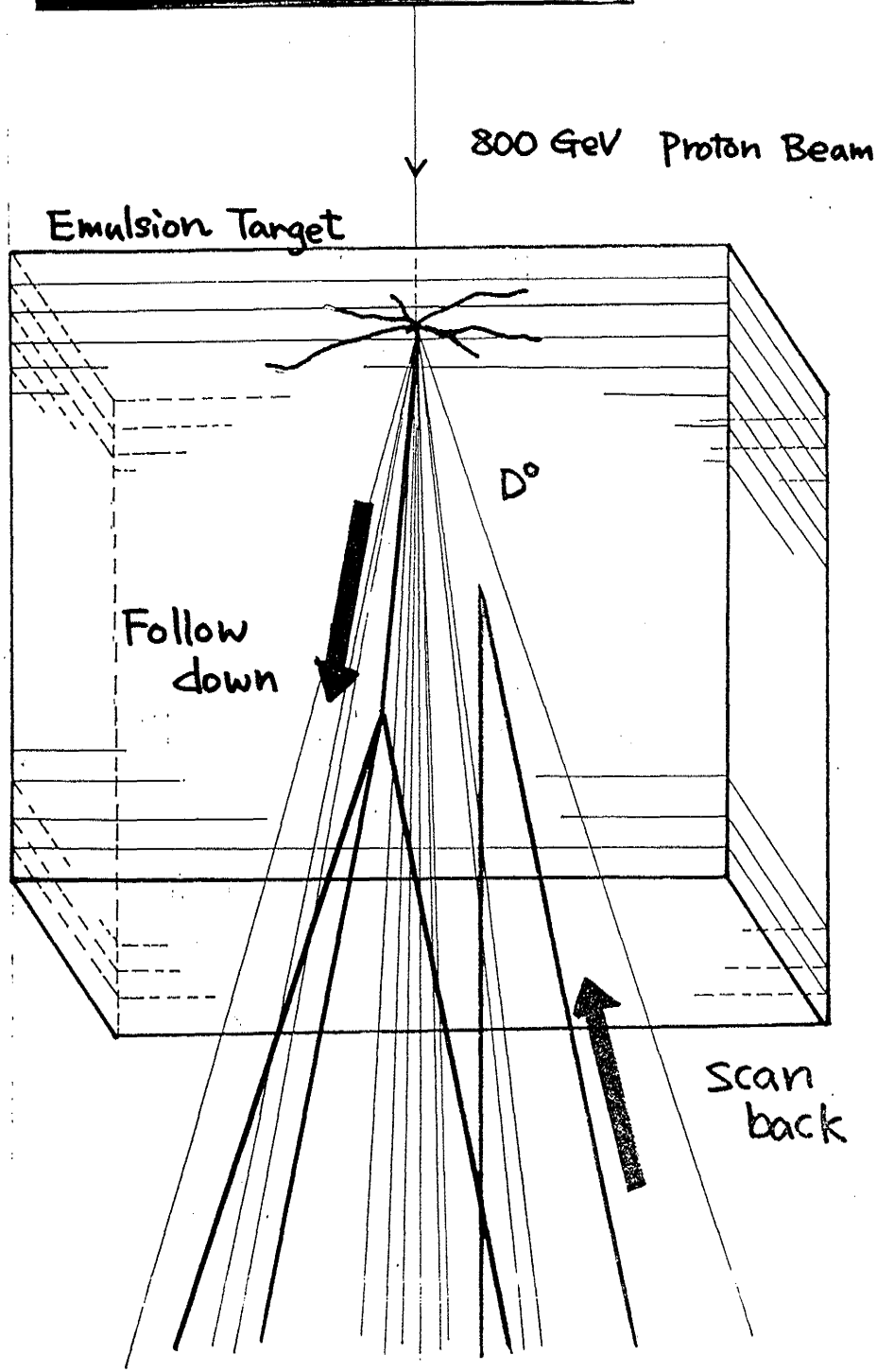

Event Selections

- $\sigma_{c\bar{c}}$ ~ small
- scanning time
- S/N ratio

Total interactions in emulsion ~ 1×10^8 int.

Data taking on Magnet Tape ~ 5×10^6

Off line selection (P_μ, $P_{T\mu}$, I.P.$_\mu$) on Data Summary Tape ~ 5×10^4

Events in fiducial volume (Found 1ry int. in emulsion) ~ 2×10^4 (18888)

NO μ from 1ry 6527

Total # of charm candidates in Emulsion after decay search 1085

N2 charm decay candidates 343

Final sample 121

- N2 with μ
- $P_T > .25$ GeV/c
- two emulsion track matched counter spectrometer and momentum analyzed

Semi-leptonic Decay of D° meson in Emulsion

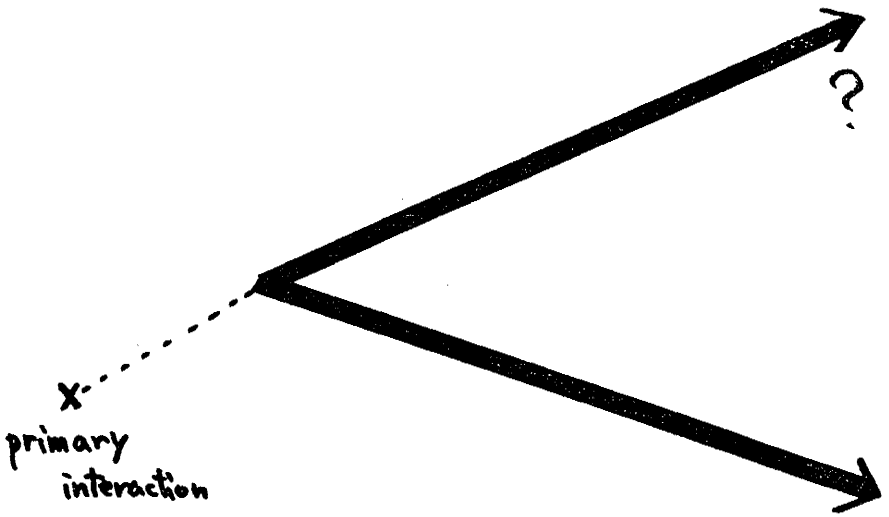

$\mu, \left(\frac{dx}{dz}\right), \left(\frac{dy}{dz}\right), P_\mu$

$D^0 \to K \mu \nu$
$\to K^* \mu \nu$
$\to \pi \mu \nu$

Branching fraction

$$f = \frac{\Gamma(D^0 \to K \mu \nu)}{\Gamma(D^0 \to \mu + \text{anything})}$$

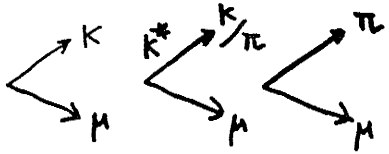

$\Gamma(D^0 \to K \mu \nu)$

1 decay vertex X $\longrightarrow$ $|V_{cs}|$, $|f_+(0)|$

5. BRANCHING FRACTION STUDY

$P_T\mu$ Method

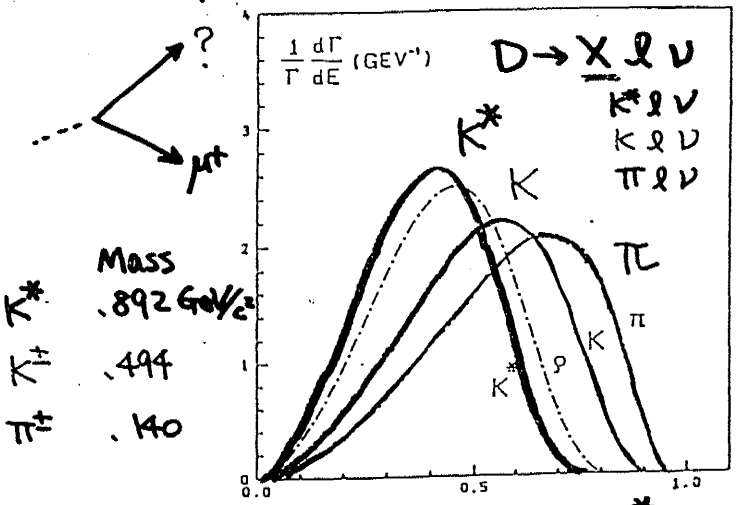

BSW model

M. Wirbel, B. Stech and M. Bauer
Z. Phys. C29(1985)

	Mass
K^*	.892 GeV/c²
$K^\pm$	.494
$\pi^\pm$	.140

E^*_ℓ Center of mass system

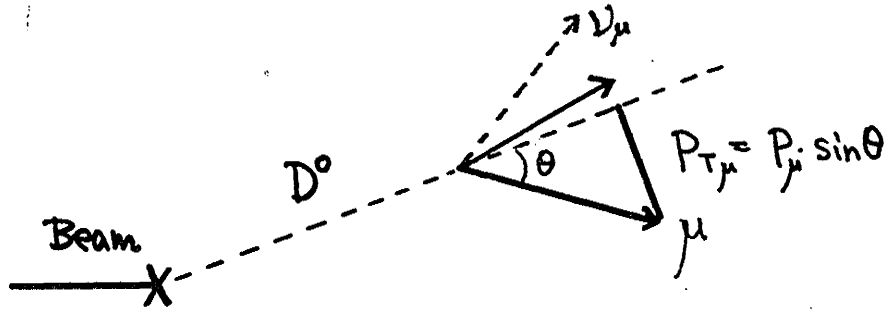

$P_{T\mu}$ Distribution

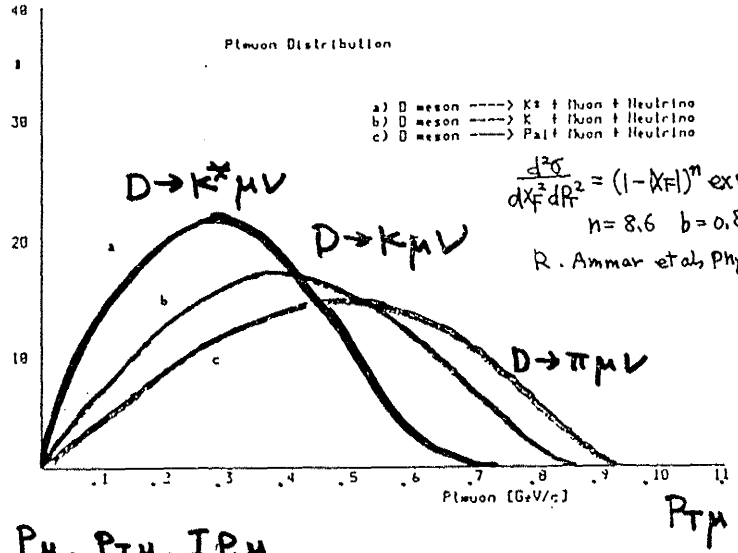

$\frac{d^2\sigma}{dx_F^2 dP_T^2} = (1-|x_F|)^n \exp(-bP_T^2)$

$n = 8.6 \quad b = 0.8$

R. Ammar et al, Phys Rev. Lett. 61(1988) 2185

3×10^6 event

$P_{T\mu}$

E653 P_μ, $P_{T\mu}$, I.P.μ

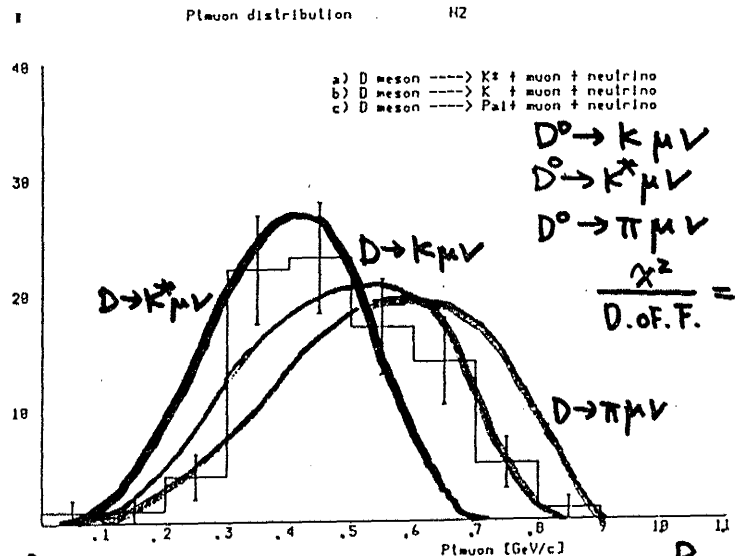

$D^0 \to K\mu\nu$ 43 %

$D^0 \to K^*\mu\nu$ 43

$D^0 \to \pi\mu\nu$ 16

$\frac{\chi^2}{D.o.F.} = 1.0$

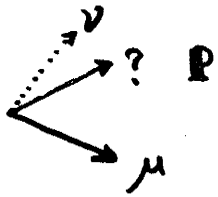

OK

Maximum likelihood $.42 \pm .14$ K, K* only

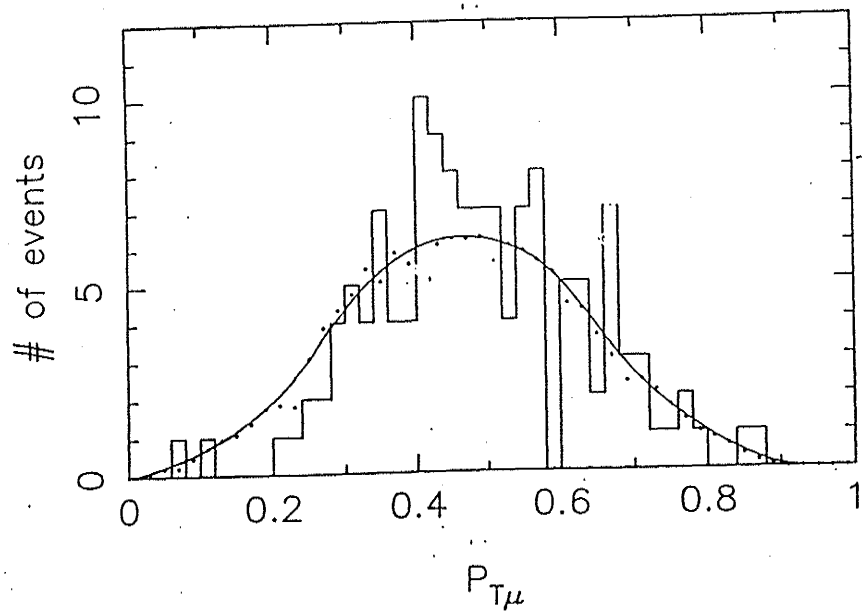

Calculation of Invariant Mass

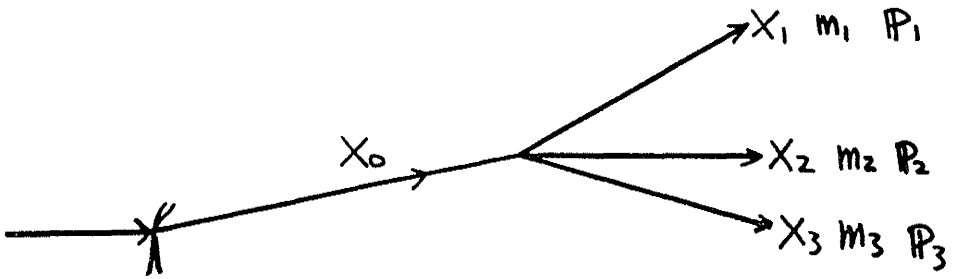

$$M_0^2 = E_0^2 - P_0^2$$

$$= \left(\sqrt{m_1^2+P_1^2} + \sqrt{m_2^2+P_2^2} + \sqrt{m_3^2+P_3^2}\right)^2 - \left(P_1 + P_2 + P_3\right)^2$$

$$= m_1^2 + m_2^2 + m_3^2 + 2\left(\sqrt{m_1^2+P_1^2}\sqrt{m_2^2+P_2^2} - P_1 \cdot P_2\right) + 2\left(\sqrt{m_2^2+P_2^2}\sqrt{m_3^2+P_3^2} - P_2 \cdot P_3\right) + 2\left(\sqrt{m_3^2+P_3^2}\sqrt{m_1^2+P_1^2} - P_3 \cdot P_1\right)$$

$$P_1 \cdot P_2 = P_{1x}P_{2x} + P_{1y}P_{2y} + P_{1z}P_{2z}$$
$$P_2 \cdot P_3 = P_{2x}P_{3x} + P_{2y}P_{3y} + P_{2z}P_{3z}$$
$$P_3 \cdot P_1 = P_{3x}P_{1x} + P_{3y}P_{1y} + P_{3z}P_{1z}$$

$$\begin{pmatrix} P_x \\ P_y \\ P_z \end{pmatrix}^{(P)} = \begin{pmatrix} \cos\theta\cos\varphi & \cos\theta\sin\varphi & -\sin\theta \\ -\sin\theta & \cos\varphi & 0 \\ \sin\theta\cos\varphi & \sin\theta\sin\varphi & \cos\theta \end{pmatrix} \begin{pmatrix} P_x \\ P_y \\ P_z \end{pmatrix}^{(B)}$$

Minimum Mass Calculation

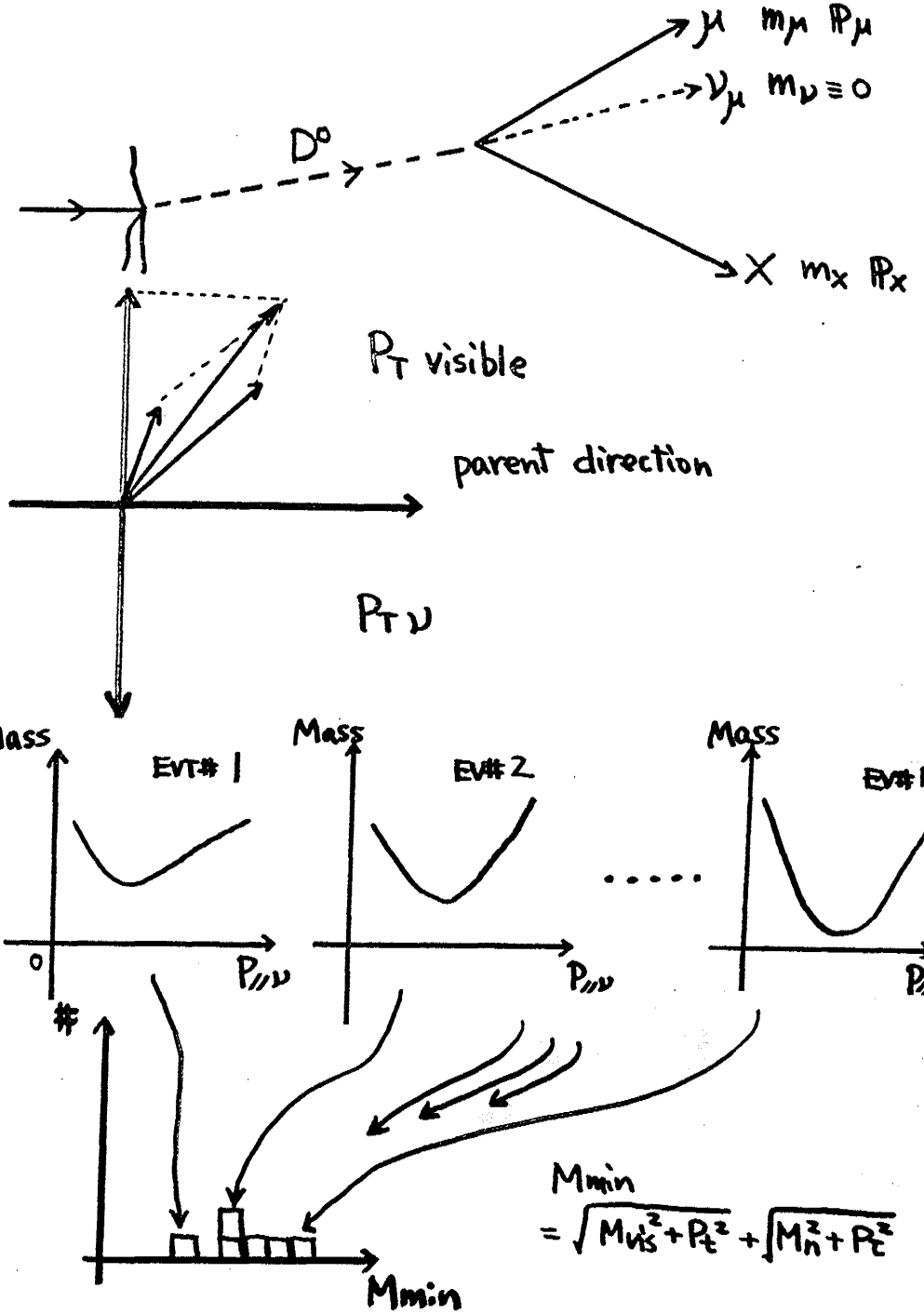

Mmin Distribution

Figure 1(b): Assume Perfect Resolution

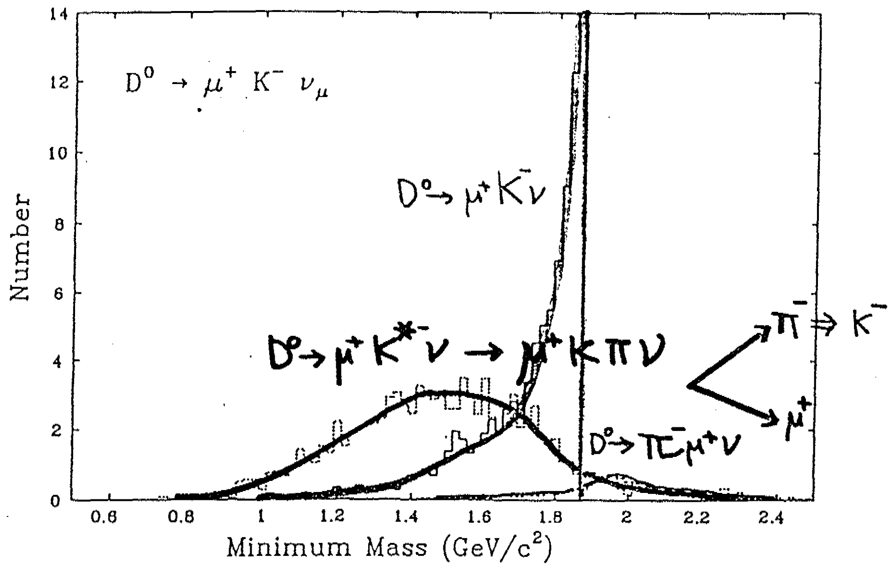

Figure 3(b): 2 μm Resolution

Emulsion

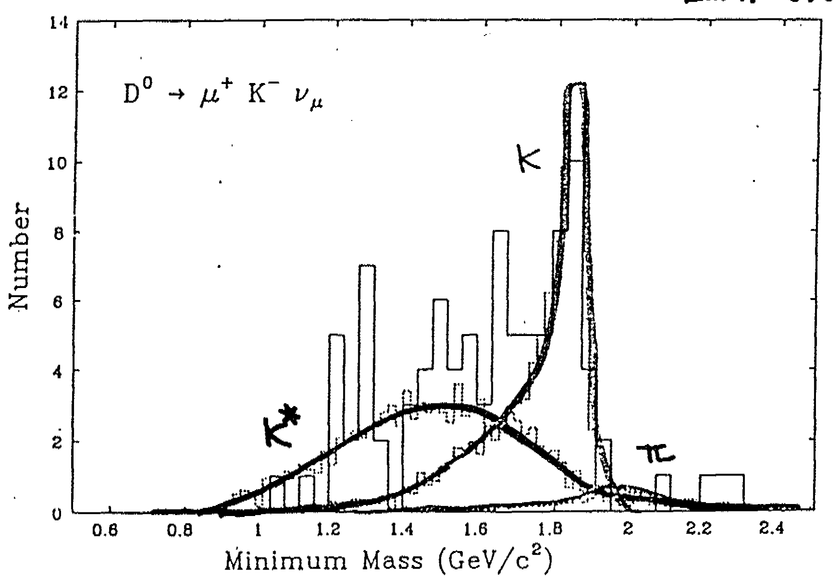

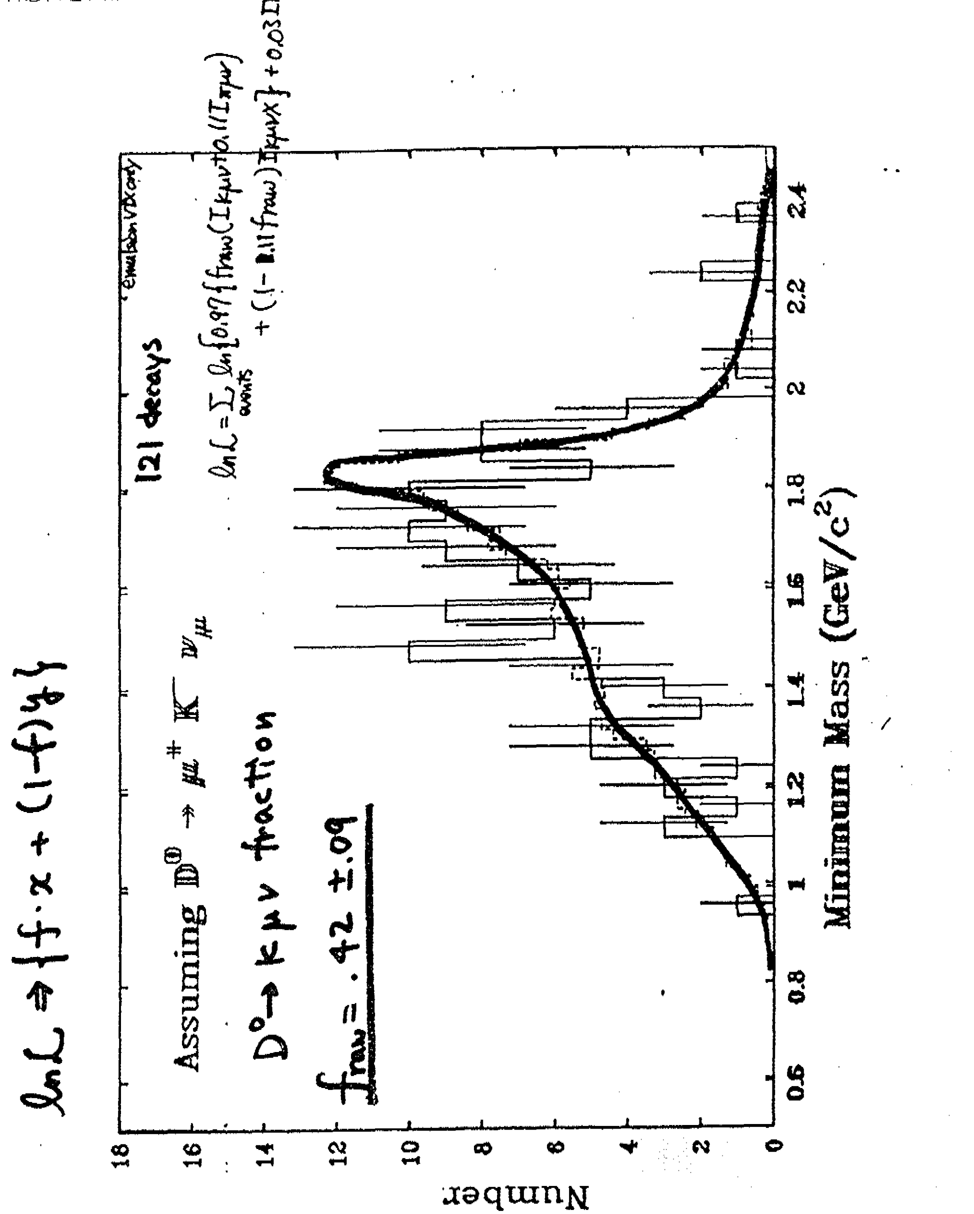

BRANCHING FRACTION STUDY
BY Mmin Distribution

$$\frac{(D^0 \to K\mu\nu)}{(D^0 \to X^-\mu\nu) + (D^0 \to K\mu\nu) + (D^0 \to \pi\mu\nu)} \equiv f$$

$X^- \equiv K^{*-}$ ($K^{*-} \to \bar{K}^0\pi^-$)

$D^0 \to X^-\mu\nu$	$f_{raw\ rate}$	$f_{corrected\ rate}$
$X^- \equiv K^{*-}$	.42 ± .09	.32 ± .05
$K^{*-}\pi^0$	.39 ± .07	.30 ± .09
$\rho^- K^0$	.43 ± .08	.29 ± .09
$\eta^0 K^-$	.46 ± .08	.34 ± .05

The values of f from the fits are not very sensitive to the choice of decay mode.
The maximum contribution of the multineutral modes is constrained by the observed N4.

$$f = .32 \pm .05\,(stat) \pm .05\,(syst)$$

Calculation of Partial Decay Width

Mmin Analysis

$$f = \frac{\Gamma(D^0 \to K\mu\nu)}{\Gamma(D^0 \to \mu X)} \qquad X \equiv \text{anything}$$

$$= .32 \pm .05 \pm .05$$

$$\Gamma_{total}^{D^0} = \frac{\hbar}{\tau(D^0)}$$

$$= (2.38 \pm 0.02) \times 10^{12}\ s^{-1}$$

$\tau(D^0) = (4.21 \pm 0.10) \times 10^{-13}$ s
PDG (1990)

$$R(D^0 \to K\mu\nu) = (.32 \pm .05 \pm .05) \times .96\,(7.7 \pm 1.2)\%$$

$$= (2.4 \pm 0.4 \pm 0.5)\%$$

$$\Gamma(D^0 \to K\mu\nu) = R(D^0 \to K\mu\nu) \cdot \Gamma_{total}^{D^0}$$

$$= \underbrace{(5.6 \pm 0.9 \pm 1.2) \times 10^{10} s^{-1}}_{\text{Published}}$$

$\Gamma(D^0 \to Ke\nu)$
(μ-e universality .96)
Phys. Rev. Lett. 66 (1991) 1819

Mark III $(7.9 \pm 1.2 \pm 0.9) \times 10^{10}\ s^{-1}$
J. Adler et al, Phys. Rev. Lett. 62 (1989) 1821

E691 $(9.1 \pm 1.1 \pm 1.4) \times 10^{10}\ s^{-1}$
J.C. Anjos et al, Phys. Rev. Lett. 62 (1989) 1587

$\Downarrow$

$(5.6 \pm 0.8 \pm 1.5) \times 10^{10}\ s^{-1}$
Preprint Fermilab-PUB-91/151

Form Factor & $|V_{cs}|$

$$\Gamma(D^0 \to K^- \mu^+ \nu_\mu) = |f_+(0)|^2 |V_{cs}|^2 (1.54 \times 10^{11})\ s^{-1}$$

$$= (5.6 \pm 0.9 \pm 1.2) \times 10^{10}\ s^{-1}$$

if $|f_+(0)| = 0.9 \pm 0.1$

$$|V_{cs}| = .86 \pm .14 \pm .16$$

if $|V_{cs}| = 0.974 \pm 0.001$

$$|f_+(0)| = .62 \pm .05 \pm .07$$

Theoretical predictions for $D^0 \to K^- \mu^+ \nu_\mu$.

Model	$\Gamma(D^0 \to K\ell\nu)$ [$\times 10^{10}$ sec^{-1}][35]	form factor $f_+(0)$
Quark Model		
GS/AW[26]	7.1	0.69
BSW[24]	8.3	0.76
GISW[25]	8.4	0.76
KS[27]	10.	0.83
Lattice QCD		
LMS[29]	4.9 ± 0.7	0.58 ± 0.04
CMHS[30]	9.5 ± 4.0	0.74 ± 0.17
BKS[31]	14.0 ± 6.0	0.90 ± 0.22
QCD sum rule		
BBD[32]	6.4 ± 3.0	$0.6^{+0.15}_{-0.10}$
DP[33]	9.7 ± 1.3	0.75 ± 0.05
AOS[34]	11.0 ± 5.0	0.8 ± 0.2

CONCLUSIONS

E653 emulsion-counter hybrid experiment

800 GeV Proton - Emulsion Reactions

Observed charm decay events in emulsion

Total # 1085 ev.

→ 121 ev.

D^0 N2 pure sample

$P_{T\mu}$ distribution → Mmin distribution

Distribution

$\Gamma(D^0 \to K\mu\nu) = (5.6 \pm 0.9 \pm 1.2) \times 10^{10}\ s^{-1}$

Partial Decay width

$|f_+(0)| = 0.62 \pm 0.05 \pm 0.07$

Form Factor ; assumed 3 generations

$|V_{cs}| = 0.86 \pm 0.14 \pm 0.16$

Model dependent ; assumed $f_+(0) = 0.7$